ELEMENT-SPECIFIC NANOPARTICLE PLACEMENT TOWARD FABRICATING MULTI-ELEMENT METASTRUCTURES

by

LEI WU

THESIS

Submitted in partial fulfillment of the requirements
for the degree of Master of Science in Material Science & Engineering at
The University of Texas at Arlington
May 2019

Arlington, Texas

Supervising Committee: Seong Jin Koh, Supervising Professor

Copyright © by Lei Wu 2019

All Rights Reserved

Acknowledgments

I am eternally grateful to all of those with whom I have had my most profound appreciation and tremendous gratitude for every support and help in one type or another to make this research being possible and successful.

To Dr. Seong Jin Koh, who took a chance on me in early 2018 and offered me a research position in his team with tuition scholarship and funding. It is the most significant opportunity for my graduate study. He saw my willingness to learn, grow and succeed in academic. During the past years, he has been an excellent professor, a friend, and a guide that encouraged me all way along.

To my team member Kishan Jayanand, a super humble and kind person that taught me respect, discipline, and manners. Shared so many scientific ideas and suggestions to help my project. I wish the best of luck on his new career and life. Also, to Nnaemeka Mcdonald Eluagu and Pushkar Kiran Gothe who given their full support to my research at any time.

I must thank Nader Hozhabri, Kevin Chambers, Huan Nguyen, and Dennis Bueno with all the nanofab technical support; without their help, this cannot be done.

I extend my gratitude to committee members, Dr. Yaowu Hao and Dr. Kyungsuk Yum for having their time in reviewing my thesis defense.

At last thanks for my parents that financially supported me so many years so I can continue my study in the US, and much more assist mentally. Moreover, a

special gratitude to my fiancée Qing Sun who had extended encouragement for my research.

All the work was supported by the National Science Foundation (CMMI-1463451).

April 17, 2019

Abstract

ELEMENT-SPECIFIC NANOPARTICLE PLACEMENT TOWARD FABRICATING MULTI-ELEMENT METASTRUCTURES

Lei Wu, MS

The University of Texas at Arlington, 2019

Supervising Professor: Seong Jin Koh

Nanoscale entities such as semiconductor nanoparticles, magnetic nanoparticles, metal nanoparticles, and dielectric nanoparticles have attracted a lot of attention due to their novel electrical, optical, and magnetic properties that their bulk materials cannot produce. These unique properties promise applications in nano-optical devices, ultra-sensitive sensors, single electron transistors, and high-density data storages. Moreover, to these captivating properties of the individual nanoparticles, it has been found that novel and scientifically important properties can be obtained when nanoparticles are arranged in specific configurations. Examples include nanoparticle dimers, hexamers, heptamers, and nanoparticle arrays. Until now, however, most studies have focused on one-element nanoparticle systems. This thesis investigates a new approach in which different-element nanoparticles can be placed on target substrate positions to construct multi-element nanoparticle metastructures.

The nanoparticle placement is carried out using electrostatic guiding structure, which guides negatively charged nanoparticles onto desired substrate

locations. Placement of different-element nanoparticles is enabled by controlling the electrostatic interactions between different-element nanoparticles and the electrostatic guiding structure. The electrostatic guiding structure was created using E-Beam lithography, thin film deposition, and formation of self-assembled monolayers (SAMs). The guiding structure contained circular wells having varying diameters from 100 nm to 200 nm. Surface modification with self-assembled monolayers (SAMs) created positively and negatively charged areas on the structure. The nanoparticles were made negatively charged by immobilizing DNA on their surfaces. The negatively charged single nanoparticles were guided by the SAMs-functionalized electrostatic guiding structure and placed on the center positions of the circular wells. By controlling the ion concentrations, pH, and circular well diameters, we were able to differentiate the placement of 30 nm and 50 nm Au nanoparticles, enabling the element-specific placement of single nanoparticles.

CONTENTS

Acknowledgments I

Abstract III

CHAPTER 1 INTRODUCTION 1

1.1 Motivation and Approach 1

1.2 Thesis Outline 1

CHAPTER 2 BACKGROUND 3

2.1 Arrays of Nano-Scale Particles 3

2.2 Applications and Fabrication of Nanostructure 6

2.3 Zeta Potential 10

2.4 Debye Length 11

2.5 Lithography Technique 13

2.6 E-Beam Lithography 14

2.7 Photoresist 16

2.8 Self-Assembled Monolayers 17

2.9 3-aminopropyltriethoxysilane (APTES) SAM's layer 19

2.10 16-mercapthohexadeconic acid (MHA) SAM's layer 20

2.11 Negatively charged DNA strands 21

2.12 Influence of DNA coverage 22

2.13 Electrostatic Funneling....................23

2.14 Thermal Oxidation....................24

2.15 Wet Etching....................25

2.16 Dry Etching....................26

2.17 Plasma-Therm Reactive Ion Etching....................28

CHAPTER 3 EXPERIMENTAL PROCEDURE....................30

3.1 Overall View of Experiment....................30

3.2 Clean Room Technical Machines....................31

3.3 Reagent Materials....................32

3.4 Wafer Preparation....................34

3.5 Thermal Oxidation....................35

3.6 Spin Coating....................36

3.7 E-Beam Lithography....................37

3.8 Development....................42

3.9 E-Beam Evaporation....................43

3.10 Lift-off with Clean Process....................43

3.11 DNA Gold Nanoparticle Conjugate....................44

3.12 SAM's Layer Formation....................48

3.13 Au Nanoparticle Placement....................50

3.14 Au Nanoparticle Protection 51

3.15 Remove of Gold and Chrome Layers 53

3.16 Pillar-Shaped Photoresist Removal 54

3.17 SiO_2 Nanopillar Formation 54

CHAPTER 4 RESULT AND DISCUSSION 57

4.1 E-Beam Dose Effect in Lithograph 57

4.2 Type of Photoresist (2401 and 2403) 59

4.3 E-Beam Deposition Method (CHA & AJA) 60

4.4 Wet Chemical Surface Treatment 61

4.5 Ion Concentration (under wet chemical treatment) 63

4.6 Gold Plating Solution Treatment 65

4.7 Sputtering Treatment and Direct Process 66

4.8 Advanced Wet Chemical Treatment 68

4.9 Continuously Process and IPA/DI Clean 70

4.10 Ethanol/N2 Immersion 71

4.11 Long-Time Ethanol Immersion and Advanced Sputtering 73

4.12 IPA, Acetone Sonication Effects 76

4.13 Ion Concentration Effeteness 79

4.14 New Pattern Array 81

4.15 DI Water Resuspended Au Nanoparticle 83

4.16 PB Buffer pH Effeteness 84

4.17 Ion Concentration and Circle Diameter (30nm Au particle) 85

4.18 Ion Concentration and Circle Diameter (50nm Au particle) 88

4.19 Single, Double, and Triple Attachment (30nm Au particle) 90

4.20 Single, Double, and Triple Attachment (50nm Au particle) 97

4.21 APTES Stability 98

4.22 Heat Treatment for APTES Layer 99

4.23 Double SAM's Layer Formation 101

CHAPTER 5 CONCLUSION 102

REFERENCES 105

List of Figures

Fig 1 Scanning electron micrographs of an array of gold nanoparticle chains on a glass substrate[19] 4

Fig 2 Shone an infra-red laser at a precise arrangement causes the sensor to emit UV light (in blue)[20] 5

Fig 3 Different options for electron devices using silicon nanowires. The top drawing a show a general 3-D view of a silicon nanowire device with metallic source/drain regions and the surrounding gate. The cross sections b–e illustrates different device concepts: b Conventional nanowire MOSFET, c Schottky Barrier FET, d Junctionless FET and e Tunnel FET[22] 6

Fig 4 Schematic cut in the width direction of a planar (a) and a nanowire-based (b) charge trapping memory cell. The arrows indicate the field lines in the device in programming or erase operation. In the nanowire device, the field lines are denser in the bottom oxide. Therefore the exchange of carriers between the charge trapping layer and the silicon transistor body is enhanced, and the charge exchange between the charge trapping layer and the gate electrode is reduced[22] 7

Fig 5 Schematic view of VLS growth of silicon nanowires. A Gold particle formed on the growth substrate. b VLS growth using silane as silicon precursor[22] 8

Fig 6 Schematic diagram of nanopillar fabrication by nanosphere lithography. Step 1: spin coat a hexagonally close-packed monolayer of polystyrene beads on substrates. Step 2: tailor the size of the beads' "resist" by oxygen plasma etching. Step 3: etch the exposed semiconductor areas by deep reactive ion etching using the "Bosch" process[22] 9

Fig 7 Schematic representation of ionic charges around a charged particle in an aqueous media[34] 10

Fig 8 Naïve view and realistic view and carrier concentration[40] 12

Fig 9 A typical sequence of lithographic processing steps [30] 13

Fig 10 schematic view of projection printing and direct writing[42] 15

Fig 11 Differences of positive photoresist and negative photoresist after expose under light[45] 17

Fig 12 schematic view of Self-Assembled Monolayer[47] 18

Fig 13 Surface modification of SiO_2 with APTES 19

Fig 14 Surface modification of Au with MHA 20

Fig 15 DNA structure[52] 21

Fig 16 DNA loading (# DNA strands/nanoparticle) vs. NaCl concentration for A10, T10, and PEG spacers on 15 nm gold nanoparticles[56] 23

Fig 17 **a**. A nanoparticle in a colloid is electrostatically guided onto a circle center. **b**. Once a nanoparticle occupies a circle, the approach of other nanoparticles is prohibited. Inside the circle: positively charged; outside the circle: negatively charged; and nanoparticle: negatively charged[57] 24

Fig 18 Simple Ideal of Wet Etching[60] 25

Fig 19 Ion generation by the collision of electrons and neutral atoms[63] 27

Fig 20 Reaction steps of dry etching[54] 28

Fig 21 **(a)** Au particle placement done, **(b)** PR coat on surface, **(c)** RIE to remove the PR above the surface, **(d)** wet etching to remove the Cr and Au layer but with PR protected Au particle will remain 29

Fig 22 Schematic representation of experiment Overview 31

Fig 23 Cleaned Si Wafer 34

Fig 24 Diced 4 inches wafer 36

Fig 25 Actual Chip with mark on it 37

Fig 26 SEM image of E-beam pattern (Smallest Unit) 41

Fig 27 E-beam pattern array design 41

Fig 28 Schematic processes from spin coating to development 42

Fig 29 Schematic side view after deposition 43

Fig 30 Schematic side view after lift-off and clean process 44

Fig 31 Schematic side of DTT break the disulfide bond 45

Fig 32 Schematic working principal of NAP-5 46

Fig 33 DNA strands coated on gold nanoparticle surface 48

Fig 34 SAM's Layer Formation 51

Fig 35 Photoresist being removed 53

Fig 36 E-beam deposited Au and Cr layer being removed 53

Fig 37 Gold Nanoparticle exposed on surface 54

Fig 38 SiO_2 nanopillar formed via RIE 55

Fig 39 SEM 45-degree SiO_2 nanopillars with 150nm height 56

Fig 40 Sample #1, 2, 3, 4, 2403 PR, overall view 57

Fig 41 Sample #2, 2, 3, 4, 2403 PR pillar shape 58

Fig 42 Sample #1, 2403 PR, the overall, small, and large size SEM view 59

Fig 43 Sample #2, 2401 PR, overall, small, and large size view 60

Fig 44 Sample #1, 2401 PR, AJA, overall, small, and large size view 61

Fig 45 Sample #2, 2401 PR, CHA, overall, small, and large size view 61

Fig 46 Sample #2, AJA, SPP SEM, overall, small, and large area size view 62

Fig 48 Sample #2, ph7.5_1mM_SPP SEM, overall, small, and large area size view 64

Fig 47 Sample #1, ph7.5_0.1mM_SPP SEM, overall, small, and large area size view 64

Fig 49 Sample #3, ph7.5_5mM_SPP SEM, overall, small, and large area size view 65

Fig 51 Sample #2, SPP SEM, selectivity, small, and large area size view 67

Fig 50 Sample #1, SPP SEM, selectivity, small, and large area size view 67

Fig 52 Sample #1-5 from tow row to bottom, SPP SEM, overall, selectivity, and large size area view 69

Fig 53 Sample #1 SPP SEM, overall, selectivity, and large middle small size area view 70

Fig 54 Sample 2 SPP SEM, overall, selectivity, and large middle small size area view .. 71

Fig 55 Sample 1 SPP SEM, overall, selectivity, and large middle small size area view .. 72

Fig 56 Sample 3 SPP SEM, overall, selectivity, and large middle small size area view .. 72

Fig 57 Sample 2 SPP SEM, overall, selectivity, large middle small size area view, and surface features 73

Fig 58 Sample 1 SPP SEM, selectivity, overall and large small size area view 74

Fig 59 Sample 2 SPP SEM, selectivity, overall and large small size area view 74

Fig 61 Sample 4 SPP SEM, selectivity, overall and large small size area view 75

Fig 60 Sample 3 SPP SEM, selectivity, and large small size area view 75

Fig 62 Sample 1 SPP SEM, selectivity, overall, large, medium, and small size area view 77

Fig 63 Sample 2 SPP SEM, selectivity, overall, large, medium, and small size area view 77

Fig 64 Sample 3 SPP SEM, selectivity, overall, large, medium, and small size area view 78

Fig 65 Sample 4 SPP SEM, selectivity, overall, large, medium, and small size area view 78

Fig 66 Sample 1 SPP SEM, 0.2mL ion concentration 80

Fig 67 Sample 2 SPP SEM, 1mL ion concentration 80

Fig 68 Sample 3 SPP SEM, 0.2mL+1mL ion concentration 81

Fig 69 New Pattern #1, top left 100nm, top right 110nm, bottom left 120nm, and bottom right 160nm 82

Fig 70 New Pattern #1, top left 120nm, top right 130nm, bottom left 140nm, and bottom right 180nm 82

Fig 71 0.02mM, 0.1mM, and 1mM ion concentration for 30nm gold nanoparticle placement SEM with different circle diameters (Partial location) 86

Fig 72 Column chart of circle diameter vs particle (30nm) attachment with different ion concentration 87

Fig 73 0.02mM, 0.1mM, and 1mM ion concentration for 50nm gold nanoparticle placement SEM with different circle diameters (Partial location) 89

Fig 74 Column chart of circle diameter vs particle (50nm) attachment with different ion concentration 90

Fig 75 0.005mM, 0.01mM, and 0.1mM ion concentration for 30nm and 50nm gold nanoparticle placement SEM with circle diameters from 100nm to 180nm (Partial location) 95

Fig 76 Column chart of circle diameter, ion concentration with single, double, and triple attachment 96

Fig 77 Column chart of circle diameter, ion concentration with single attachment 97

Fig 78 130-19nm alternating pattern, after 0.005mM 50nm+0.1mM 30nm particle placement 98

Fig 79 Different temperature heat treatment result of multi nanoparticle placement 100

Fig 80 Double SAM's layer formation results with alternating pattern circle 101

List of Tables

Table 1 Characteristics of positive and negative photoresists 16

Table 2 Oxidation conditions of the furnace.. 35

Table 3 pH values with the differ ion concentration and DI water.................................. 84

Table 4 30nm particle Attachment with differ ion concentration and circle diameter 87

Table 5 50nm particle Attachment with differ ion concentration and circle diameter 89

Table 6 30nm particle Attachment with differ ion concentration and circle diameter in 8X8 plus 7X7 array.. 95

CHAPTER 1 INTRODUCTION

1.1 Motivation and Approach

The words Nano and nanotechnology were introduced to our world long time ago. Modern society and human life have been changing by nanotechnology in so many ways that we do not even realize[1,2]. This developing field of research is taking us to the new frontier of science and technology. Over the past decades, nanoscale entities such as nanoparticles, nanopillars, nanotubes, and their nanoarrays have attracted a lot of attention due to their unique electrical, mechanical, and optical properties[3]. For these nanoscale entities to be utilized for practical applications, however, it would require that they can be placed on desired substrate locations in systematic ways. To fulfill these requirements, many novel nanoparticle placement methods have been demonstrated over the past decades. Until now, however, they have been limited to the placement for one-element nanoparticles. In this study, we investigate a new approach in which different-element nanoparticles are placed on specific substrate positions[4]. This new approach could create a new classes of nanoparticle metastructures that one-element nanoparticle systems could not produce, which may promise many applications[4] in the fields of nano-optical devices[5,6], ultra-sensitive sensor[7], ultra-high-density data storage[8,9], and nano-transistors.

1.2 Thesis Outline

Chapter 1, a brief statement of this research's motivation and how this thesis is going to approach the new method with the discussion in detail.

Chapter2, Basic knowledge is going to introduce in this chapter, including all the methodologies and different techniques. Generally, most of the relevant background and experimental setups.

Chapter 3, the procedure of experiment from substrate preparation to Au nanoparticle placement, and one application are going to discuss. Every chemical reagents and experiment instruments (cleanroom) will be mention. Process list: substrate preparation, E-Beam lithography, development, E-Beam deposition, lift-off, DNA nanoparticle conjugate, SAM's layer, Au nanoparticle placement, wet/dry etching and formation of SiO_2 nanopillars as the application.

Chapter 4, this section talks about the experimental results within changing different parameters and methods to achieve substrate surface clean conditions, and the total nanoscale control of Au nanoparticle placement via PB ion concentration, pH value, type of Au nanoparticle(Size), and pattern circle diameter.

Chapter 5, depends on all the results and discussions there is a thesis summary present in this chapter, and also some future development with prospects.

CHAPTER 2 BACKGROUND

The topic of this thesis is to show a new approach and a discovery of how to fabricate ordered arrays of Au nanoparticles on patterned substrates with the precise position and specific elements. In this background section, there is couples brief description of various techniques and applications that how this type of nanostructure can be used in different ways, followed by some basic understanding of the experimental procedure and fabrication steps.

2.1 Arrays of Nano-Scale Particles

The development of nanoscale electronic and photonic devices[10] will require a combination of the high throughput of lithographic patterning[11,12] and the high resolution and chemical precision afforded by self-assembly[13,14]. For most of the potential applications in nanotechnology relays on virtually defect-free arrays of nano-scale particles over large areas[15]. The incorporation of nanomaterials with dimensions of less than 10 nm into functional devices has been hindered by the disparity between their size and the 100 nm feature sizes that can be routinely generated by lithography[16]. Recent years guided self-assembly of colloidal particles on patterned templates has been shown to produce ordered arrays of colloidal particles[17], but the particle size still holds the critical limitation of this technique. A well-developed robust process of using nanoparticle measuring much less than 50nm in size can result in defect-free, large-area arrays[18].

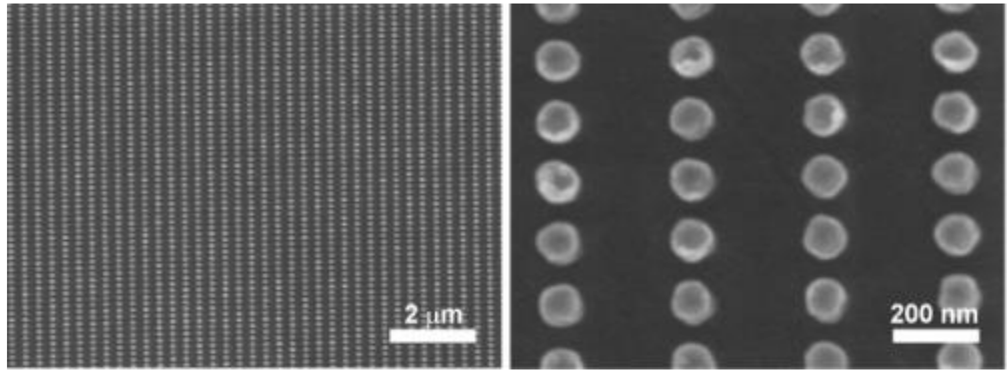

Fig 1 Scanning electron micrographs of an array of gold nanoparticle chains on a glass substrate[19]

In a recent study, researchers from the University of Bath and Northwestern University find out using the gold nanoparticle array to develop a new type of sensor platform. Claim to be 100 times more sensitive than the current sensors. There are many significant figures of merit, surface lattice resonances in the metal nanoparticle arrays, and vast potential for biomolecular and chemical sensing in either gas or liquid media. They put gold disk-shaped nanoparticle on a glass slide, then shone an infra-red laser at a precise arrangement of the nanoparticles, which are going to emit an unusual amount of ultraviolet light. So, this feature gives the underlying mechanism of how the sensor can work, if a molecular bond to the gold nanoparticle array surface, there is an effectiveness to the electrons at the gold surface resulting from the change of the amount of ultraviolet light they emit. In other words, the amount of ultraviolet light emitted can be used to determine the molecular type because every different molecular has significant ultraviolet emission. This technique could enable ultra-sensitive detection for super low

concentration and small volumes of biological markers for early-stage diagnostic screening for rare diseases[20].

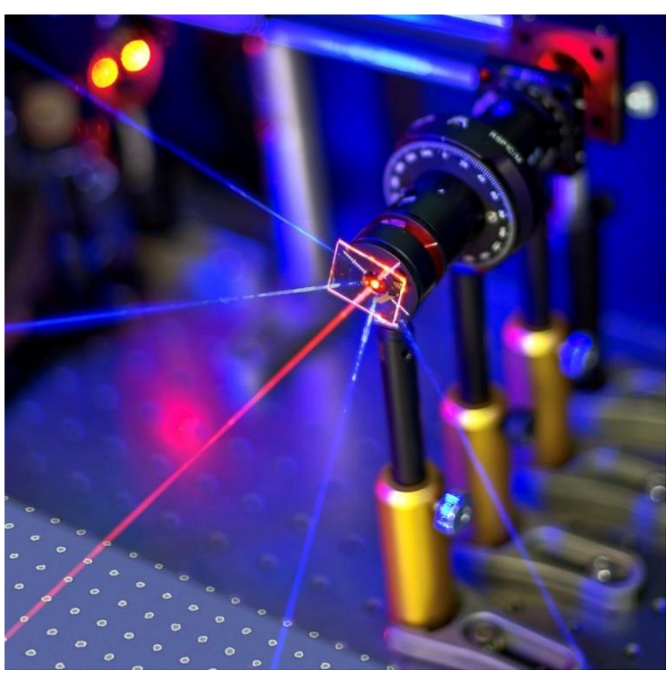

Fig 2 Shone an infra-red laser at a precise arrangement causes the sensor to emit UV light (in blue)[20]

Magnetic nanoparticles are a different kind of nanoparticles beside the gold nanoparticles. This type of particle arrays represents an essential class of artificial nanostructure materials. With the size of few nanometers to 20 nanometers in their diameter, the magnetic properties can change drastically. A typical example is FePt nanoparticles, which has a high magnetocrystalline anisotropy allows the use of small, thermally stable magnetic grains. Moreover, it also has better chemical stability compared with other hard magnetic materials. In addition, the possession

of its well-defined boundaries and tiny size are quite suitable to reach ultra-high storage densities with reduced noise[21].

2.2 Applications and Fabrication of Nanostructure

Silicon can exhibit unique properties if it reaches a 1D shape, the behavior of Si nanopillars as quasi 1D[22]. Which means the band gap will increase for the smaller diameter. Because of this quasi 1D behavior[23], silicon nanopillar can be modified in electron devices in different ways. Like field effect device, with the nanopillar wrapped around by the gate electrode (Fig 1), the active region of the device can have the optimum gate coupling, in other words the device's top scaling

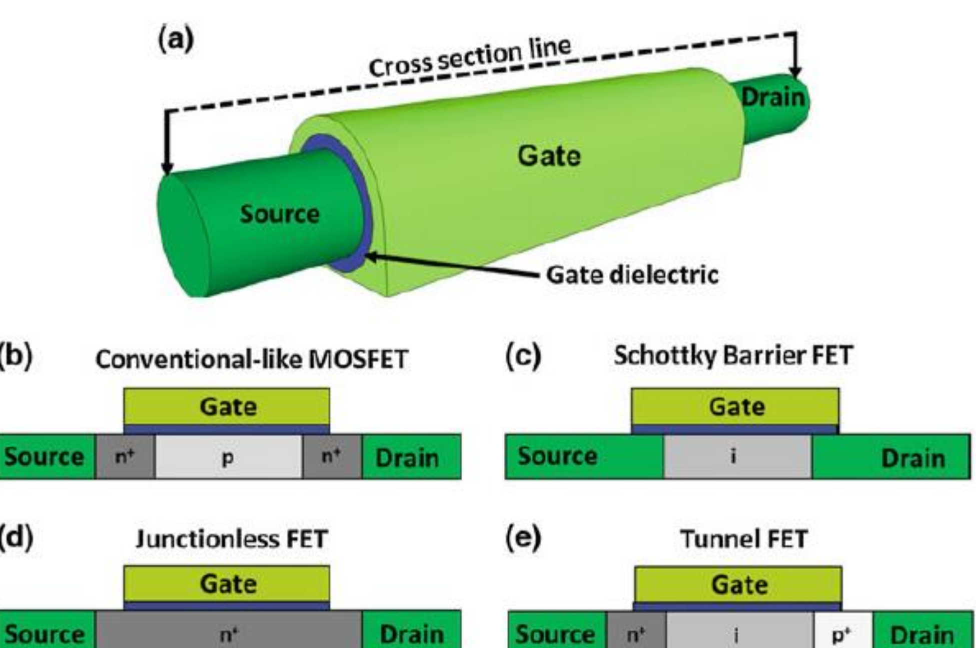

Fig 3 Different options for electron devices using silicon nanowires. The top drawing a show a general 3-D view of a silicon nanowire device with metallic source/drain regions and the surrounding gate. The cross sections b–e illustrates different device concepts: b Conventional nanowire MOSFET, c Schottky Barrier FET, d Junctionless FET and e Tunnel FET[22]

behavior may be achieved[24], because the super thin silicon thickness would be good enough to make the full depletion with a low voltage.

Another classical approach within memories of the semiconductor, specifically NADA Flash know as floating-gate transistors[25]. Because the underlying physical reason, the top oxide, and tunnel oxide cannot be control separately, this is why nanopillar structure and a low extent tri-gate can give a unique choice to solve the problem[26]. Due to the geometry of the nanopillar, it will automatically generate a higher field at the bottom oxide while the diameter of the nanopillar can take over the extension of the field increase (Fig 3).

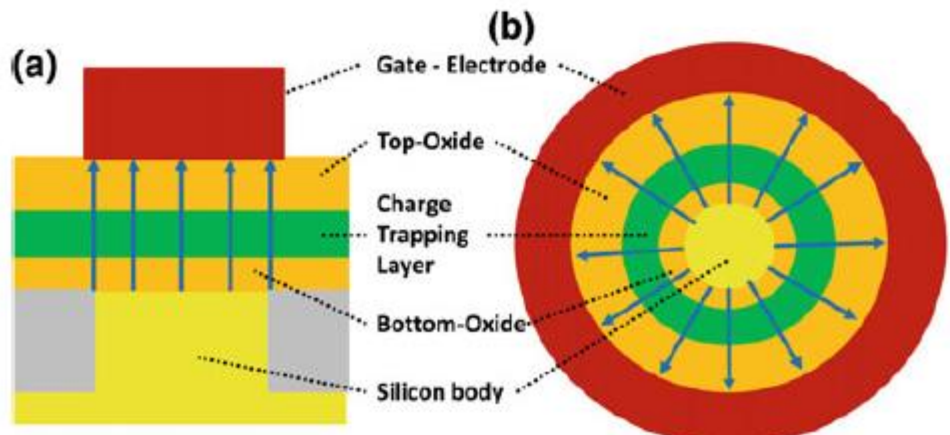

Fig 4 Schematic cut in the width direction of a planar (a) and a nanowire-based (b) charge trapping memory cell. The arrows indicate the field lines in the device in programming or erase operation. In the nanowire device, the field lines are denser in the bottom oxide. Therefore the exchange of carriers between the charge trapping layer and the silicon transistor body is enhanced, and the charge exchange between the charge trapping layer and the gate electrode is reduced[22]

In 1964, Wagner and Ellis published a paper that first described a prominent nanopillar synthesis method, vapor liquid solid (VLS) and introduced the growth mechanism happens by the material phase changes which are mediated through a catalyst particle[27]. In the case Si being evaporated, the Si gas (SiH_4, $SiHCL_3$) can be collector by the catalyst particles which gold is used in most situations. The first stage Au nanoparticles placement on the substrate can be done either by the coalescence of the gold thin film or by dispersion of synthesized Au particles. For a quite long time, there is a limitation of critical diameter for growth due to the thermodynamic consideration[28], until 1998 Morales and Lieber proved that diameter below 20nm could be achieved[29]. As explained above, in general, this type of fabrication method named bottom-up techniques.

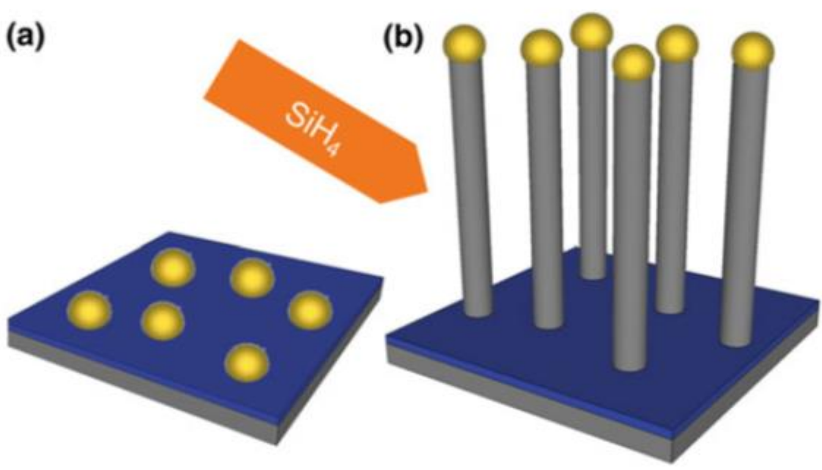

Fig 5 Schematic view of VLS growth of silicon nanowires. A Gold particle formed on the growth substrate. b VLS growth using silane as silicon precursor[22]

Another reversed way to produce nanopillar is called top-down techniques. Other researchers have been using methods like nanosphere lithography (NSL) to fabricate nanopillars; it is an economical technique to generate a single layer of nanoscale features. The nanosphere was created by apply planar ordered arrays of nanometer-sized polystyrene nanobeads as lithography mask. The next step is to conduct conventional reactive ion etching[30,31]. With this process nanopillars and nanopillar structure liked shape can be achieved (columnar and spike). Not only but also to generate high aspect ratio Si nanopillars, which involves high-density plasma in ion etching. The size of the polystyrene nanospheres can control the size of nanopillars. Also, oxygen plasma can tailor the nanosphere diameter. More of that their packing density affects the flow rate of the reactive ion etchants; all these parameters can be controlled to result from the different shape of nanopillars.

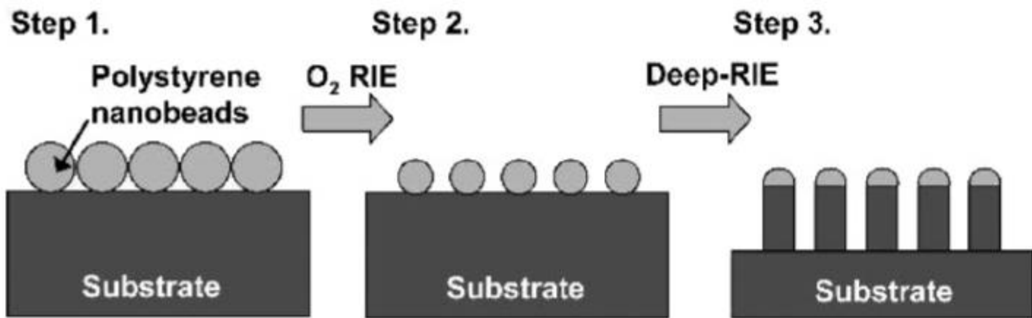

Fig 6 Schematic diagram of nanopillar fabrication by nanosphere lithography. Step 1: spin coat a hexagonally close-packed monolayer of polystyrene beads on substrates. Step 2: tailor the size of the beads' "resist" by oxygen plasma etching. Step 3: etch the exposed semiconductor areas by deep reactive ion etching using the "Bosch" process[22]

2.3 Zeta Potential

Zeta Potential is the magnitude of the repulsion force or attraction force between particles when solid particles immersed in an aqueous colloidal solution[32,33]. Au nanoparticle acts as a hard mask to help the etching process, so zeta potential taking a specific insight into the mechanism of the dispersion. The concept deals with the electrostatic interaction between the gold surface, SiO_2 surface, and gold nanoparticles also can use to assess the stability of the colloidal system.

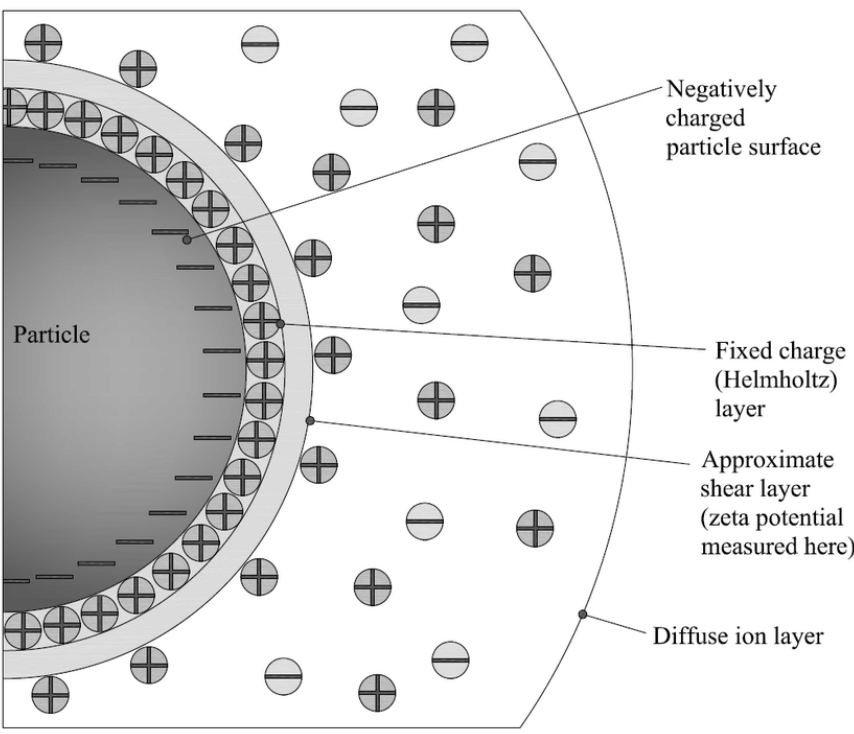

Fig 7 Schematic representation of ionic charges around a charged particle in an aqueous media[34]

The net charge can control the distribution of ions covered surrounding the interfacial area at the particle surface. There is an increased concentration of differently charged ions that not far away from the particle surface; this forms an electrical double layer around each particle. From the above figure, the double layer exists as two parts, the inner region which called stern layer in this layer ions are firmly bonded with each other[35], then an outer region named diffused layer which all the ions are less tightly associated. There is a notional boundary within this diffused layer know as slipping plane (shear plan), the zeta potential is the potential right at this boundary[36,37].

Zeta potential indicates inherent stability; in other words, a dispersion stability state refers to all the particles in this colloidal system have a significant positive (or negative) zeta potential, so they repel each other. Otherwise, the system can show the dispersion instability means all the particles have low zeta potential and nearly no force to prevent them from coming to each other. It is the same when applying to the substrate surface[38].

2.4 Debye Length

Debye length is an abstract concept, think about there is a positively charged plate and a material having negative mobile charges, they have some distance separate each other. Consider the charged plate and the material are insulated, no currents can flow between them. However, the electrical field will be generated,

with the field line start from the positive charged plate and end at the negative charges inside the material. As show the below.

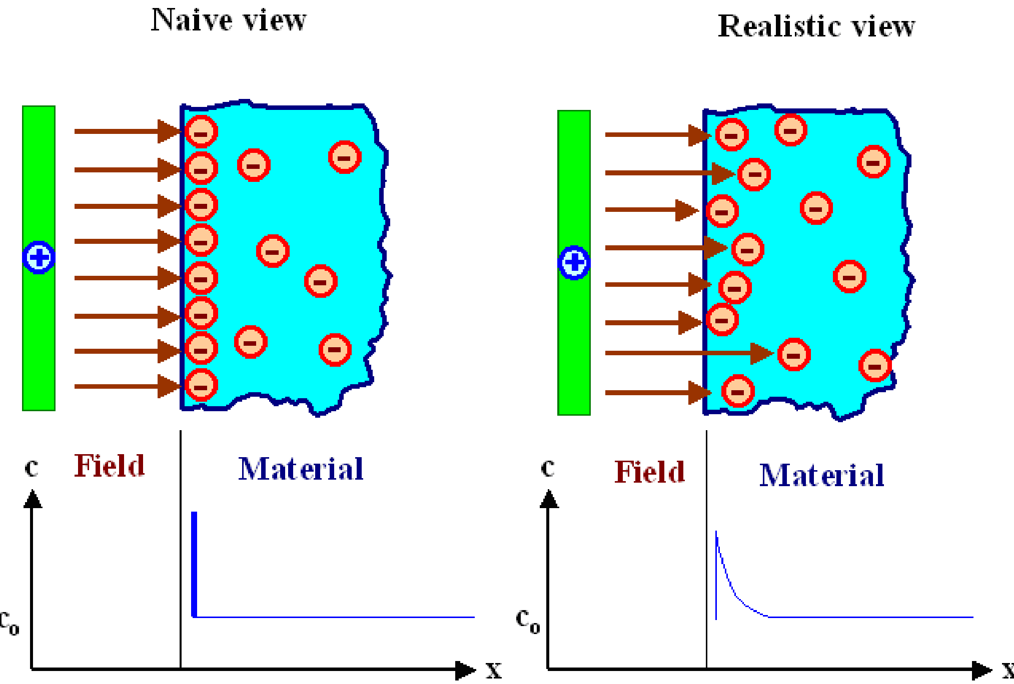

Fig 8 Naïve view and realistic view and carrier concentration[40]

The naïve view shows that every field line which starting from the positively charged plate ends on the negatively charged carrier inside the material perfectly. Because the negatively enough charged carriers in material move t to the surface then screen the field thoroughly, in other words, it prevents the penetration of the material, which the concentration of carriers at the surface would be a function with a super steep slope. In a realistic view, this is more physically sensible by the concentration level that varies smoothly within some distance; we called this distance as Debye Length[39]. The thesis carried out gold nanoparticle placement, which involves a phosphate buffer solution to adjust the Debye length[40].

2.5 Lithography Technique

The word ‘lithos’ comes from Greek, means stone, and ‘graphia’ means to write. So, the direct translation would be writing on stones. In here the lithography is a fabrication technique for integrated circuit requires a variety of chemical and physical process conduct on the silicon wafer, or we can say semiconductors. Three significant steps in lithography are film deposition, patterning, and semiconductor doping. Films of conductors and insulators are customarily used to connect or isolate transistors and side components. Regions of silicon doping can manipulate the conductivity of the silicon result in a change of voltage for a specific application. For most of our complex circuitry microelectronic devices, the fundamental of all process is lithography[41].

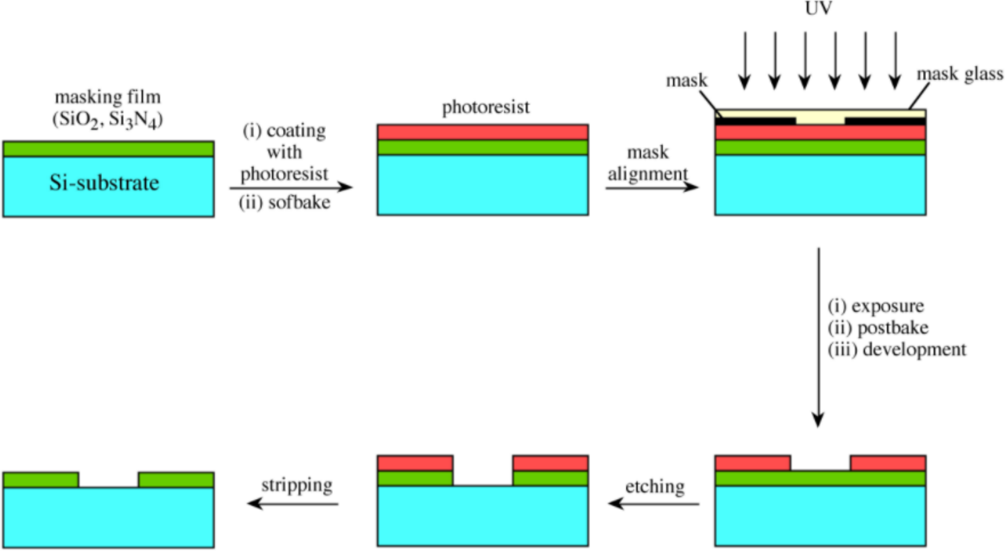

Fig 9 A typical sequence of lithographic processing steps [30]

In the case of the semiconductor industry, optical lithography is a quite common choice for building complex structures by which a light-sensitive polymer, called photoresist. Generally, a photoresist coverage can be done by spin coating, then use light to transfer a geometric pattern (hard photomask) to the light-sensitive photoresist, here is the UV light. With the exposed silicon wafer followed by a development process to remove useless photoresist and left the pillar-shaped PR on the substrate surface. In the later etching step, these remaining photoresists turn to a cover which protects the underneath substrate which can create a hard material pattern on the surface from deposition. The model can be defined by the different type of photoresist (positive or negative)[41].

2.6 E-Beam Lithography

Let us look back from the past 20 years to present, the components and parts in our modern production are becoming smaller and smaller. Such as the cellphone we use every day; the innovation of fabrication technology made a phone not just a phone. The theme under the spotlight is miniaturization, especially in the electronics industry the feature size of semiconductor devices is shrinking every year. Electron-Beam lithography could be a solution to the best quality, plus a reasonable writing speed and a possibly high level of integration of complex devices[42].

Instead of use UV light to expose the photoresist coated on the substrate surface, the electron beam can fabricate patterns having nanometer feature size. With two different types of exposures, projection printing, and direct writing.

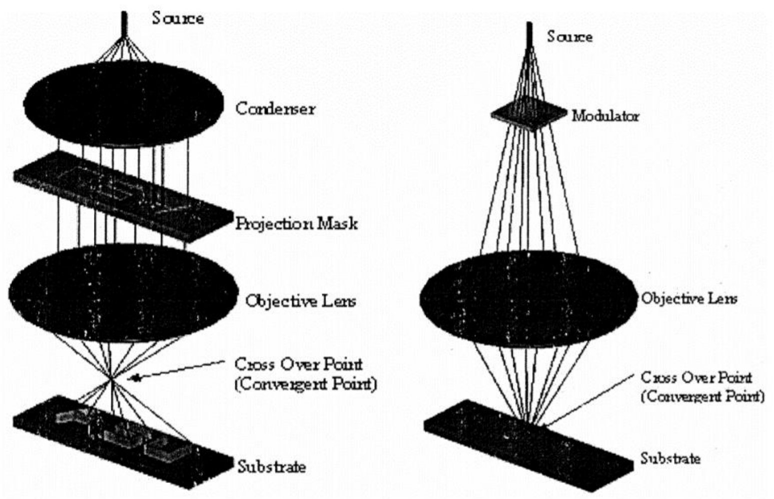

Fig 10 schematic view of projection printing and direct writing[42]

Projection printing requires a mask with patterns already on it; a relativity large sized electron beam is parallel projected through the mask on the substrate coated with photoresist and controlled by a high precision lens system. For direct writing, it is even simple that a tiny point of electron beam hit directly on the photoresist coated substrate, the pattern directory is programmed ahead in the computer which can be sent the order to move the substrate stage to move. The 10-50 Kev electrons give a significant tiny wavelength adjust by the energy density in order to write precise features in the nanometer scale. In this thesis, the direct writing method is used to get rid of the use of mask and time consuming[43].

2.7 Photoresist

Characteristics of **positive** photoresists	Characteristics of **negative** photoresists
1. Excellent resolution 2. Stable against developers 3. Can be developed in aqueous developers 4. Bad resistance in etching or implantation processes 5. Bad adhesion on the wafer	1. High sensitiveness 2. Fair adhesion 3. Excellent resistance against etching or implantation processes 4. Cheaper than positive resists 5. Lower resolution 6. Organic developers are needed (toxic)

Table 1 Characteristics of positive and negative photoresists

The photoresist is another critical point in the process of lithography. It is usually an organic polymer which super light sensitive, the chemical structure will change if expose it under ultraviolet light (UV). Resist can be coated on the substrate surface, then a hard mask with patterns applied to above the substrate surface, so the patterns block light to go through. Meanwhile, the unpatterned area of the resist will be exposed to light. According to the different type of photoresist, the exposed result can differ. This result will show after the development step, which the exposed wafer is developed in dipping solvent bath. For the positive resist case, the area exposes to the light becomes more soluble in the developer. Means the exposed resist then be washed away by the developer solution, leave windows of the bare underlying material, in other words, a copy of the exact pattern of the hard mask remains on the wafer. It is the other way around for the negative

resist, the part being exposed turn to crosslinked or polymerized, and even more difficult to

dissolve in the developer. Then the negative resist can remain on the surface of the substrate, and the developer solution only removes the unexposed region[44].

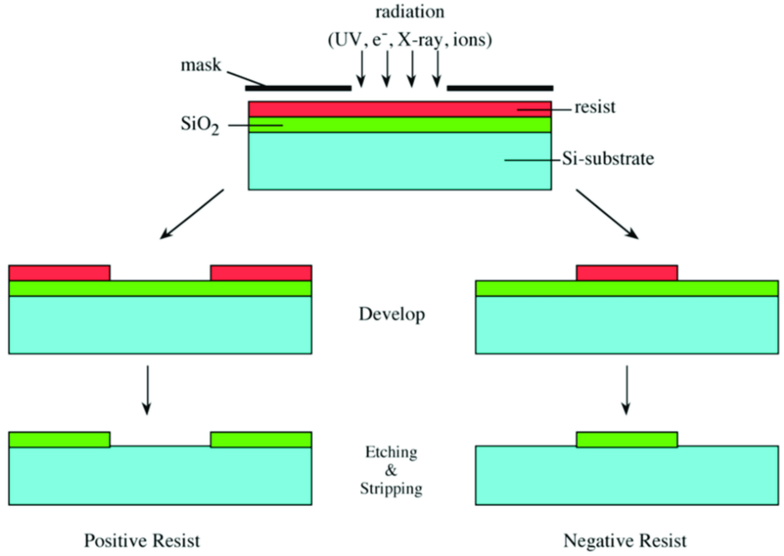

Fig 11 Differences of positive photoresist and negative photoresist after expose under light[45]

2.8 Self-Assembled Monolayers

For the metal and metal oxide, their bare surface tends to adsorb adventitious materials (organic) effortlessly due to these adsorbates. They can decrease the free energy of the interface between the metal (or metal oxide) and the ambient environment. More than that, adsorbates also can alter the properties of interfacial, give significant impact to the metal and metal oxide's nanostructure stability. Therefore, the self-assembled organic material on the surface can act as a barrier against agglomeration, because of their physical or electrical features. Even

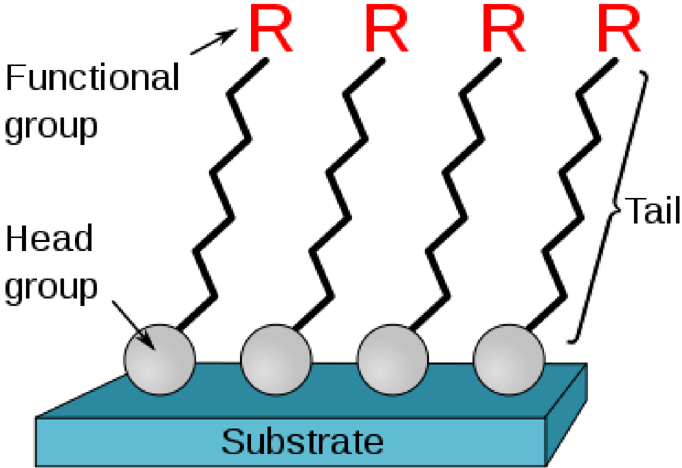

Fig 12 schematic view of Self-Assembled Monolayer[47]

lower the reactivity of the atoms on the surface or play the role of an electrically insulating layer[46]. This one molecule thick film of material is a self-assembled monolayer; we usually call it SAM's layer. The formation processes are usually taking place by the adsorption of molecular constituents from gas or solution phase on to the surface of solids or in the ordered ranging on the surface of the liquid. All the adsorbates can spontaneously organize into a crystalline structure; there is no specialized tools or extreme environment require. The molecules that form SAM's layer have a chemical functionality know as a headgroup, which states a specific affinity for a substrate, in some cases, it even has a significant high affinity for the surface and displaces adsorbed adventitious organic materials. Once the deposition occurs, a chemical bond forms with the surface are rendering a permanent modification of the substrate. On the other side of the headgroup, a functional group is attached; the specific application can modify this function group. For example,

carboxyl and amine terminated functional groups can be used to form negative and positive surface charge layer on the silicon oxide and gold substrate[48].

2.9 3-aminopropyltriethoxysilane (APTES) SAM's layer

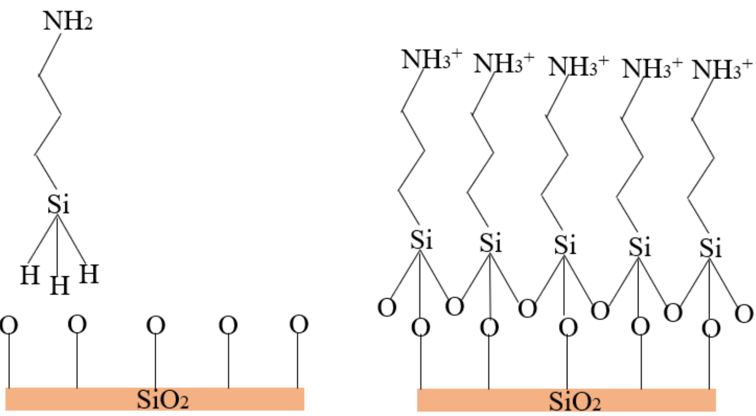

Fig 13 Surface modification of SiO_2 with APTES

In this thesis, there is two different SAM's layer will be introduced. This first amine terminated function group, APTES is a popular choice of the coupling agent. It allows for later attachment of molecules via its terminal amines and exhibits self-assembly. Here we use APTES on the silicon dioxide surface to form the layer, the hydroxylation of silicon dioxide takes the first place, then subsequent hydrolysis of APTES ethoxy group while the ethanol dislocated from the molecule[49]. With this configuration, the aminopropyl-terminated groups are pointing toward the liquid or gas phase, but away from the solid substrate, leave the amine groups available for later functionalization. The confirmation and density of this monolayer can be profoundly affected by the solvent used during the formation; in this study, we use APTES to attract functionalized gold nanoparticles via the

positive charged aminopropyl-terminated group to the negative charged DNA covered gold nanoparticles[50].

2.10 16-mercapthohexadeconic acid (MHA) SAM's layer

The second SAM's layer is 16-mercapthohexadeconic acid (MHA). It is a quite well know the method for the formation of SAM's layer on the gold surface since the MHA has the sulfur-containing alkanethiols group. Deposition of the gold layer on the substrate gives the inert behavior for chemisorption of most polar organic function groups[51]. The research found the disulfide alkanethiol can have a stable formation of chemisorption bond. So, the gold layer can be negatively charged due to MHA's -COO^- terminated group. With the APTES gives positively charged surface by the -$NH3^+$ terminated group, these negatively and positively charged SAM's layer form an electrostatic guiding structure which can guild the negatively charged Au nanoparticle to the expected location. Theoretically the -COO^- terminated group here is for pushing away nanoparticles and without any attachment.

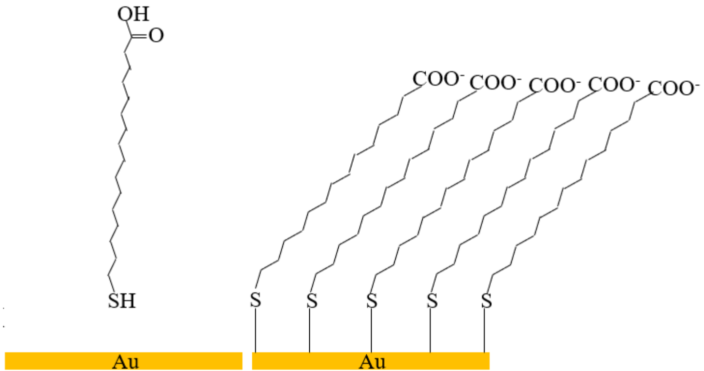

Fig 14 Surface modification of Au with MHA

2.11 Negatively charged DNA strands

We know DNA is a large molecule which made up of nucleotides, and every nucleotide contains a nucleobase [Adenine (A), Thymine (T), Cytosine (C), or Guanine (G)], a sugar group, and a phosphate group. The bonds connected between nucleotides are covalent bonds, but every two polynucleotides from nucleobase are connected via hydrogen bond in a specific order which adenine dependably combined with thymine, and cytosine dependably matches with guanine (A-T, C-G). Overall, DNA is helical in structure bonded through hydrogen bonds. To be able to get single-stranded DNA requires increasing in temperature and decreasing the salt[52].

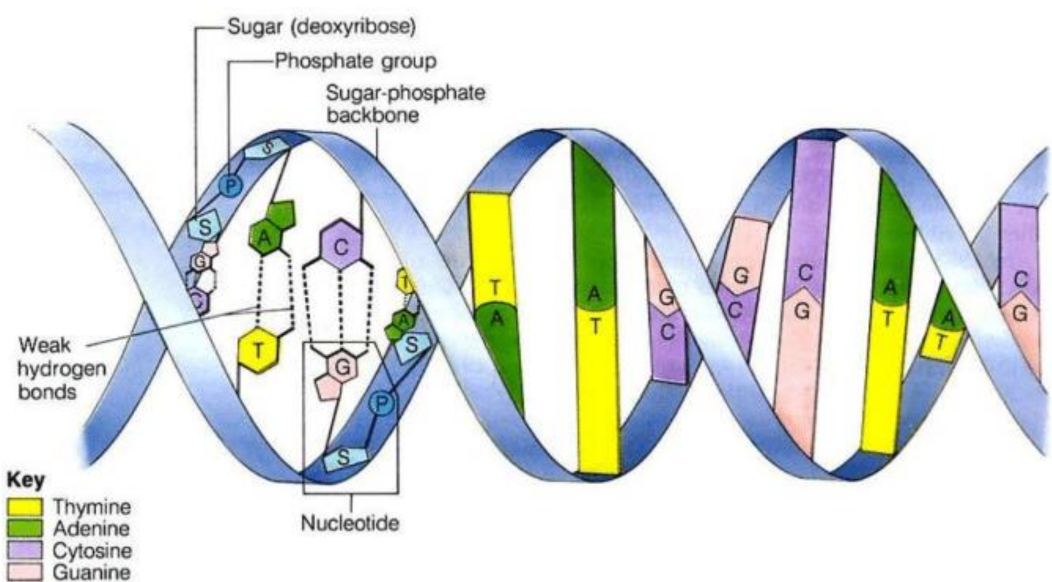

Fig 15 DNA structure[52]

The reason why DNA negatively charged is that the phosphate group carry negatively charged oxygen by releasing hydrogen ions[53]. In this thesis,

electrophoretic isolation of discrete gold nanoparticle/DNA conjugates was used. The nanoparticle surface charge was regulated by the number of DNA strands that attached to the nanoparticle; the increasing of the DNA strands increases the overall surface negative charge of the conjugates[54].

2.12 Influence of DNA coverage

The recent study shows that salt concentration and spacer composition is the variables that affect DNA coverage on the nanoparticle. The thickness of the oligonucleotides progresses with NaCl concentration which is principally attributed to the screening impact of counter ions reduced the repulsive force between DNA strands and resulted in more strands can be attached[55]. The maximum screening is achieved at a salt concentration around 0.7M, and DNA loading keeps relatively constant. For the spacer composition, A_{10}, T_{10}, or PEG spacer was used. Because of the negative charge of DNA, spacer regions formed nucleotide bases express inter-strand repulsion, and DNA loading was restricted. As a result, the adenine (A_{10}) are easy likely to lie on the nanoparticle surface than thymine (T_{10}) due to the considerable relative affinity; The PEG gives the best packing densities by instance formation of SAM's layer lack of the intermolecular repulsions and interactions between PEG and nanoparticle surface[56].

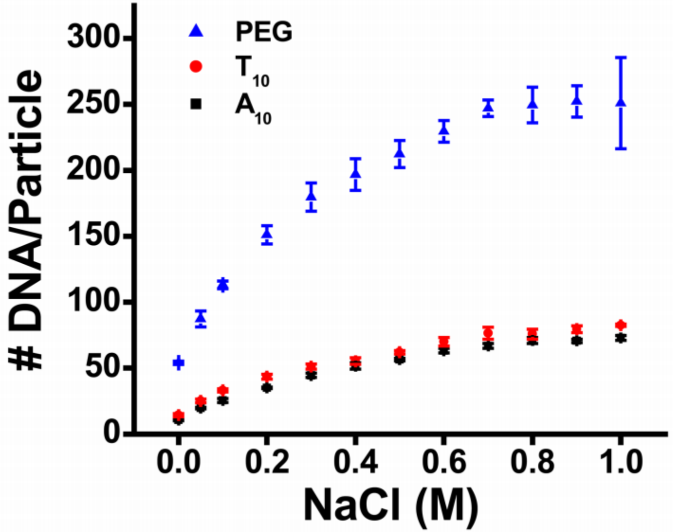

Fig 16 DNA loading (# DNA strands/nanoparticle) vs. NaCl concentration for A10, T10, and PEG spacers on 15 nm gold nanoparticles[56]

2.13 Electrostatic Funneling

This is a critical point of the entire study, to precisely place a single gold nanoparticle onto the desired substrate location we developed a new method which can be processed on a large scale with nanoscale accuracy. Charged nanoparticles can be guided in a colloid through their electrostatic potential energy gradient, then place them onto a specific spot in a self-limiting way. Fig 15 shows the schematic view. The substrate surface is functionalized with positively and negatively charged SAM's layer; this builds an electrostatic guiding structure. So, the single negative charged nanoparticle will be guided and placed at the target area, which is inside the circle. The region outside the circle is gold surface attached with MHA SAM's layer express negative charge, and inside the circle is SiO_2 surface coated with

APTES Sam's layer express positive charge. Once a nanoparticle occupies the circle, it prohibits an approach of other nanoparticles[57].

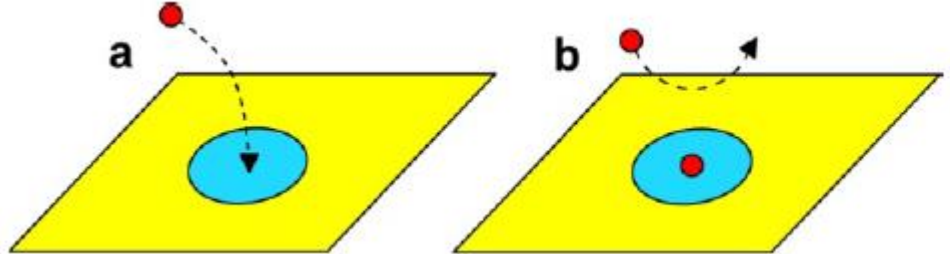

Fig 17 **a**. A nanoparticle in a colloid is electrostatically guided onto a circle center. **b**. Once a nanoparticle occupies a circle, the approach of other nanoparticles is prohibited. Inside the circle: positively charged; outside the circle: negatively charged; and nanoparticle: negatively charged[57]

2.14 Thermal Oxidation

An accessible overview of thermal oxidation in this thesis is trying to grow a silicon dioxide layer on the standard silicon wafer. Not like bear Silicon substrate, the stable silicon dioxide layer is a better interface mainly used for isolation in semiconductor devices. Although the PCVD of oxide is a possible way, the quality of deposited oxide is under the thermally grown oxide. Since it is a quite refined process, the oxide can be finely controlled with a specific application[58]. The silicon dioxide layer grows by the thermal oxidation has excellent electrical properties and oxide density which means it is packed surface. Thermal oxidation of silicon is considered as a chemical process, the first oxidant from the ambient reach the oxide-ambient interface, they will be starting to penetrate the surface then begin to diffuse through the existing oxide once they get enough energy and stop when they arrive the oxide-silicon interface. Second, they start interacting with the surface

silicon atoms which produce the SiO2 as the chemical reaction. Last because of the combination of oxidant and silicon atoms, the newly formed molecule has a new crystalline arrangement, a volume expansion happened and increase the surface height. All the processes are conducted in an oxidation furnace. This very first step played an essential role in the development of silicon integrated circuit technology[59].

2.15 Wet Etching

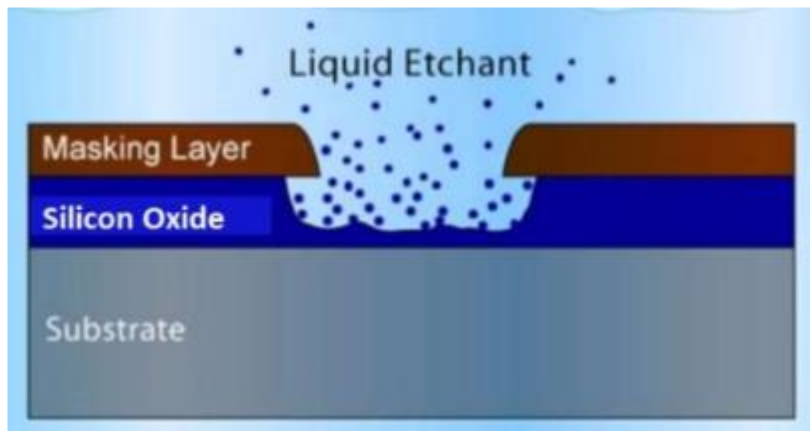

Fig 18 Simple Ideal of Wet Etching[60]

As the name of this section, it is a material removal process which relies on specific etchants or liquid chemicals to remove materials from the substrate. The desired pattern can be defined by a mask placed on top of the substrate. It is just like the lithography; the mask does not protect those materials will be etched away with the liquid chemicals. In this thesis, we are not using any mask as the protector but a photoresist to cover up our desire area instead. Because of the wet etching can be considered as a chemical reaction, there are a couple of steps usually involved. (a) The liquid etchant diffuses onto the unprotected area. (b) The reaction happens;

materials start to be etched away. Generally, this is a redox reaction, and it entails the oxidation of the material then dissolving the oxidized material. (c) At the reacted surface, byproducts diffusion started. A specific case in our research is used gold etchant and chrome etchant to get rid of the 15nm Au layer and 5nm Cr layer without harming the gold nanoparticles inside the pattern circle[61].

2.16 Dry Etching

In semiconductor manufacturing, dry etching is one of the most frequently used processes. As we discussed the wet etching above, it is inadequate for feature size control especially the small-scale features. Therefore, the dry etching method gives better process option. In dry etching instead of using chemical etchant, a plasma or etchant gasses help remove the substrate material[62]. The process can be done by utilizing the high kinetic energy of chemical reaction, particle beams or both together. Understand the dry etching needs some knowledge of plasma, an "ionized gas" which contains pretty much same number of ions and electrons. So, it is considered as an electrically neutral state, in other words, the ion density and electron density are substantially equal, and they can be referred to as the plasma density.

The dry etching typically conducted in an etching chamber; with the applied radiofrequency power an electric field is generated. Electrons now getting accelerated vis this electric field and gaining kinetic energy, then starting to collide

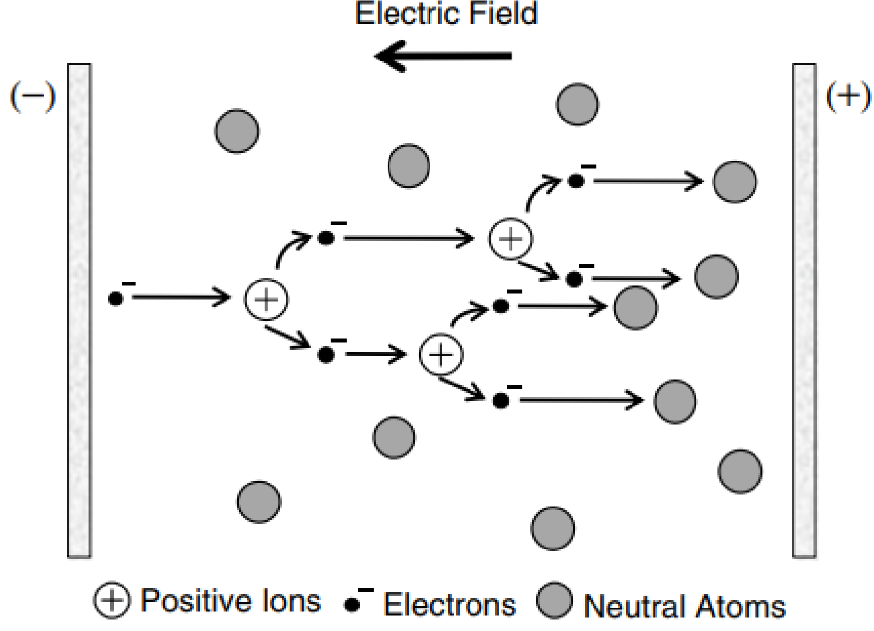

Fig 19 Ion generation by the collision of electrons and neutral atoms[63]

with molecules and atoms. Once the acquired kinetic energy of an electron exceeds the ionization voltage, the outermost shell electron of the atom is expelled. Because of the loss of the electron, the neutral state atom now becomes an ion. The new expelled electron and the colliding electron then getting accelerate under the same electric field to collide with other neutral atoms to create more electrons and ions. The number of electrons and ions will eventually pass a threshold level, resulting in the form a plasma. Dry etching also processed in couple steps, (a) Reactive species are created in the plasma; (b) Transportation and adsorption of species at the etch target film; (c) At the etch target film surface reaction being started, meanwhile etch byproducts are produced, and (d) Etch byproducts leave from the

surface of the etch target film[54]. Fig below shows the Reaction steps of dry etching for the case of Si etching with CF4.

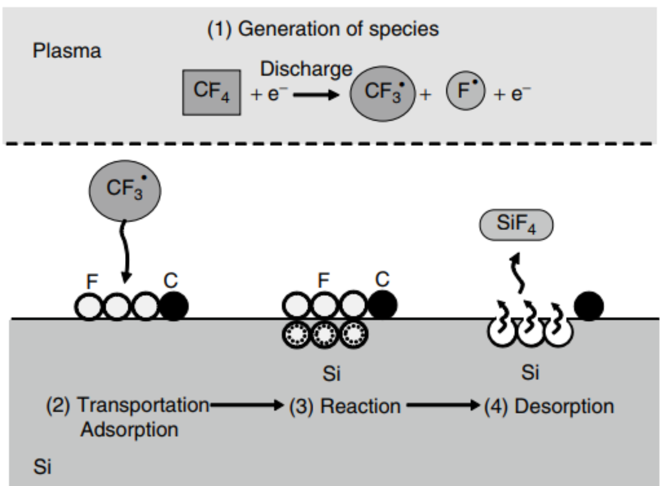

Fig 20 Reaction steps of dry etching[54]

2.17 Plasma-Therm Reactive Ion Etching

As we discussed in previous wet etching section since after the gold nanoparticles were successfully placed on the exact location, we need to process wet etching to remove the Cr and Ag surface. However, also, we have to find out a way to protect the Au nanoparticle not being removed from the wet etching. So, another layer of photoresist will be spin coated on the substrate surface to cover up the gold nanoparticle which inside the pattern circle, then introduce the plasma therm reactive ion etching which can ash the photoresist above the gold surface. This is a highly controllable process that can etch quite precise thickness in order to not harm the PR inside the pattern circle protecting the Au nanoparticle but remove another PR that covered just above the surface[65]. One significant advantage

to RIE over other forms of etching is that the process can be designed to be highly anisotropic, allowing for much more exceptional resolution and higher aspect ratios.

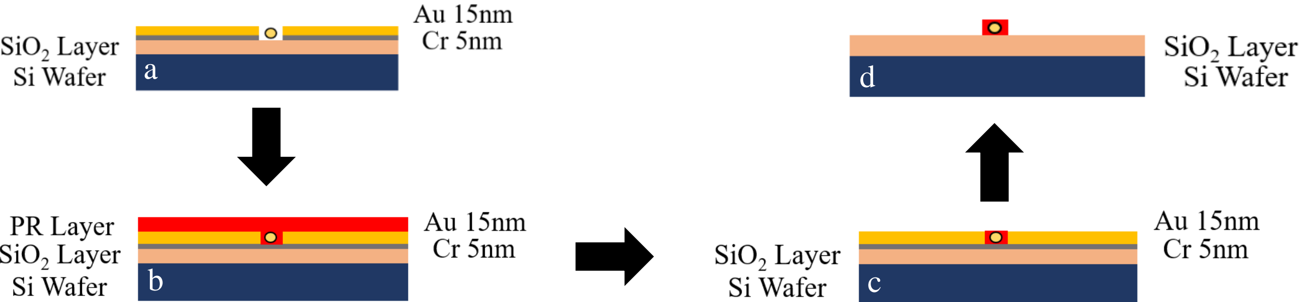

Fig 21 **(a)** Au particle placement done, **(b)** PR coat on surface, **(c)** RIE to remove the PR above the surface, **(d)** wet etching to remove the Cr and Au layer but with PR protected Au particle will remain

CHAPTER 3 EXPERIMENTAL PROCEDURE

3.1 Overall View of Experiment

To be able to fabricate the nanopillar shaped SiO_2, everything starts with a bare Si wafer. The wafer needs to go through the clean surface process.

Prepares piranha solution (H_2SO_4:H_2O_2=3:1) to clean the organic compound on the substrate surface, follow by acetone sonication. Load the wafer into the thermal furnace overnight to form a thin SiO_2 layer around 280nm. Cut substrate to small rectangle pieces, spin-coated with negative photoresist followed by e-beam expose with designed patterns. Develop sample with ma-D525 to remove the unexposed photoresist, then e-beam deposit 5nm of Cr and 15nm of gold on the substrate surface followed by lift-off via acetone sonication. Surface clean carried out with IPA sonication to make sure to remove the scum of negative photoresist. (Previous HF, NH_4F, H_2O_2, sputtering, UV Ozone, and acetone sonication confirm not useful) Stored in the ethanol.

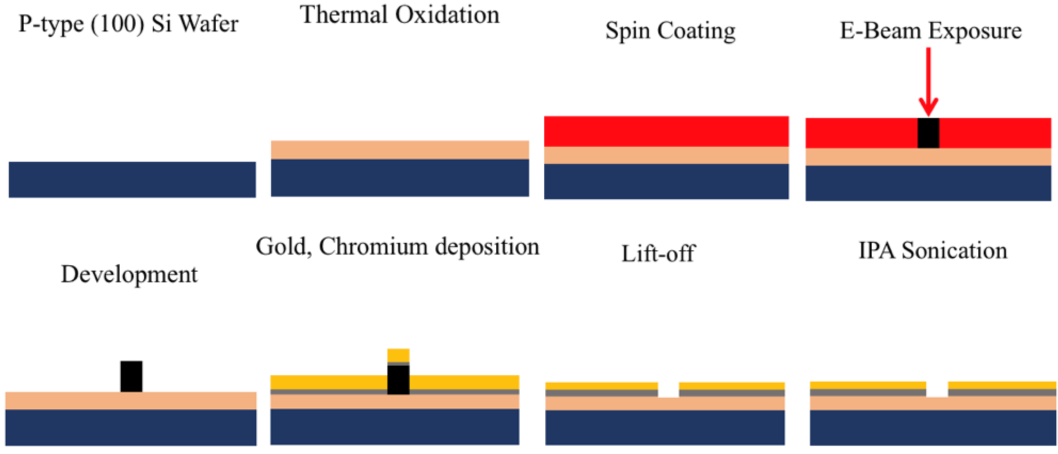

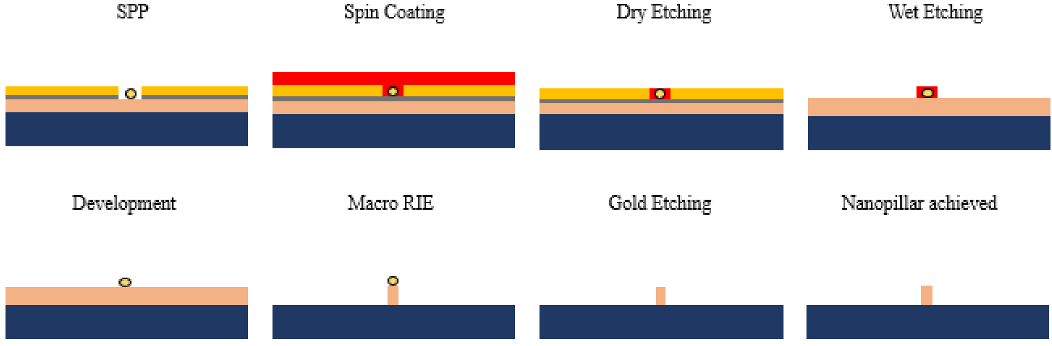

Fig 22 Schematic representation of experiment Overview

3.2 Clean Room Technical Machines

- Tystar, Oxidation Furnace
- Ocean optics reflectometer
- Gaertner stokes ellipsometer
- Branson 2501, Ultra-Sonication Bath
- Disco DAD3220 Automatic Dicing Saw
- Cole-Parmer HP30A Photolithography Hot Plate
- Headway, Spin Coater
- ZEISS Supra 55 VP Scanning Electron Microscope
- ZEISS 1540XB Cross Beam E-Beam Writer
- AJA International, E-beam evaporator
- CHA Solution E-Beam-Evaporator
- Millipore DI water purification system

- Teaching Fab, Weighing Scale
- Plasma-Therm, Plasma Etcher
- Macro RIE
- Eppendorf 5418, Centrifuge
- Vortexes

3.3 Reagent Materials

- P-Type (100) Si wafer, Nova Electronic Materials
- Sulfuric acid solution
- Hydrogen peroxide solution
- DI water
- Liquid acetone
- Liquid methanol
- Liquid IPA
- Solid Cr
- Solid Ag
- ma-N 2401 negativity E-beam photoresist, Microchem
- ma-D 525 photoresist developer, Microchem
- Hydrogen fluoride solution
- Ammonium fluoride powder
- Synthetic oligonucleotide probe-DNA with disulfide linker, BioBasic

- DL-Dithiothreitol (DTT), Sigma-Aldrich
- 30nm Gold Nanospheres, Bare (Citrate), NanoComposix
- 50nm Gold Nanospheres, Bare (Citrate), NanoComposix
- NAP-5 filter column, GE Healthcare
- Sodium Chloride (>99.5%), Sigma-Aldrich
- Sodium Hydroxide, Sigma-Aldrich
- Tris-EDTA buffer solution, Sigma-Aldrich
- 3-Aminopropyltriethoxysilane (APTES), Sigma-Aldrich
- 16-Mercaptohexadecanoic acid, Sigma-Aldrich
- Sodium phosphate monobasic monohydrate, Sigma-Aldrich
- Sodium phosphate dibasic heptahydrate, Sigma-Aldrich
- Hydrochloric acid, Sigma-Aldrich
- Chrome etchant
- Gold etchant

3.4 Wafer Preparation

A 4 inches Si wafer will start with the clean process. The first step is piranha solution cleaning and followed with acetone sonication should be done before the thermal oxidation. Piranha solution was made by a mix of sulfuric acid and hydrogen peroxide (3:1) in an open glass beaker, suggested volume is 60ml of H_2SO_4, 20ml of H_2O_2, must wear appropriate protection.

- Immerse the wafer into the piranha solution for 30 minutes
- Transfer wafer to a DI water container for 5 minutes
- Wash it under running DI water,
- Dry with N_2
- Acetone sonication the wafer for 15 minutes
- Rinse with an acetone squeeze bottle
- N_2 dry

This step is to make sure the removal of organic compounds and a thin oxide layer on the wafer surface. Make sure the piranha solution being preparade freshly every time before use.

Fig 23 Cleaned Si Wafer

3.5 Thermal Oxidation

After a clean process wafer is ready to subject to the thermal oxidation furnace. This step is to form a thin SiO_2 layer on the bare Si surface, in the study we choose thermal oxidation method because it gives packed SiO_2 film and surface is uninformed.

The oxidation conditions of the furnace are listed below.

Dry Oxidation	H_2O: 0sccm, O_2: 3000sccm, N_2: 0sccm, Temperature: 1100C, Time: 300s
Wet Oxidation	H_2O: 5000sccm, O_2: 3000sccm, N_2: 0sccm, Temperature: 1100C, Time: 300s
Annealing	H_2O: 0sccm, O_2: 0sccm, N_2: 2000sccm, Temperature: 1100C, Time: 3600s

Table 2 Oxidation conditions of the furnace

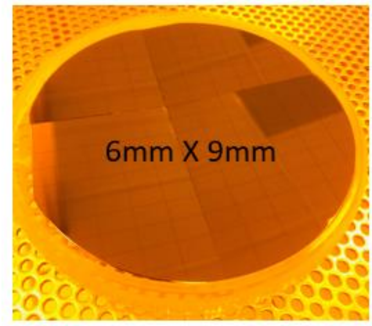

Fig 24 Diced 4 inches wafer

The above oxidation recipe can grow around 260-280nm thickness of SiO_2 layer, normally show dark red surface compare with the bare Si surface. Then the whole wafer will be diced into small pieces (6mm by 9mm) for experimental use.

3.6 Spin Coating

Every sample preparation batch we can normally process nine substrate chips as three chips parallel to each other for 1 row, and a total of three rows. The substrate was first

- Clean with acetone sonication for 10 minutes
- Rinse with acetone, methanol, and IPA
- Dry with N_2 gently
- A dehydration step, 200℃ for 20 minutes
- Place the substrate on the spin coater
- Drop photoresist on the substrate surface (slightly cover)
- Strat the spin coating with under conditions

  Step 1: 500 RPM, 100RPM/s, 5 seconds

Step 2: 3000RPM, 1000RPM/s, 30 seconds

- Transfer the substrate to the 90°C hotplates for 1 minute

The dehydration process is used to remove the moisture on the substrate surface in order to make good contact between photoresist and substrate. ma-N

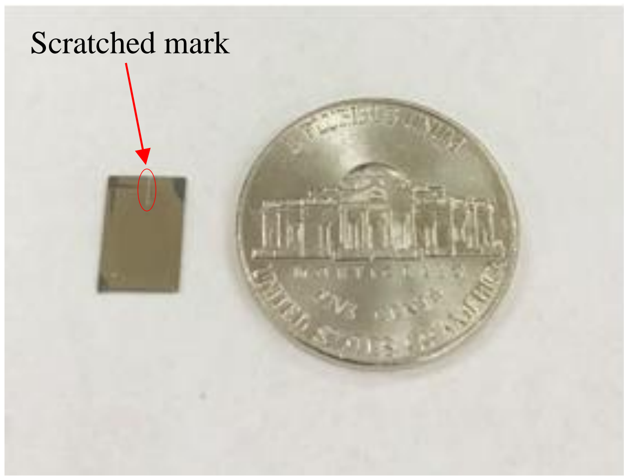

Fig 25 Actual Chip with mark on it

2401 negative e-beam photoresist was used in the spin coating. As the resist data index shows, this setup can result in a thin resist film on the surface about 100nm. Use a diamond pen to make a scratch on each chip after the 90°C bake out; the scratch is meant to be as a navigation mark which helps locate e-beam writing pattern area.

3.7 E-Beam Lithography

NPGS software work with e-beam writer to draw the pattern, specifically expose the surface photoresist to create the desired pictures. Because of the negative

photoresist, the parts being exposed will be hardening. The pattern file was previously designed in AutoCAD and loaded into the e-beam writer.

- Use AutoCAD software to design the pattern
- Save the pattern file as AutoCAD 2004 format (.dxf)
- Copy the file to a flash drive
- Copy the file from flash drive to the right-side PC in e-beam room
- Set the directory as C:/NPGS/Projects/Pradeep
- Choose the correct folder (C:/NPGS/Projects/Pradeep) in "Current Project Directory" in NPGS main window
- Choose "Design CAD Files" in Display File Types on NPGS main window
- Select any run files (. dc2) right click to choose "Design CAD LT"
- In "Design CAD LT 2000" screen, Ctrl + A then delete all existing patterns
- Import the new file from "file" sub-list
- "Save-Save to current NPGS project" under NPGS sub-list
- Rename the file
- Close the "Design CAD LT 2000" window
- Reentry the new file's "Design CAD LT 2000"
- Ctrl + A, choose all the pattern

- Click the button with an exclamation point on it
- Click the dash line button appeared at the right side of the window
- Choose “dashed” for line type
- Set line scale as 1 and line width as 0
- “Save-Save to current NPGS project” under NPGS sub-list
- Overwrite use the same file name
- Close the window
- Back to the NPGS window
- Select the new pattern (dc2) file
- Right click choose “Run File Editor”
- Same way above to open an existing run file (rf6)
- Right click choose “Run File Editor”
- Copy the entry of fun file (rf6) into the (dc2) file for 1 entry type and 2entry type
- In 1 entry type right side of the window set first three as YES, NO, and NO
- In 3 entry type choose array then put correct parameters
    1. Layer => Normal Writing
    2. Origin Offset => (0,0)
    3. Magnification => as large as possible, e.g., 18000

4. Center-to-Center Distance (nm) => as small as possible, e.g., 2.19
5. Line Spacing (nm) => as small as possible, e.g., 2.19
6. Aperture #: 3 (10 μm)
7. Measured Beam Current (pA): put the measured current (using the Faraday cup)
8. Multiple Pass Mode => Disable
9. Area Dose: 150 ($\mu C/cm^2$) works well for ma-N 2401

- Save the run file with the name you want
- The new pattern run file is ready to go

A good focus on the sample surface is a significant step for a quality e-beam lithography process. The below are a standing e-beam writer setup for resulting in a decent pattern shape. The pattern was located 1mm under the bottom mark tip; this is an easy way to make sure once after the process started, for any reason if we want to check the substrate pattern conditions and results use SEM, we can quickly locate the exposed area.

- Magnitude: 100K
- Exposure dose: 180 $\mu C/cm^2$
- Aperture size: 10mm
- Electron high tension (EHT): 10kV

The basic pattern is built by nanoscale circles with square, cross, and circle. Each three of them (total nine shapes) combine as one unit, from unit A to unit I the circle size increase by about 10nm for each unit, so the unit A usually has size

around 80nm, then the unit I should have close to 160nm. This nine units of patter we call them one section, the entire patter is a combine of 9 of sections with the 3x3 arrangement. The below are the Schematic representation of e-beam lithography pattern, the circle's order and arrangement can be adjusted through AutoCAD, in fact, we do have some other shape of patterns used for testing gold nanoparticle attachment by changing the phosphate buffer ion concentration, pH value, and pattern circle diameter.

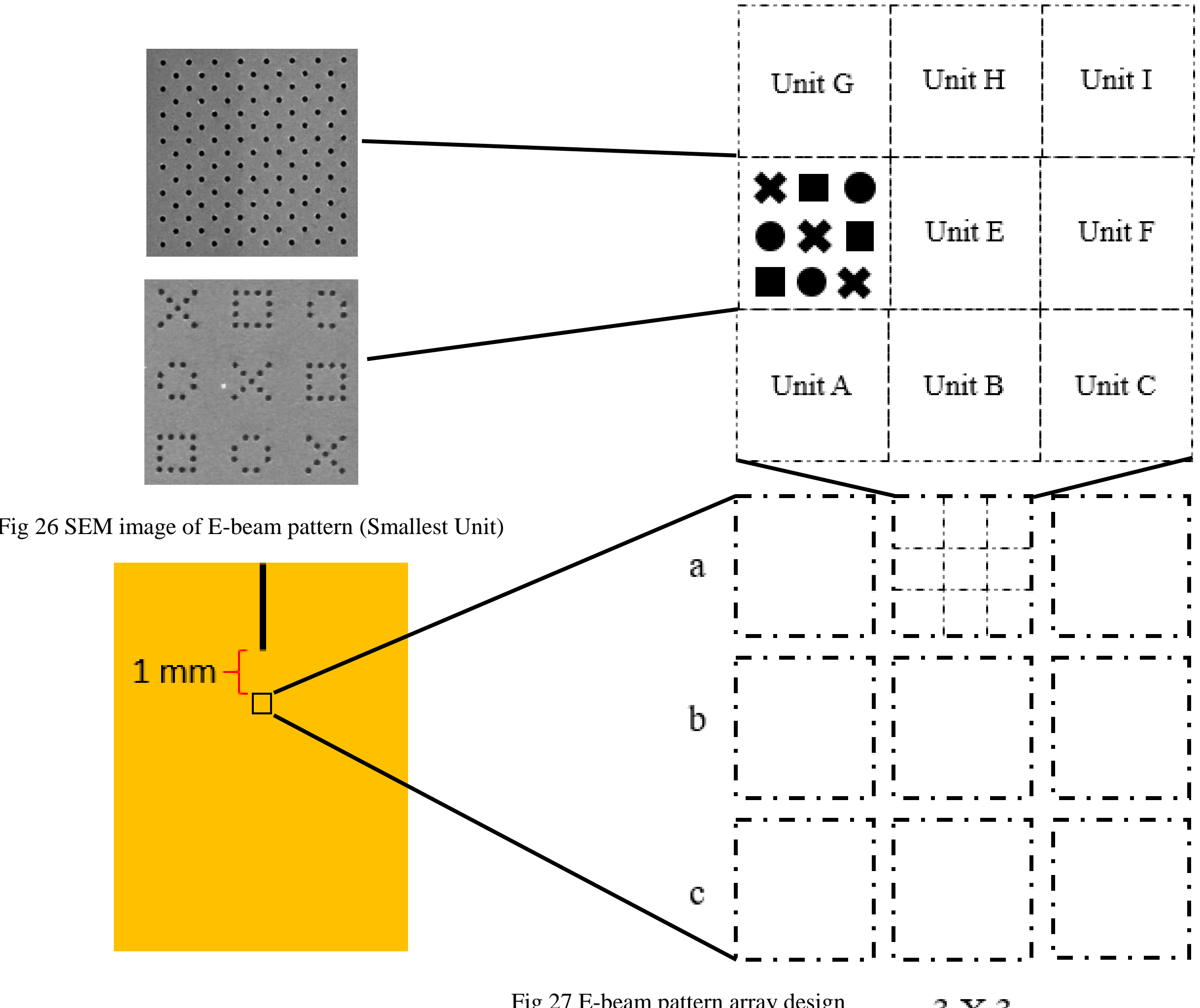

Fig 26 SEM image of E-beam pattern (Smallest Unit)

Fig 27 E-beam pattern array design

3.8 Development

As we mentioned before ma-N 2401 is a negative photoresist, the parts being exposed become insoluble when immure into photoresist developer. This process needs to act right after the e-beam lithography in case the photoresist gets contaminated by lights or moisture. Ma-D 525 is the photoresist developer we used for this step

- Immersion the sample in Ma-D 525 for 10 seconds
- Transfer the sample in DI water container for 10 minutes (change the DI water every two and a half minutes)
- Dry with N2 (blow very carefully since the insoluble resist Nano-size cylinder maybe destroy)

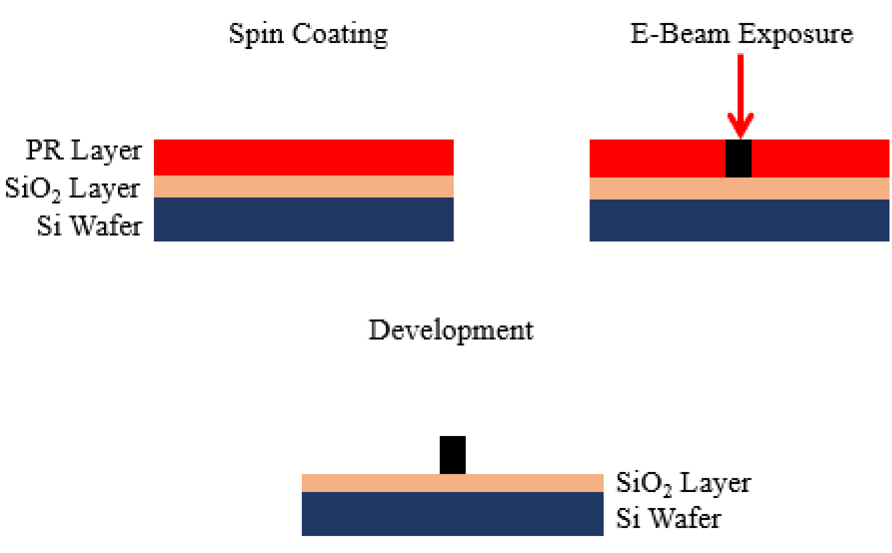

Fig 28 Schematic processes from spin coating to development

3.9 E-Beam Evaporation

The next step is to evaporate 15nm of Cr and 15nm Ag on the substrate surface use AJA international or CHA Solution, they are both electron beam evaporator, which AJA is more manually functionalized, and CHA is a totally automatic tool. The entire evaporation process needs to be under a high vacuum chamber to avoid contamination. Here the Cr layer deposited before Ag is acting as a glue for the second gold layer, it can create a better adhesion between the gold layer and the substrate surface.

Fig 29 Schematic side view after deposition

3.10 Lift-off with Clean Process

An immediate lift-off process after deposition needs to be done. The lift-off step is to make sure all the exposed photoresist pillars will be removed from the substrate and leaving a 30nm depth circle on the surface.

- Put the substrate in the acetone ultra-sonication bath for 15 minutes
- Take out the substrate, rinse with the acetone squeeze bottle
- N_2 dry
- Repeat above three steps for four times, a total 1 hour of lift-off
- Put substrate in the IPA ultra-sonication bath for 15 minutes

- Take out the substrate, rinse with IPA squeeze bottle
- N_2 dry
- Repeat above three steps for four times, total of 1 hour of cleaning

The previous UV-Ozone step is now useless for the clean substrate step. Due to the formation of gold oxide on the surface, all the samples need to store in the ethanol overnight and change the storage ethanol every two days.

Fig 30 Schematic side view after lift-off and clean process

3.11 DNA Gold Nanoparticle Conjugate

The substrate preparation was done discuss; now we will talk about the second part of this research, single particle placement. It starts with the preparation of gold conjugate. As the previous chapter mentioned the DNA strands attached on the surface of gold nanoparticle relay on pH, salt and ion concentration.

Synthetic oligonucleotide probe-DNA with disulfide linker was used in our experiment, because of its disulfide bond (for a stable storage state) we must break the bond before applying it to the gold nanoparticle. DL-Dithiothreitol is the chemical for this cleavage reaction. The DL-Dithiothreitol bottle needs to take out from the refrigerator and set in room temperature for at least 30 minutes to avoid

the formation of moisture. Weight the DL- Dithiothreitol powder use the test tube on a scale. To be able to reach 0.1M of DTT solution we need to weight 0.0154g of DTT for every 1 mL of phosphate buffer we added. Adjust the amount of the phosphate buffer use the ratio, have the 0.1M DTT solution ready for the next process.

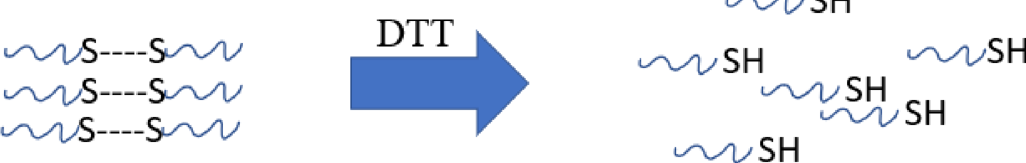

Fig 31 Schematic side of DTT break the disulfide bond

- Take out the DNA tube from the freezer
- Set in room temperature for about 30 minutes
- Centrifuge the DNA tube at 3000 rpm for 3 minutes (make sure all the DNA molecules move to the bottom of the tube)
- Pipette 120μL of the 0.1M DTT solution into the DNA tube (release it when tip touch the bottom)
- Wait for 2 minutes to let the DNA rehydrate
- Shake the tube by hand gently for one minute
- Wrap up the tube with foil
- Set it on the vortex for two and half hours (lowest speed)
- Take NAP-5 filter column out from the fridge
- Allow it to equilibrate under room temperature for at least 1 hour

- Remove both top and bottom caps and let the storage buffer to drain completely
- Pipette 15mL of fresh DI water into the filter column (1mL each time, total 15 times)
- Let it drain
- Pipette 120μL of DNA/DTT into the filter column
- Let it drain
- Pipette 380μL of DI water into the filter column
- Let it drain
- Pipette 100μL of DI water into the filter column
- Let it drain
- Pipette the last 300μL of DI water into the filter column
- Collect the 300μL DNA/DI drain droplet in a new test tube

This filter column helps to select oligonucleotides in the DNA/DTT by their size. The column inside is made with a porous matrix structure, which can allow small size oligonucleotides to pass through the gel bed but stop the large ones.

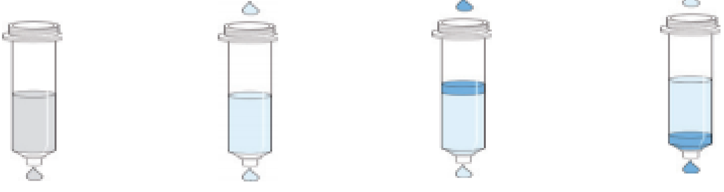

Fig 32 Schematic working principal of NAP-5

- Collect 2mL of 30nm gold nanoparticle colloid in the test tube
- Centrifuge the gold nanoparticle colloid at 4000 rcf for 10 minutes
- Take out 1950μL of the gold nanoparticle colloid supernatant
- Shake well the rest 50μL gold nanoparticles
- Ready the 300μL of DNA/DI that collected from the NAP-5 filter column step
- Slow pipette 14.58μL of 500mM citrate buffer (pH 7.5) into the 300μL DNA/DI
- Pipette 2.25μL of HCl to the same 300μL DNA/DI, adjust the pH to around 2.5
- Pipette the DNA/Citrate-HCl buffer into the 50μL gold nanoparticle colloid
- Incubate for 5 minutes on the vortex (lowest speed)
- Pipette 15μL of 1M NaOH to the above conjugates to raise the pH to around 7
- Pipette 650μL of Tris-EDTA buffer into the conjugates, handshake well
- Transfer the conjugates into a new test tube
- Centrifuge at 4000 rcf for 10 minutes
- Take out the supernatant
- Resuspend in 1mL Tris-EDTA buffer (pH8)

- Repeat above three purification steps for three more times
- Keep store the conjugates in the fridge

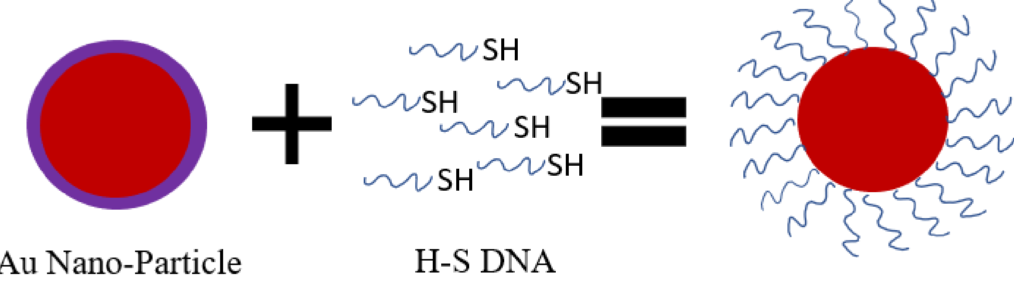

Fig 33 DNA strands coated on gold nanoparticle surface

3.12 SAM's Layer Formation

Self-Assembled Monolayer is the key for our single nanoparticle placement; it is the fundamental blocks of the electrostatic funneling technique. The DNA-functionalized gold nanoparticle can be guild onto the silicon oxide surface with the APTES positive charged layer form on the SiO_2 area and MHA negative charge layer form on the gold surface area.

The APTES SAM's layer will be conductor first to form the positively charged surface on the SiO_2 area due to the aminopropyl-terminated groups. The sample substrate was stored in ethanol for overnight already.

- Prepare a test tube (2mL)
- Pipette 950µL of pure ethanol into the tube
- Pipette 30µL of pH 13 DI water into the tube

- Pipette 20µL of APTES into the tube
- Vortex the total 1000µL of APTES mixture solution for 10 seconds (highest speed)
- Rinse the sample with the ethanol squeeze bottle
- Immerse it in the APTEX mixture solution for 60 minutes
- Prepare wash step tubes (6 of them)
- Pipette 1mL of pH 13 ethanol for the each first three tubes
- Pipette 1mL of pure ethanol for each remaining three tubes
- Rinse the sample in each tube for 30 seconds
- N_2 dry

Make sure to wash the tweezer by ethanol squeeze bottle every time the substrate transfer to next tube, also between the third tube and fourth tube rinse the sample with the ethanol squeeze bottle because the ethanol pH has a significant change from pH 13 to pH 7.

The MHA solution can be prepared ahead to get ready for the sample. Once the APTES layer formation is done, the second MHA SAM's layer can be started immediately. The correct ratio for MHA/ethanol mixture is MHA: ethanol=0.014:1000, which means every 0.014 gram of MHA needs to dissolve in 1000µL of ethanol.

- Weight the MHA powder in the test tube via the weighing scale
- Pipette the correct amount of pure ethanol into the tube

- Sonicate the MHA/ethanol tube for 5 minutes
- Pipette HCl to the MHA solution with every 1μL HCl to 1000μL of MHA/ethanol solution
- Immerse the sample in the MHA solution for at least two and a half hours
- Prepare wash step tubes (6 of them)
- Pipette 1mL of pH 2 ethanol for the each first three tubes
- Pipette 1mL of pure ethanol for each remaining three tubes
- Rinse the sample in each tube for 30 seconds
- N_2 dry

Make sure to wash the tweezer by ethanol squeeze bottle every time the substrate transfer to next tube, also between the third tube and fourth tube rinse the sample with the ethanol squeeze bottle because the ethanol pH has a significant change from pH 2 to pH 7.

Now the surface will be covered by positively charged APTES aminopropyl-terminated group layer on the SiO_2 surface, and negatively charged MHA $-COO^-$ terminated group layer on the gold surface.

3.13 Au Nanoparticle Placement

The gold nanoparticle conjugate was stored in the refrigerator.

- Take 50μL of the conjugate colloid into a test tube
- Centrifuged the colloid at 4000rcf for 10minutes

- Suspended with pH 7.5 phosphate buffer (Ion concentration can vary)
- Shake well by hand
- Ready the substrate in the hybridization chamber
- Apply 10µL of the phosphate buffer/Au nanoparticle colloid on the substrate surface for 10minutes
- Prepare four test tubes
- Pipette first three tubes with DI water
- Pipette last test tube with pure ethanol
- Wash substrate in each DI tube for 10s and a quick dip in ethanol tube
- N_2 dry,
- Store sample in a clean test tube

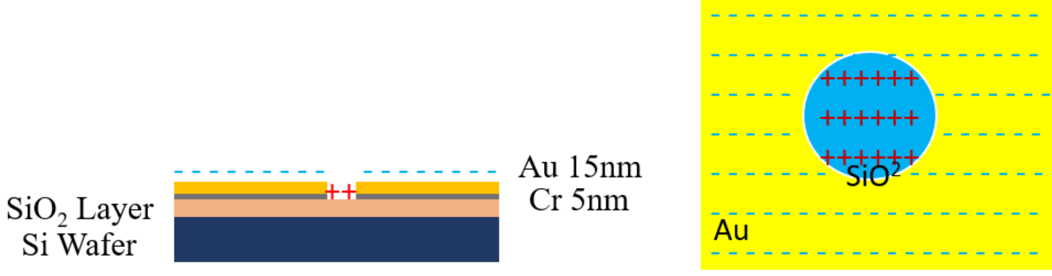

Fig 34 SAM's Layer Formation

3.14 Au Nanoparticle Protection

The gold nanoparticle was placed at the exact location via the electrostatic funneling technic. The next we need to get rid of the Au and Cr layer use gold and chrome etchant while the fixed gold nanoparticles are not being removed. The same

photoresist we used in lithograph can still work here for the gold nanoparticle protection. Spin coat the substrate with the same spin coating recipe:

I. 500 RPM, 100RPM/s, 5 seconds

II. 3000 RPM, 1000RPM/s, 30seconds

Followed by the pre-bake at 90°C for 60 seconds, then take the sample under the UV light for 2 minutes at room temperature. As we know the photoresist will be polymerized forming interlocking result in hardened the resist. This step is to make the surface photoresist a good condition which can be easily controlled in the later etching process. The substrate is ready for the resist strip step; a Plasma-therm etcher was used for the process. It is under a controllable manner which can result in gold surface exposed, but the cylinder-shaped nanoscale circle still covered photoresist with nanoparticle in it. The resist thickness on the surface is about 100nm, so the below setup was tested for the resist strip.

I. Power: 50W

II. Pressure: 300mTorr

III. O_2 Flow: 100 SCCM

IV. Time: 420 Seconds

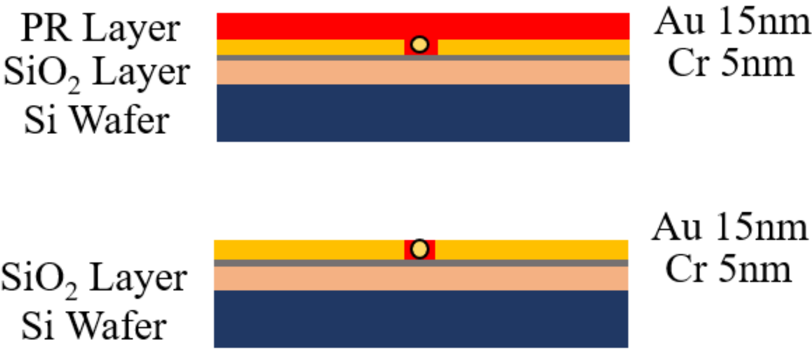

Fig 35 Photoresist being removed

3.15 Remove of Gold and Chrome Layers

Now we have the gold layer exposed at the top of the substrate, and the chemical etching will be conduct for the removal of both gold and chrome thin film. From the etchant chemical manufactures index, the gold etches rate was around 2.8nm/s, and the chrome etch rate was about 4nm/s. Since we have 10nm of chrome and 20nm of gold the etch time can be quickly calculated. Immures the substrate first in the gold etchant for 8 seconds this is an over-etch process, which can make sure all the first layer gold can be removed. Follow by DI water rinse for 2 minutes to clean out the gold etchant and possible tiny gold pieces. Then place the substrate into the chrome etchant for 8 seconds, over-etch also was involved since the bottom SiO_2 layer will not be affected by the chrome etchant.

Fig 36 E-beam deposited Au and Cr layer being removed

3.16 Pillar-Shaped Photoresist Removal

Successful removal of the gold and chrome layer will leave the photoresist protected nanoparticles on the surface. This is the last step we need to do before the nanopillar formation. The same process oxygen plasma etch will be used just like the resist strip section. Time setup here is on purpose for over-etching to get rid of all the resist; in other words, the gold nanoparticle can be exposed correctly.

I. Power: 50W
II. Pressure: 300mTorr
III. O_2 Flow: 100 SCCM
IV. Time: 500 Seconds

Fig 37 Gold Nanoparticle exposed on surface

3.17 SiO_2 Nanopillar Formation

In this section, we are going to fabricate the silicon oxide nanopillar through the Marco RIE. Usually, before the process, conduct a cleaning process step for the RIE chamber is necessary, vent and open the chamber, use IPA solution and lint-free wipes to clean the inside parts of the chamber. Pump down the machine and conduct an oxygen dry etching process which helps remove all the polymers and contaminations. The oxygen dry etching clean setup shows below.

I. Power: 750W

II. Pressure: 150mTorr

III. O_2 Flow: 11SCCM

IV. Time: 1200 Seconds

After the clean process, the substrate now placed in the center of the chamber which ensures the etching uniformity. The nanopillar height and shape can be adjusted via the CF_4, O_2, power, pressure and time. To be able to get a nanopillar with around 150nm height the below recipe was used.

I. Power: 500W

II. Pressure: 150mTorr

III. CF_4: 20sccm

IV. O_2: 1.2sccm

V. Time: 100s

Fig 38 SiO_2 nanopillar formed via RIE

Many steps we have been going through is to make the gold nanoparticle can be placed on the substrate surface with at the exact location via the design. The gold nanoparticle's main job is to act like a mask (a hat) to protect the underlayer SiO_2 during the RIE process, so a nanopillar shaped SiO_2 cylinder can be fabricated. Once we did with the formation, the gold nanoparticle can be removed from the surface through the gold etchant.

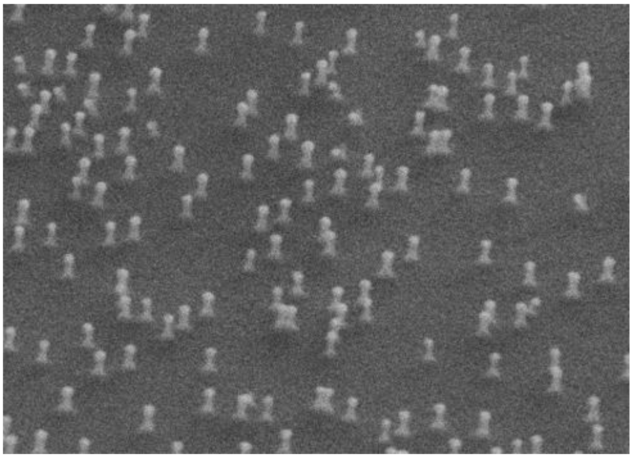

Fig 39 SEM 45-degree SiO_2 nanopillars with 150nm height

CHAPTER 4 RESULT AND DISCUSSION

4.1 E-Beam Dose Effect in Lithograph

Sample #1 2403 dose 160 $\mu C/cm^2$, 5nm Cr, 15nm Au, develop time 45s

Sample #2 2403 dose 180 $\mu C/cm^2$, 5nm Cr, 15nm Au, develop time 45s

Sample #3 2403 dose 200 $\mu C/cm^2$, 5nm Cr, 15nm Au, develop time 45s

Sample #4 2403 dose 220 $\mu C/cm^2$, 5nm Cr, 15nm Au, develop time 45s

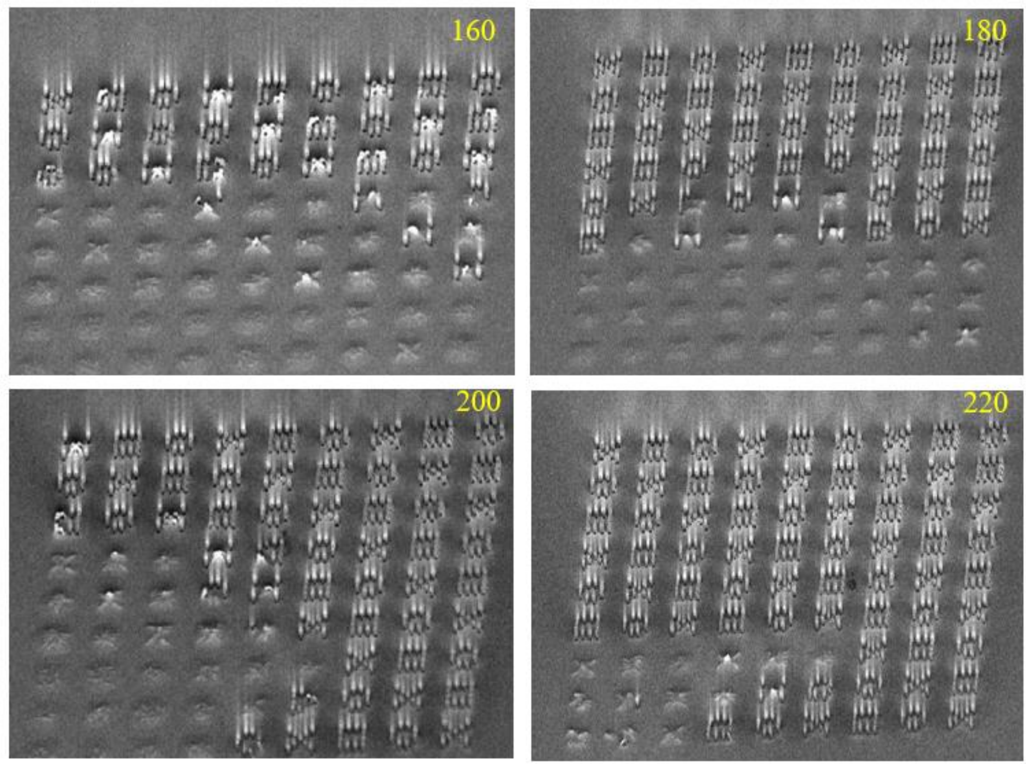

Fig 40 Sample #1, 2, 3, 4, 2403 PR, overall view

With 2403 photoresist, E-beam writing under dose 160, 180, 200, and 220. The above picture shows the photoresist pillar after the 5nm of Cr and 15nm of Au

deposited on the surface and before the lift-off process. All the samples processed with 45 seconds of development. Which is too long for the 2403 PR, because of the missing PR pillars find in the small size area of the patterns. As a result, the large dose gives thick PR pillar and hard being removed during the development, and the gold deposition was covering those small sized areas. In other words, the development time for 2403 PR needs some adjust between 30 to 45 seconds — the PR shapes in large magnitude show below.

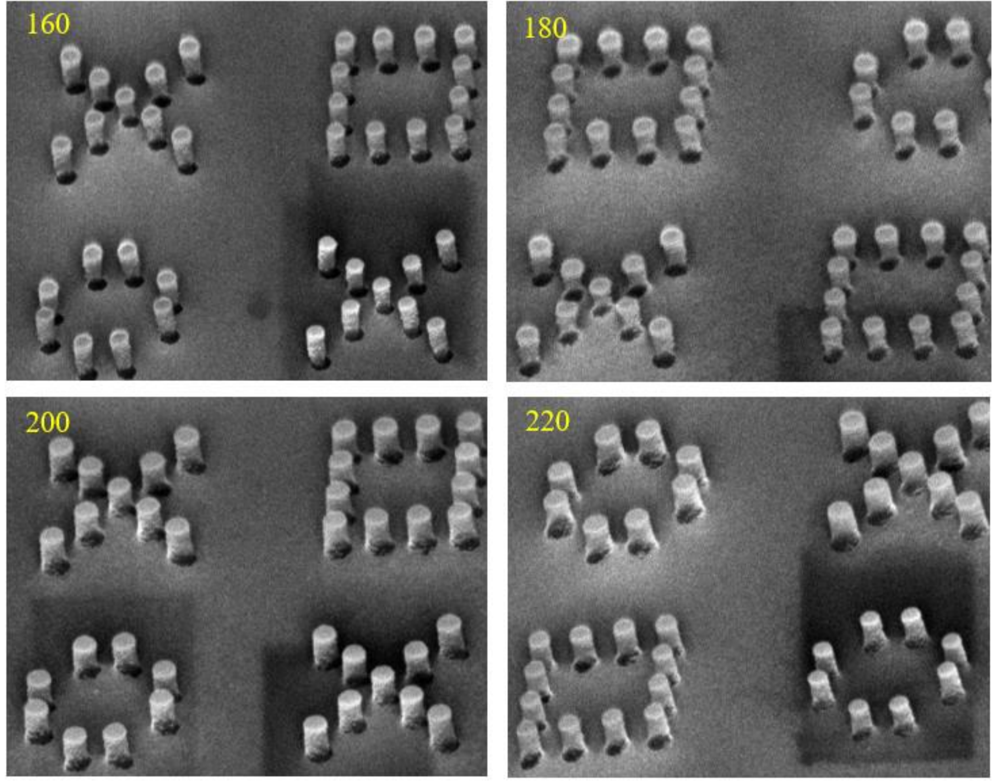

Fig 41 Sample #2, 2, 3, 4, 2403 PR pillar shape

4.2 Type of Photoresist (2401 and 2403)

Sample #1 2403 dose 160 $\mu C/cm^2$, 5nm Cr, 15nm Au, develop time 40s

Sample #2 2401 dose 160 $\mu C/cm^2$, 5nm Cr, 15nm Au, develop time 10s

From the e-beam dose effect, we believe the dose size is not the critical point in the process (between 160 $\mu C/cm^2$ to 180 $\mu C/cm^2$ is a good range), but the photoresist type can be a quite issue. Keep the dose at 160 $\mu C/cm^2$ with changing of development time from 45 seconds to 40 seconds for 2403 PR. The small size now has a better feature, more patterns survived. However, some patterns have photoresist left on the surface, and the large size pattern edges showing roughness which can be a problem for future particle placement. Features show in under pictures.

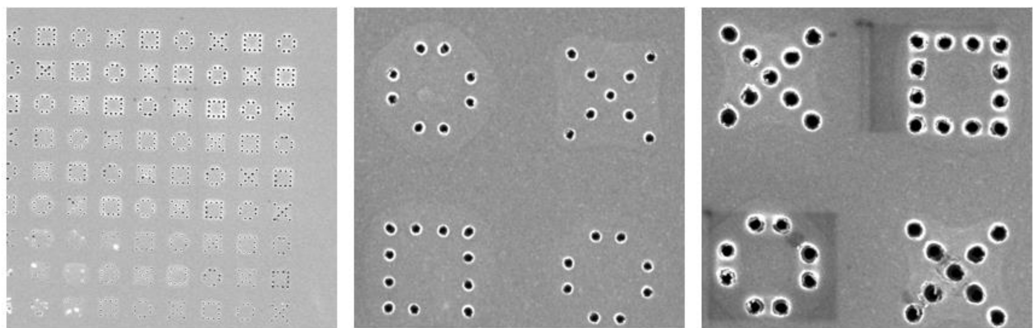

Fig 42 Sample #1, 2403 PR, the overall, small, and large size SEM view

Because of the new adjustment for the CHA solution and after several tests using 2403 photoresist, we decided to go back using 2401 again to see if the previous lift-off problem may be solved. The result shows that the lift-off problem

is getting way better than before. 15minutes of lift-off may need to extend for a little bit more time. Since the small size still has some PR left around the pattern. More test needs to be done to confirm the 2401 result if it works then we do not need to use 2403 at all. Below is 2401 PR pattern.

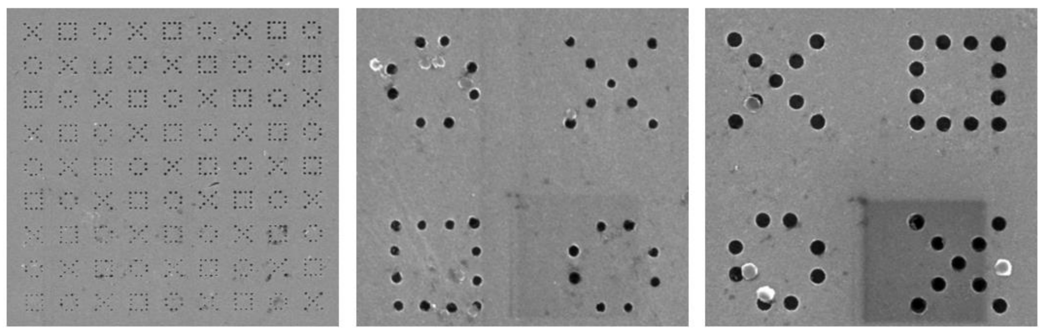

Fig 43 Sample #2, 2401 PR, overall, small, and large size

4.3 E-Beam Deposition Method (CHA & AJA)

Sample #1 2401 dose 160, 5nm Cr, 15nm Au, develop time 10s (AJA)

Sample #2 2401 dose 160, 5nm Cr, 15nm Au, develop time 10s (CHA)

For the confirmation of the result, we conducted once more of the 2401 PR and conventional deposition with CHA. Moreover, we also did one sample with all the same conditions but used AJA instead of CHA to deposit the Cr and Au, since from the CHA incident we believe the E-beam deposition method and parameters can be a significant reason to the following lift-off process. In other words, the thickness should still be the critical thing to consider. As the SEM result, we can be sure that 2401 PR with CHA and AJA deposition are both works well, it can be

concluded that the E-beam pattern preparation steps are confirmed, and the further process can be initiated.

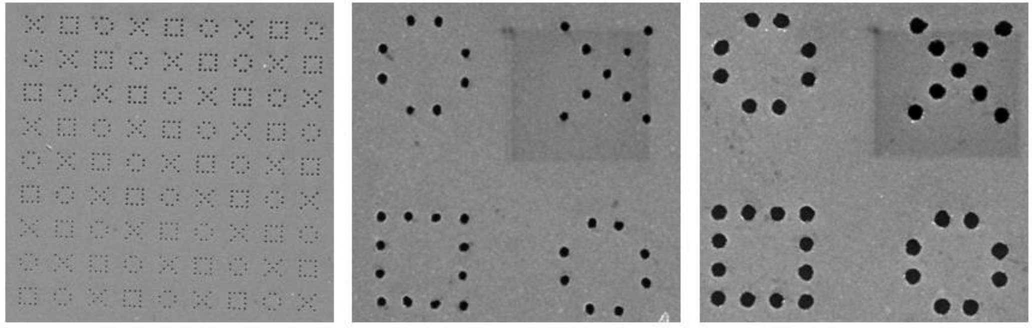

Fig 44 Sample #1, 2401 PR, AJA, overall, small, and large size view

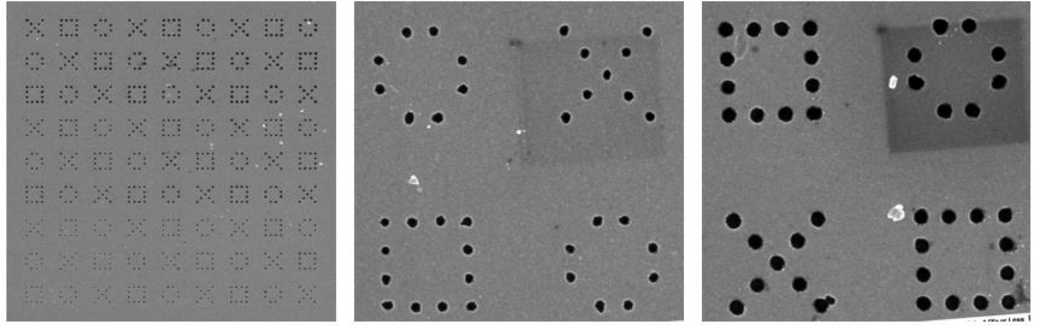

Fig 45 Sample #2, 2401 PR, CHA, overall, small, and large size view

4.4 Wet Chemical Surface Treatment

#1 HF (50:1) 2 min NH_4F 3min H_2O_2 30min AJA

#2 HF (50:1) 2 min NH_4F 3min H_2O_2 30min CHA

We did the SPP experiment with the samples which under new established E-beam lithography preparation process. The surface treatment was conducted with wet chemical (HF (50:1) 2 min NH_4F 3min H_2O_2 30min). The difference between

the two samples are the E-beam deposition method, one was for CHA, and another was AJA. The SEM result showed the gold nanoparticle can be attached within the pattern circle quickly in the large diameter area, but not quite in the small size area. The most problem is the gold nanoparticles were attached within all the gold surface, except the pattern region. This is what suppose not to happen; we believe the future work needs to be focus on pH value and ion concentration optimization. The sample must be stored in ethanol for at least one day to let the oxide remove from the gold surface. The both CHA and AJA sample give the same result, here only showing the AJA sample SEM.

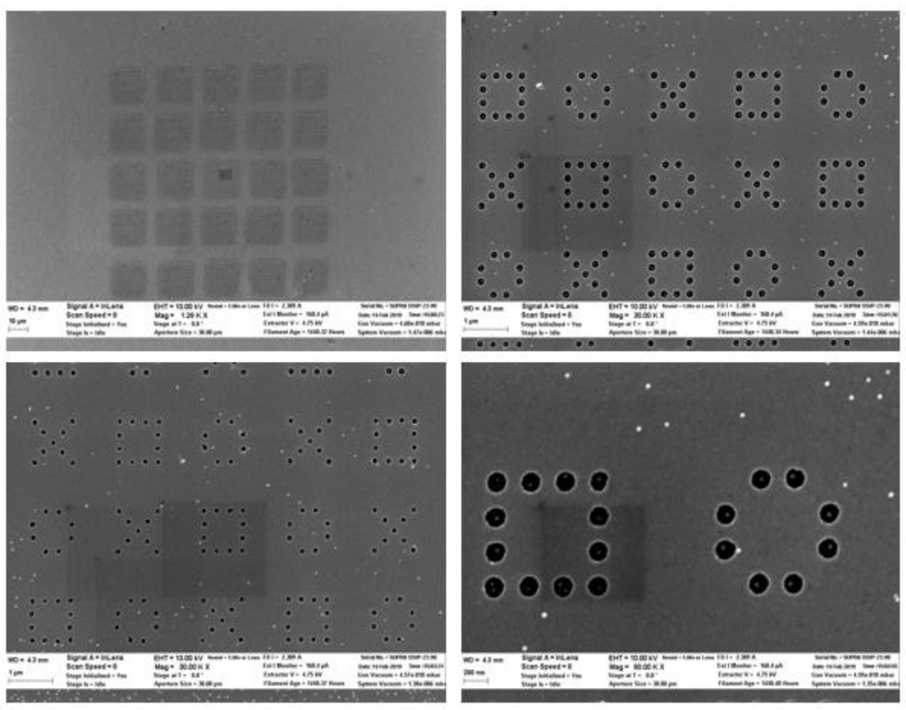

Fig 46 Sample #2, AJA, SPP SEM, overall, small, and large area size view

4.5 Ion Concentration (under wet chemical treatment)

#1 HF (50:1) 2 min NH_4F 3min H_2O_2 30min (0.1mM)

#2 HF (50:1) 2 min NH_4F 3min H_2O_2 30min (1mM)

#3 HF (50:1) 2 min NH_4F 3min H_2O_2 30min (5mM)

Tested 3 samples use 7.5pH and 0.1mM 1mM 5mM PB, the nanoparticle droplet time is 5 minutes. The SEM did not show many differences between all three. The selectivity still not good, and big size pattern show some particles attachment, the small size pattern nearly no attachment. Compare the results which did before with the pH 6.75 1mM PB sample; it is easy to tell that the change of the pH from 6.75 to 7.5 did not solve the gold surface nanoparticle attachment problem. Also, still cannot tell the ion concentration may affect the placement. The nanoparticle droplet time reduced from 30 minutes to 5 minutes did not affect the gold surface attachment but decrease the particle placement in the SiO_2 circle. Since the large pattern area now has fewer particle attaches, and the small size area barely has the attachment.

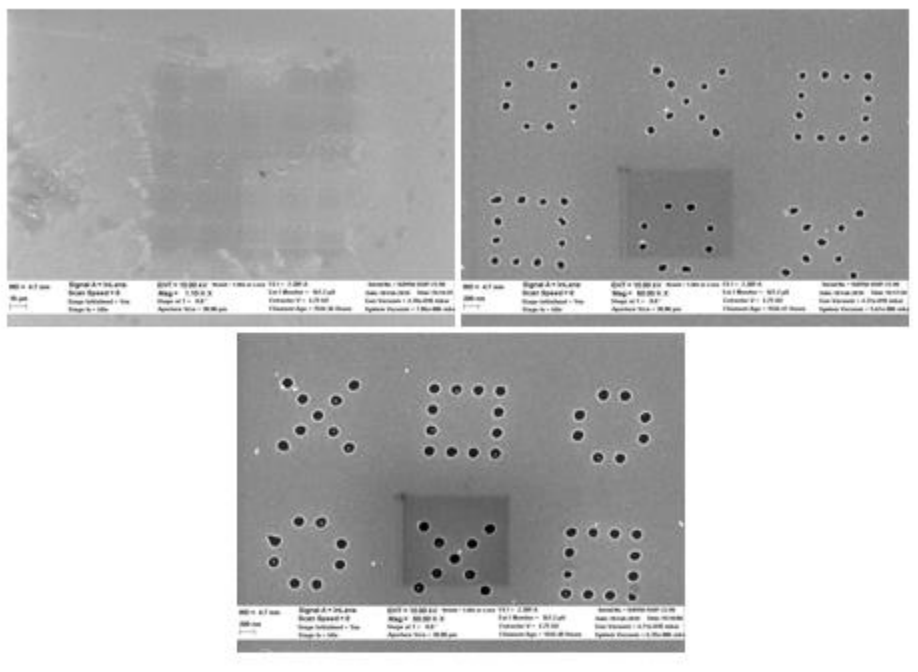

Fig 47 Sample #1, ph7.5_0.1mM_SPP SEM, overall, small, and large area size view

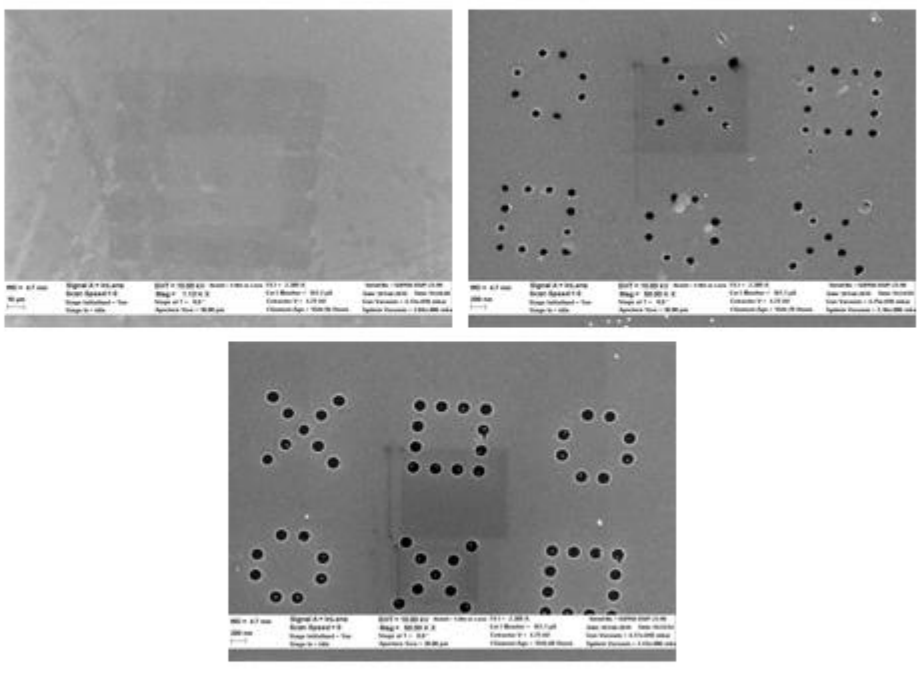

Fig 48 Sample #2, ph7.5_1mM_SPP SEM, overall, small, and large area size view

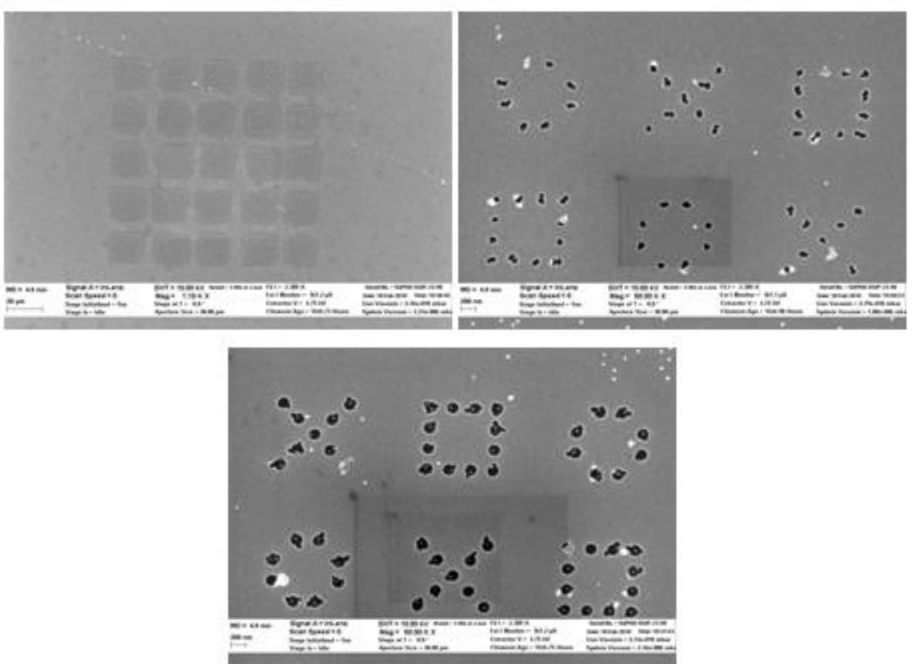

Fig 49 Sample #3, ph7.5_5mM_SPP SEM, overall, small, and large area size view

4.6 Gold Plating Solution Treatment

#1 HF (50:1) 2 min NH_4F 3min H_2O_2 30min (1mM 7.5pH)

Gold plating solution treatment

Before the SPP experiment, we try to do a gold plating coverage on the sample. Which was heat gold plating solution to 65C and put the sample into the solution for 45s and wash with large amount DI water then process normal SPP. The result shows a disastrous result, the nanoparticles were attached on the gold surface everywhere, and the selectivity is sure no acceptable. The gold plating treatment is not a solution at this moment.

4.7 Sputtering Treatment and Direct Process

#1 Ar Sputtering, Power: 300w, Pressure: 150 mTorr, time: 120s

#2 No UV O-Zone treatment

We try to skip the general clean process (HF, NH_4F, H_2O_2) and go straight to the acetone sonication & UV ozone cleaning; both samples are processed continuously means from the sample preparation to the single particle placement has no waiting or stopping. The sample 1 which was clean by both acetone sonication & UV ozone 10 minutes each and repeat five times, then do Ar spattering (Power: 300w, Pressure: 150 mTorr, time: 120s) the result shows failed particles attached all over the surface, the selectivity also not well. Sample 2 which did only five times acetone sonication 10minutes each time, no UV O-zone treatment. This sample shows a better result, the selectivity is quite good, and the surface is not covered with particle-like before, the pattern area also very clean, but there are some line-shaped area over some surface which only the line area has particles attached, it is a discovery, and may cause by the sample overlap during acetone sonication. Sample 2 still seems on the right track.

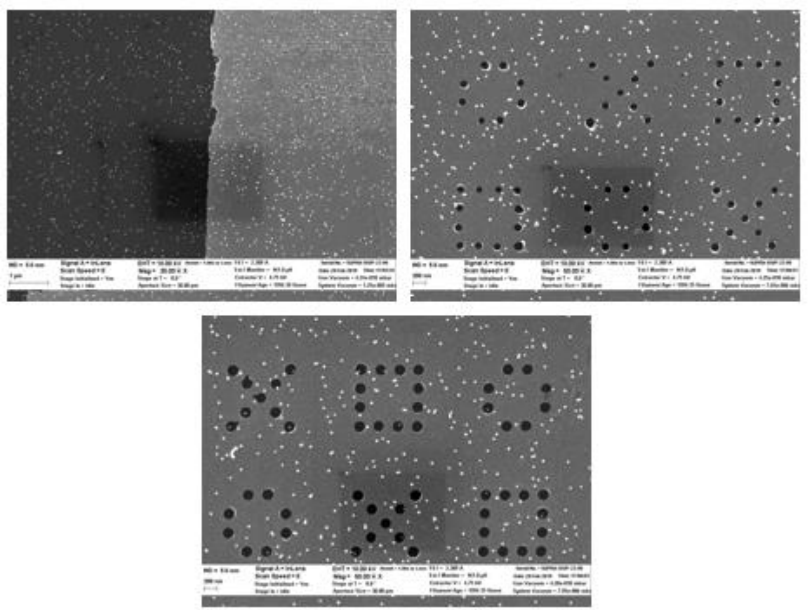

Fig 50 Sample #1, SPP SEM, selectivity, small, and large area size view

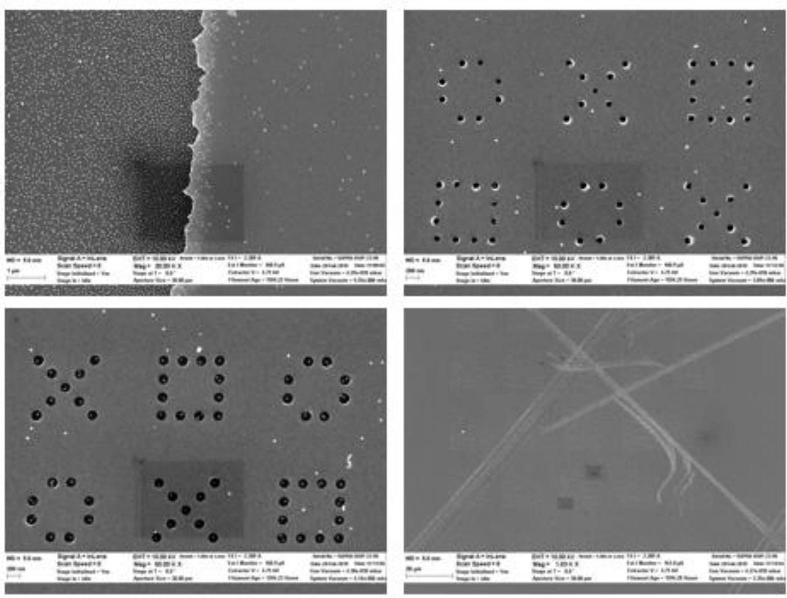

Fig 51 Sample #2, SPP SEM, selectivity, small, and large area size view

4.8 Advanced Wet Chemical Treatment

#1 HF (50:1) 2 min NH_4F 3min H_2O_2 30min

#2 HF (50:1) 2 min NH_4F 3min H_2O_2 30min, HCl treatment

#3 HF (50:1) 2 min NH_4F 3min Piranha 30min

#4 HF (50:1) 2 min NH_4F 3min Piranha 30min, HCl treatment

#5 Acetone Sonication X 5 [Overnight ethanol]

Since the UV Ozone treatment did not help for the surface cleaning. We try to figure out if the chemical treatment with HCl dip may help the surface conditions. Since the H_2O_2 and Piranha solution can both somehow help the surface cleanness, we set the sample as the above to check the treatment differences. Moreover, sample #5 is for one more time to confirm the UV Ozone treatment may not be useful.

The results are frustrating; all the five samples are failed at this time. Chemical treatment is not a right choice for surface cleaning. Even the sample #5 is not success compare with the same condition sample #2 we did before. After rechecking the experimental procedure for couple times and compare the details of two experiment steps. We think the direct process SPP after substrate clean can be a key for successful SPP result. The ethanol storage and overnight maybe contaminated the surface conditions. We plan to have a continues process from substrate preparation to SPP.

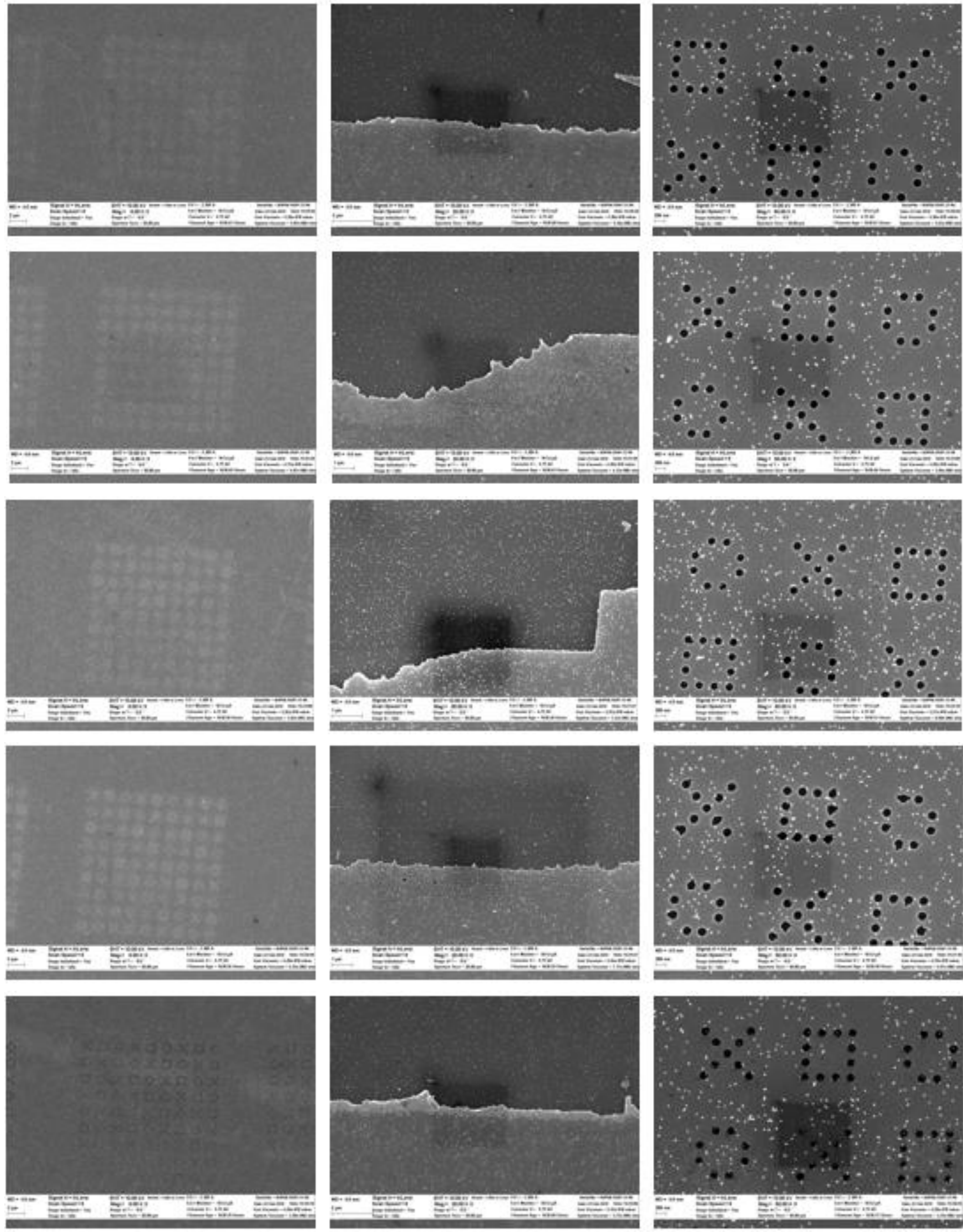

Fig 52 Sample #1-5 from tow row to bottom, SPP SEM, overall, selectivity, and large size area view

4.9 Continuously Process and IPA/DI Clean

#1 Acetone sonication – 10mins (X5) acetone, methanol, IPA

#2 Acetone sonication – 10mins (X5) acetone, methanol, DI water, IPA

This is the second time conduct direct process, start from the sample preparation to the SPP. Two samples are being processed with the same conditions and at the same time. The only difference between them is during the acetone sonication's clean step; one sample was treated with acetone, methanol, and IPA. The other one has one more step which is DI water wash between methanol and IPA. We want to see if the water moisture can affect the surface conditions. The SEM shows a quite good result; the direct process is a crucial point for SPP; in other words, the SAM's layer formation needs continuously process. The DI water seems like not quite affect that much at this point, but sample 2 does have some lift-off problem. Both surface SPP are relevant clean.

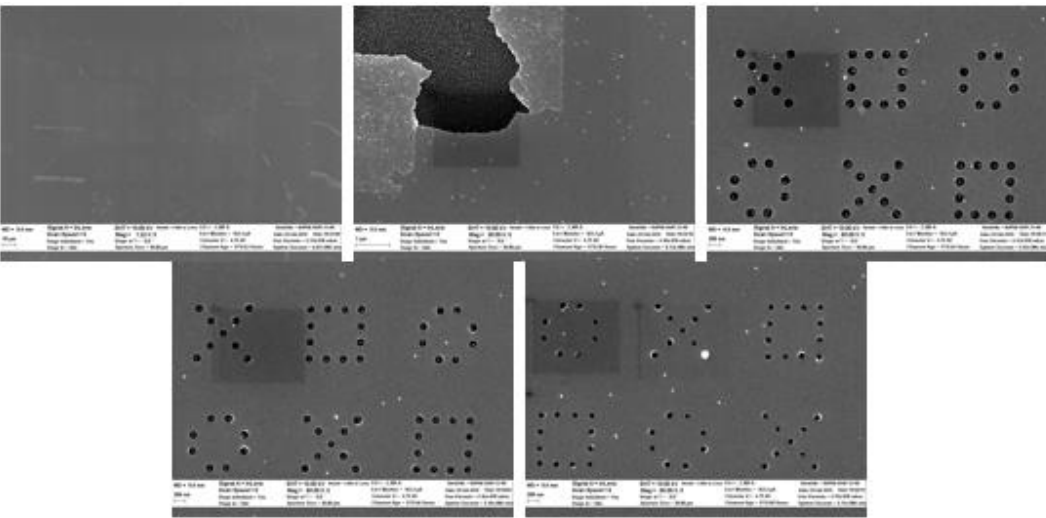

Fig 53 Sample #1 SPP SEM, overall, selectivity, and large middle small size area view

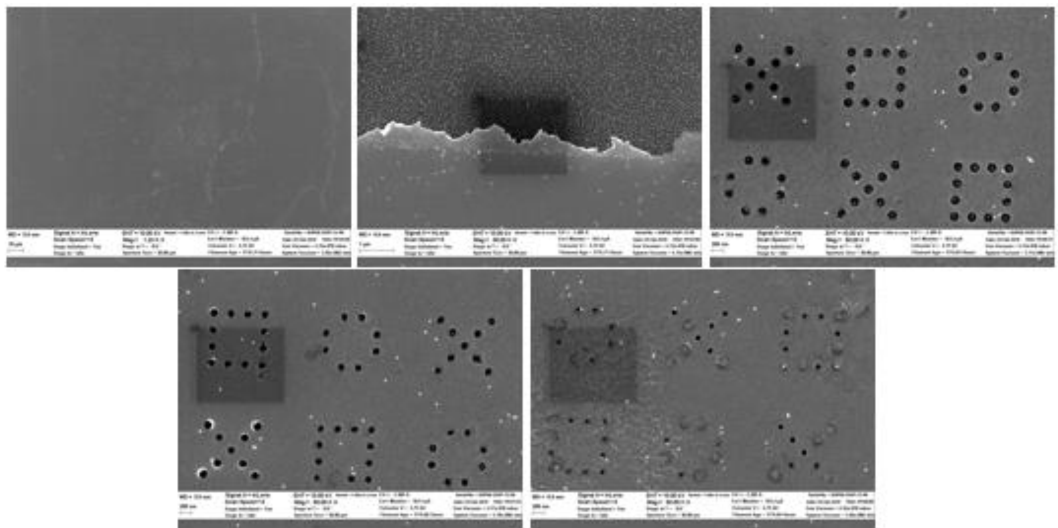

Fig 54 Sample 2 SPP SEM, overall, selectivity, and large middle small size area view

4.10 Ethanol/N2 Immersion

#1 Acetone sonication – 10mins (X5) Acetone Sonication + UV Ozone, Stored in ethanol, four days

#2 Acetone sonication – 10mins (X5) Acetone Sonication Only, Stored in ethanol, four days

#3 Acetone sonication – 10mins (X5) Acetone Sonication Only, Stored in N2, overnight

This sample set up is for a long-time ethanol immersion check. Both sample 1 and sample 2 are stored in ethanol for more than four days. Sample 1 is cleaned with acetone sonication and UV Ozone, and sample 2 did only with acetone sonication. Sample 3 was made the day before and stored in N_2 for just overnight. The SEM shows the UV Ozone steps is not helping the surface clean.

Moreover, seems the N_2 immersion kind same as ethanol immersion, so the problem may not come from either ethanol or N_2; because the overnight storage can affect the surface condition no matter how we store the sample. Also, the long-time storage may help the substrate surface conditions.

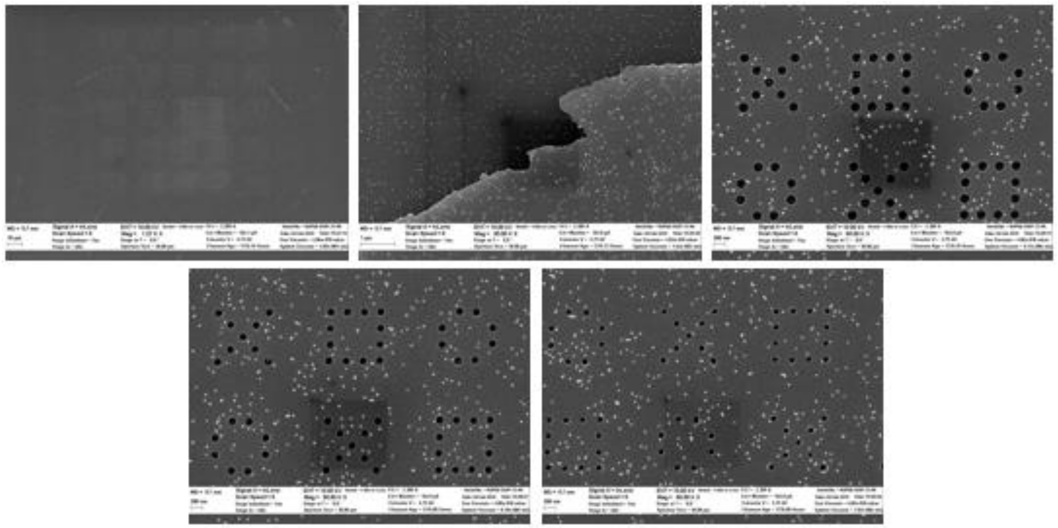

Fig 55 Sample 1 SPP SEM, overall, selectivity, and large middle small size area view

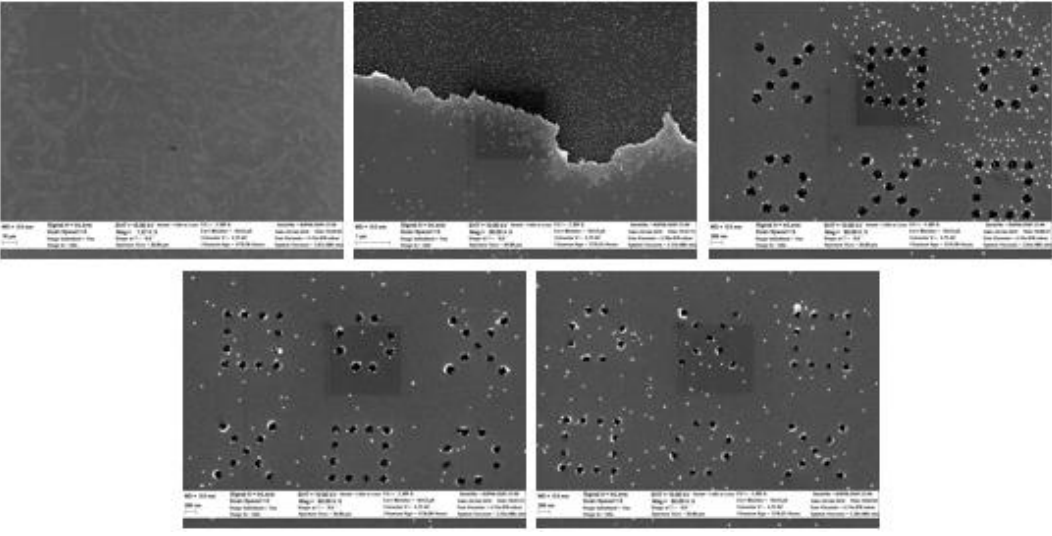

Fig 56 Sample 3 SPP SEM, overall, selectivity, and large middle small size area view

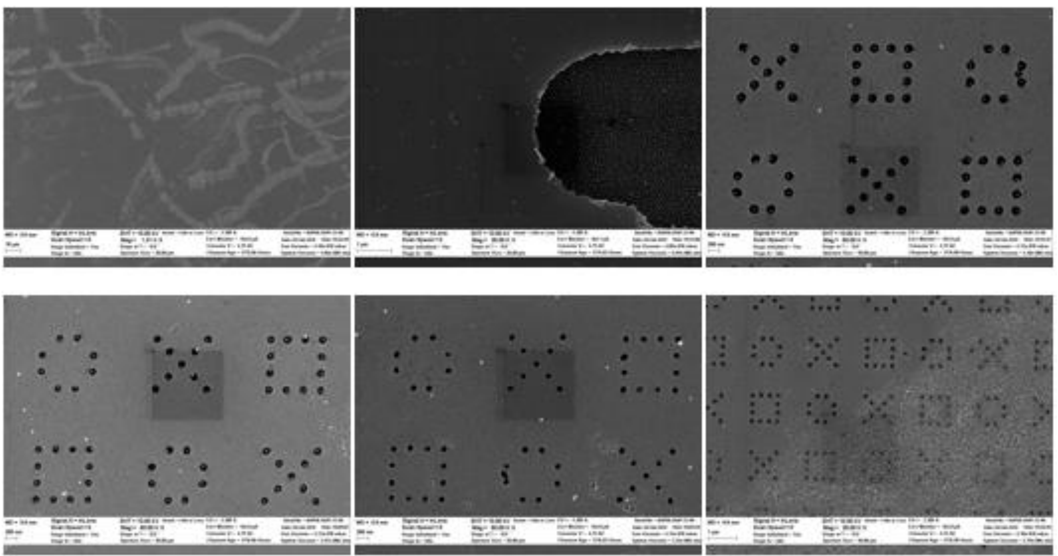

Fig 57 Sample 2 SPP SEM, overall, selectivity, large middle small size area view, and surface features

4.11 Long-Time Ethanol Immersion and Advanced Sputtering

#1 Acetone sonication & UV Ozone Stored in ethanol, 5days, O_2

#2 Acetone sonication & UV Ozone Stored in ethanol, 5days, O_2+CHF_3

#3 Acetone sonication & UV Ozone Stored in ethanol, 5days, CHF_3

#4 Acetone sonication & UV Ozone Stored in ethanol, 5days, Piranha

This surface spattering test batch was not a success. All the four above cleaning test show failed clean surface condition. From this date, we can confirm that UV Ozone can be out of the concerning as a clear cycle step. The acetone sonication or IPA sonication should only be used in the cleaning step. Later experiment will be conducted to confirm if acetone sonication or IPA sonication

can give a better surface condition. Moreover, once more to ensure the long-time (more than three days) ethanol storage can help enhance the surface cleanness.

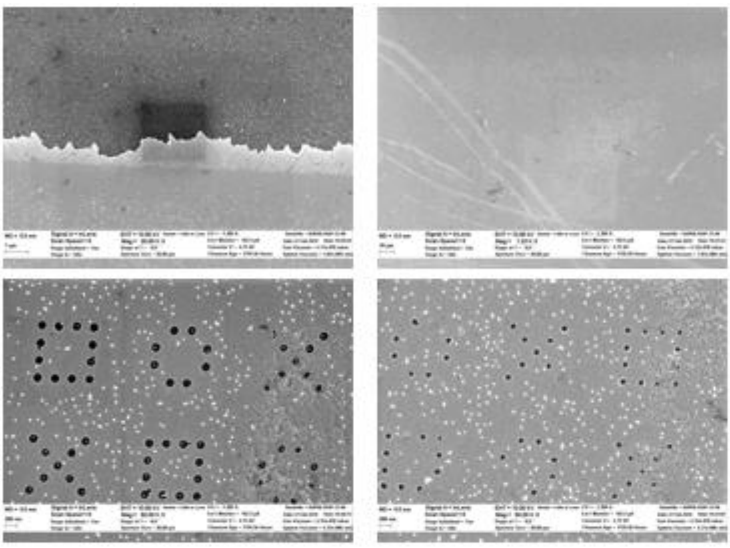

Fig 58 Sample 1 SPP SEM, selectivity, overall and large small size area view

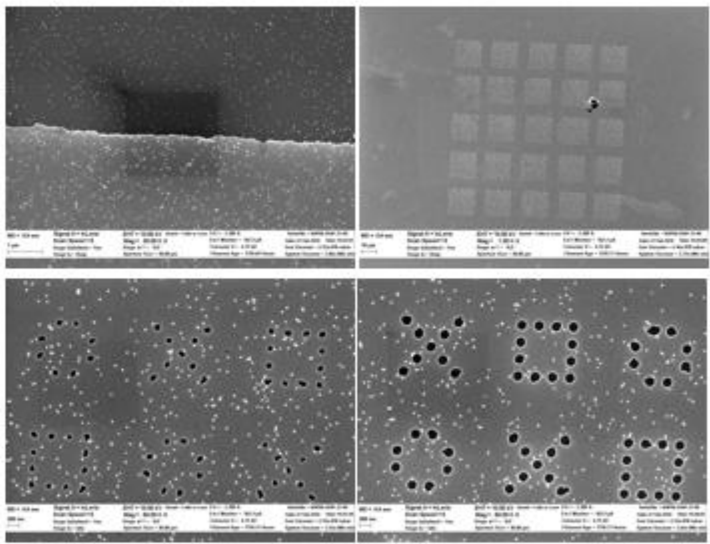

Fig 59 Sample 2 SPP SEM, selectivity, overall and large small size area view

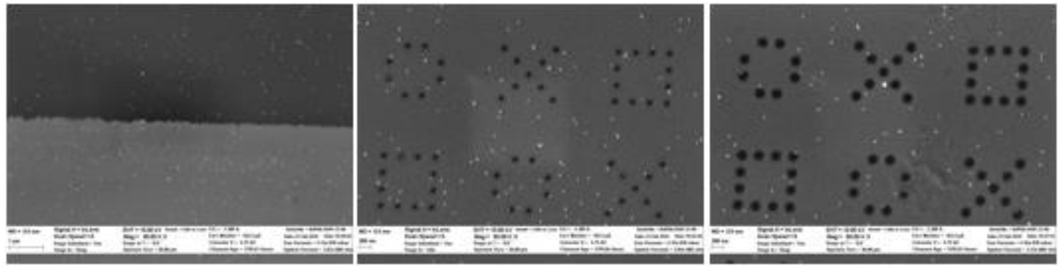

Fig 60 Sample 3 SPP SEM, selectivity, and large small size area view

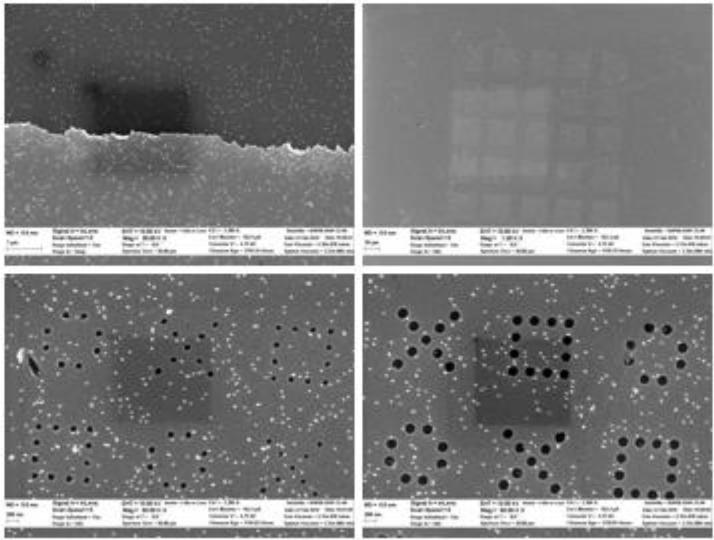

Fig 61 Sample 4 SPP SEM, selectivity, overall and large small size area view

4.12 IPA, Acetone Sonication Effects

#1 Lift-off acetone sonication 60 minutes, IPA sonication (X5) rinse with IPA, Stored in ethanol, overnight

#2 Lift-off acetone sonication 60 minutes, IPA sonication (X5) rinse with IPA, Stored in N_2, overnight

#3 Lift-off acetone sonication 60 minutes, rinse with acetone, Stored in ethanol, Overnight

#4 Acetone sonication (X5) Stored in ethanol, 6days

This is a quite success batch; all the samples that tested are showing quite good results. After this experiment, we can pretty much have some conclusions for the substrate surface clean process.

1. the UV Ozone is not useful
2. DI water step does not affect the result
3. HF, NHF_4, H_2O_2, and Piranha did not help the surface clean
4. Any sputtering cannot improve the surface condition
5. Continuously SPP process can give good results
6. Longtime ethanol storage can help the surface condition
7. N_2/ethanol overnight storage showing good result
8. IPA sonication is a better choice than acetone in the clean process

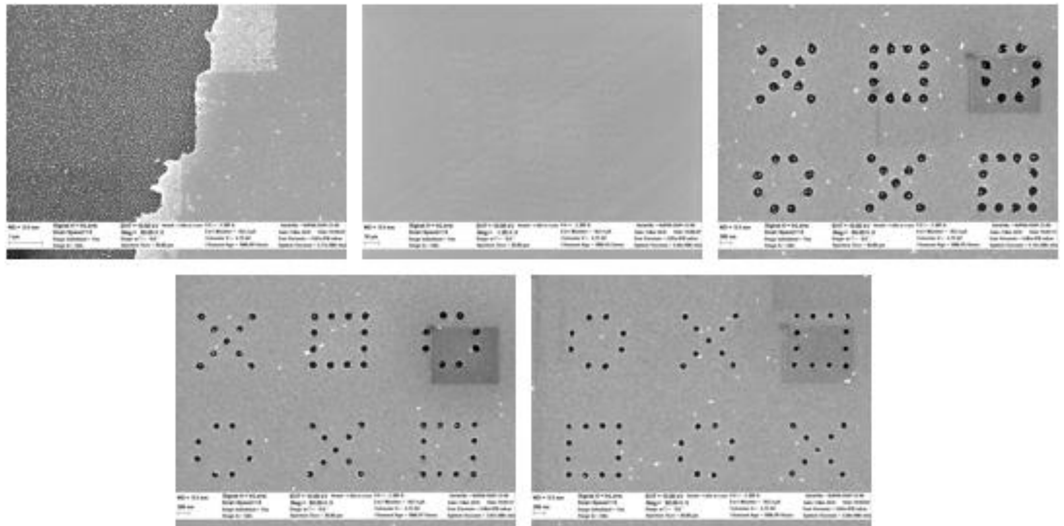

Fig 62 Sample 1 SPP SEM, selectivity, overall, large, medium, and small size area view

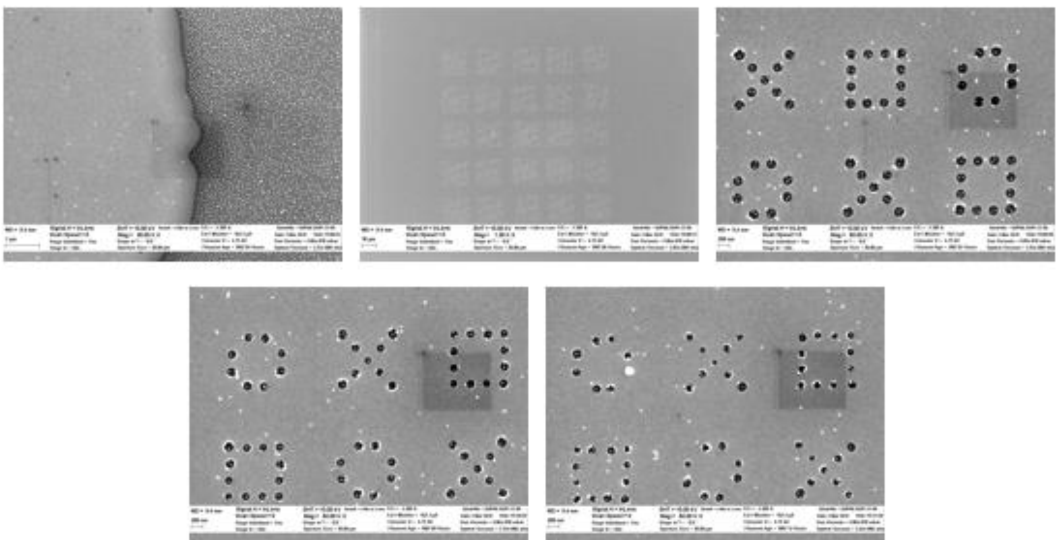

Fig 63 Sample 2 SPP SEM, selectivity, overall, large, medium, and small size area view

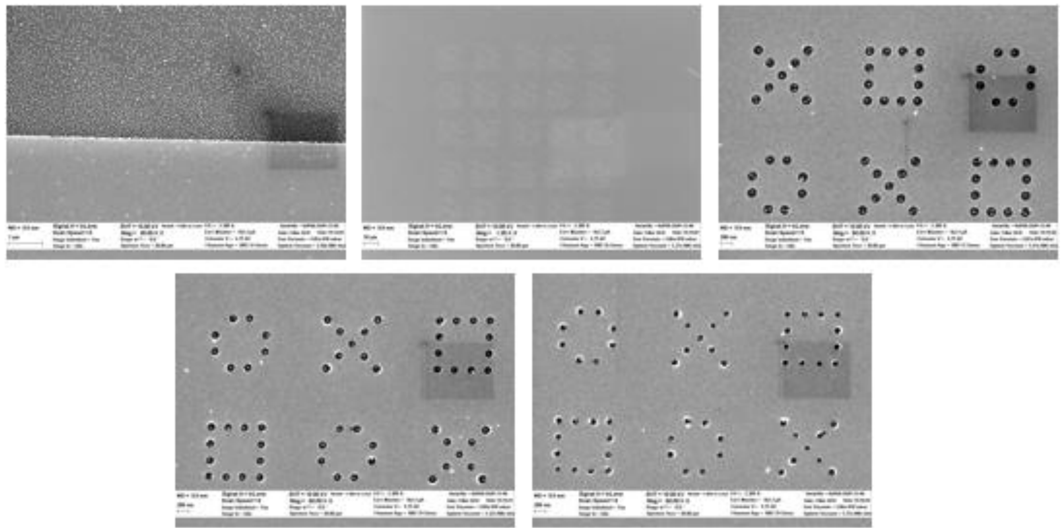

Fig 64 Sample 3 SPP SEM, selectivity, overall, large, medium, and small size area view

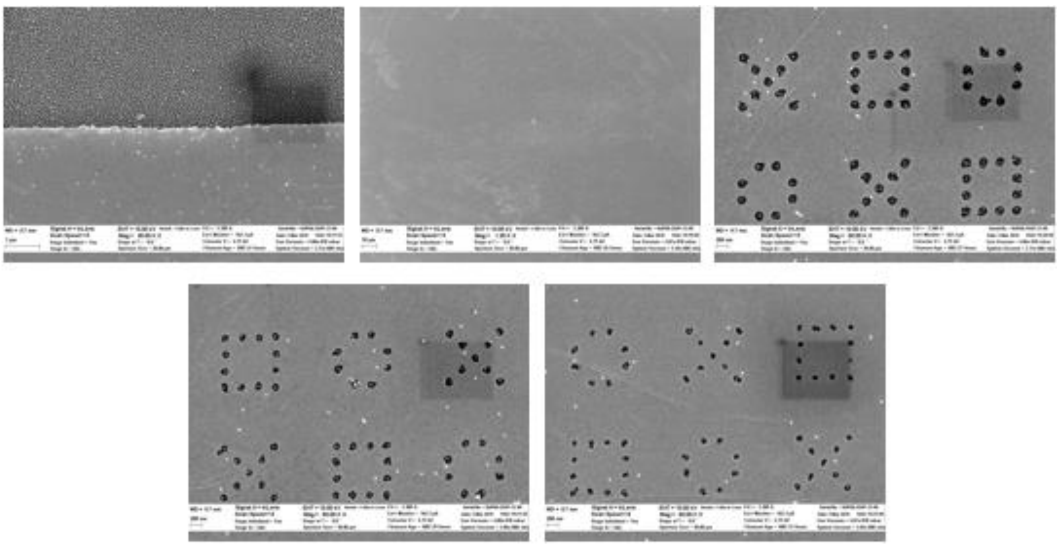

Fig 65 Sample 4 SPP SEM, selectivity, overall, large, medium, and small size area view

4.13 Ion Concentration Effeteness

#1/2/3 Lift-off acetone sonication 15minutes (X4), IPA sonication 10minutes (X2) rinse with IPA, Stored in ethanol, overnight

Since the establishment of the clean surface process from last time, we now move our research to the next step. Start from today we begin to use the new E-beam lithography pattern. The new patterns are still nano-scale circle with diameter 120nm and 160nm. Those circles are arranged to form cross, round, and parallel array; this design can allow us to study for the micro control of nanoparticle placement via ion concentration, pH value, and diameter of lithography pattern. From this first try results, we differ the ion concentration as 0.2mL and 1mL which the 0.2mL droplet gold nanoparticle should fill only one each the 160nm circle but leave the 120nm circle open. Then the 1mL droplet will cover both 120nm and 160nm circles and may have more than one particle filled in the 160nm circle. The last sample was treated first with 0.2mL then 1mL droplet, theoretically both two size diameter circle should be filled with only one particle inside. The SEM results indicated that we probably on the right track; the principle of "electrical funning" is working. The thing we need to find out is to optimize the conditions (ion concentration, pH value, and pattern diameter) to be able to reach the total modification and control of single nanoparticle placement.

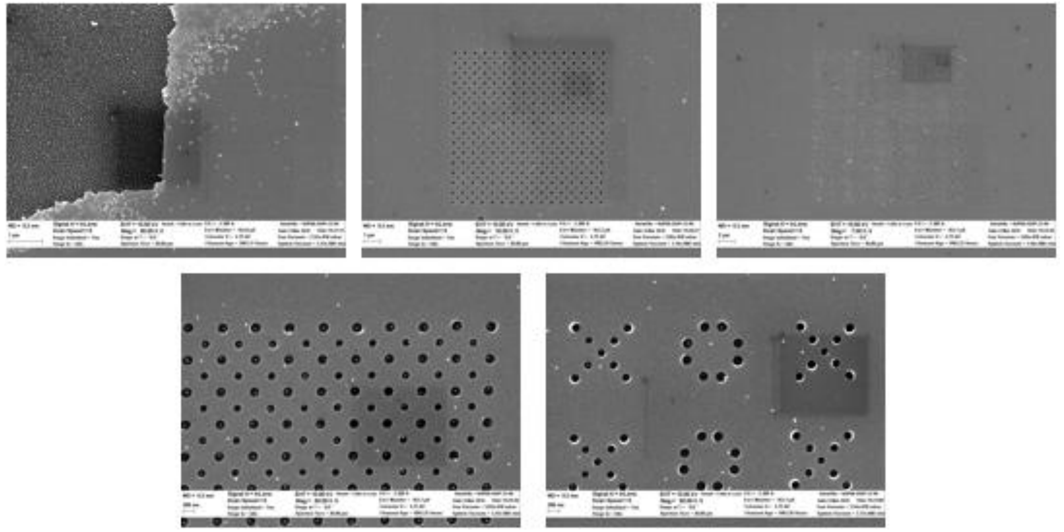

Fig 66 Sample 1 SPP SEM, 0.2mL ion concentration

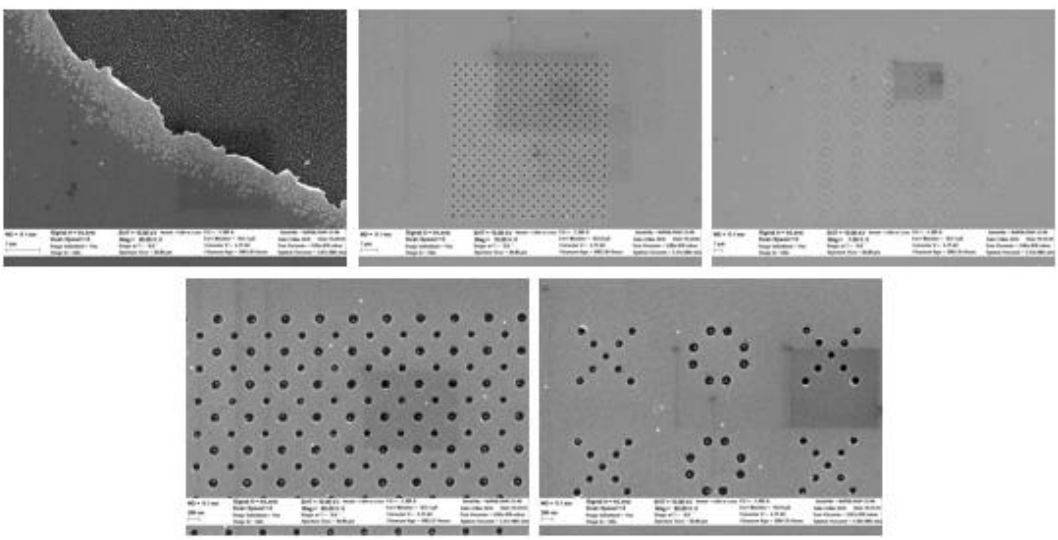

Fig 67 Sample 2 SPP SEM, 1mL ion concentration

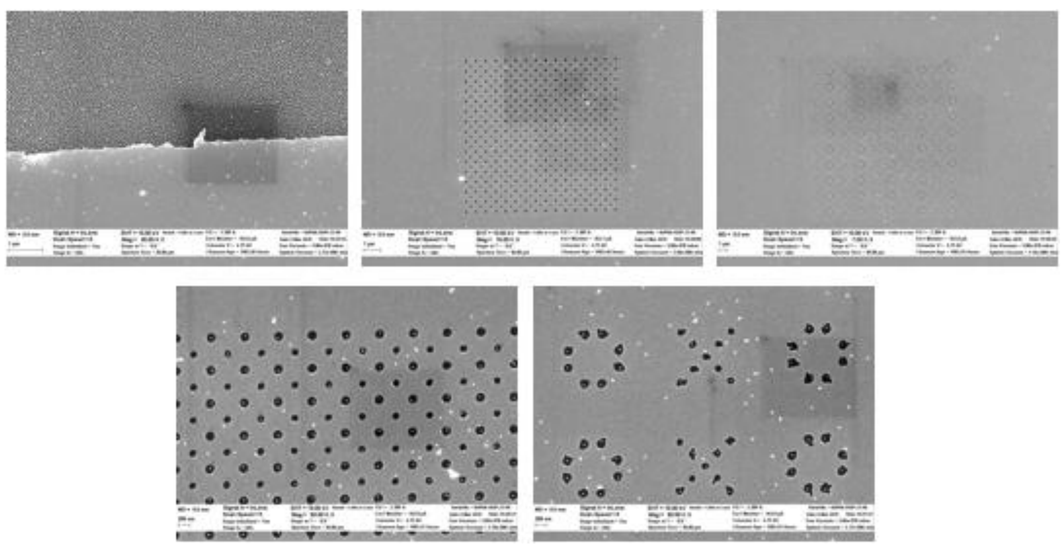

Fig 68 Sample 3 SPP SEM, 0.2mL+1mL ion concentration

4.14 New Pattern Array

New AutoCAD pattern has been made with pattern #1: diameter 100nm, 110nm, 120nm, and 160nm. Pattern #2: diameter 120nm, 130nm, 140nm, and 180nm. Both the pattern #1 and #1 are in BCS-square order, with size 26 X 26 circles on each side. The new patterns were written and developed, check under SEM without a further process to make sure if the e-beam lithography process remains the same after the change. The SEM shows that the new patterns have missing areas with 100nm and 110nm circles within pattern #1, 120nm and 130nm circles with pattern #2. Also, the circles with diameter 180nm in pattern #2 show a

poor lift-off result, some of the PR pillars have not been removing, this indicates that circle diameter should be smaller than 180nm to avoid the lift-off problem.

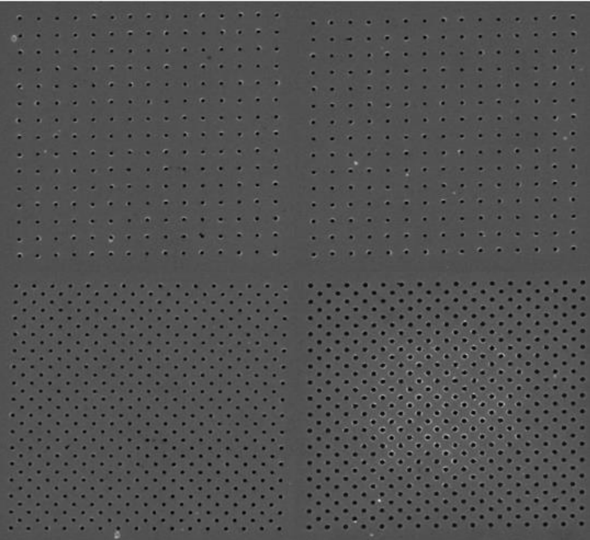

Fig 69 New Pattern #1, top left 100nm, top right 110nm, bottom left 120nm, and bottom right 160nm

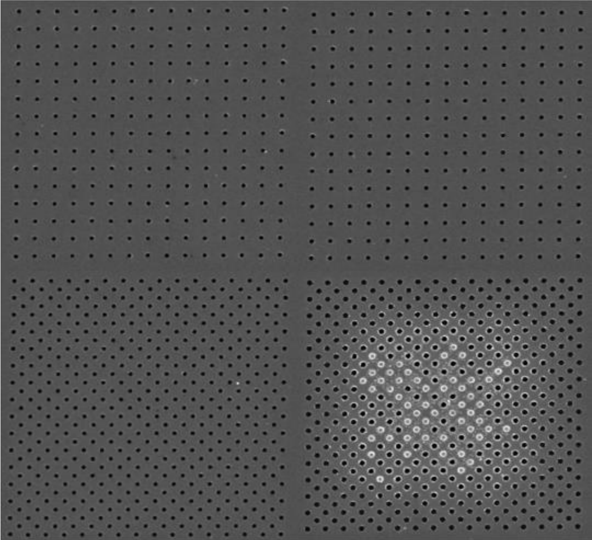

Fig 70 New Pattern #1, top left 120nm, top right 130nm, bottom left 140nm, and bottom right 180nm

4.15 DI Water Resuspended Au Nanoparticle

New step added: Wash Au nanoparticle with DI water, before resuspending in TE

#1 SPP with Au nanoparticle droplet resuspend in 0.02mM TE

#2 SPP with Au nanoparticle droplet resuspend in 0.1mM TE

#3 SPP with Au nanoparticle droplet resuspend in 1mM TE

#4 SPP with Au nanoparticle droplet resuspend in 3mM TE

With the solved surface clean condition problem and a stable clean process, we now prepare for the next step to check the Au nanoparticle placement on the substrate surface via the fixed pH value (pH 7.5), with changing of the TE buffer ion concentration through 0.02mM, 0.1mM, 1mM and 3mM. in addition, because of the different ranges of the diameter of the circles, we can also investigate the relation between the ion concentration and circle size. This is a critical concept here for nanoparticle attachment; the success micro-control of the nanoparticle placement can influence the surface modification and result in many ways of engineering applications. This process did not go well because of the new process step added in; we realize our DI water system produces the low pH Di water (around pH 5-6), since we use it to wash our Au nanoparticle, so it makes the nanoparticle colloid pH (around pH 8) below 7. The Au nanoparticle colloid being acidic and affect the particle surface ion potential, also the substrate surface SAM's layer. The MHA layer with $-COO^-$ group can be destroyed via H^+, in other words, the

electrostatic funneling technic cannot be processed successfully, in meanwhile the aggregation between Au nanoparticles occurs, the above two phenomena result in failed of Au particle placement.

4.16 PB Buffer pH Effeteness

The DI water pH problem was solved by the clean process to the DI water system. Moreover, we did a test for the pH value for the both TE buffer (originally pH=8) and PB buffer (originally pH=7.5) with each four different ion concentration, 0.02mM, 0.1mM, 1mM, and 3mM. Also, a couple of run of tests of the pure DI water from the recleaned DI water system.

	TE Buffer (pH=7.54)	PB Buffer (pH=7.5)	Pure DI Water
0.02mM	pH 6.5	pH 7.48	pH changes through the time, vary from pH 8.4 to pH 6.3
0.1mM	pH 7.03	pH 7.78	
1mM	pH 7.37	pH 7.83	
3mM	pH 7.38	pH 7.85	

Table 3 pH values with the differ ion concentration and DI water

It is obviously the TE buffer pH value cannot maintain with a desirable interval (pH 7.5), but the PB buffer shows better stability of keeping pH around 7.5. We decided to remain using PB buffer from now on for the particle placement experiment.

4.17 Ion Concentration and Circle Diameter (30nm Au particle)

This is the most successful results for Au nanoparticle placement since this year. We solved the new AutoCAD pattern missing problem; we now have the updated lithography patterns: Body-Centered circle with 16X16 plus 15X15 alternated array for 100nm, 110nm, 120nm, 130nm, 140nm, 160nm, and 170nm in diameter. This setup covers seven different diameters of the circle, with the fixed pH value (7.5) of PB buffer and control the four different ion concentration: 0.02mM, 0.1mM, 1mM, and 3mM. The expected results follow with the low ion concentration Au nanoparticle placement gives a low attachment rate and increase with the increasing circle diameter. The high ion concentration Au nanoparticle placement gives a high attachment rate, and even double or triple attachment find in specific circle diameter. The counted attachment with diameters and ion concentration shows below:

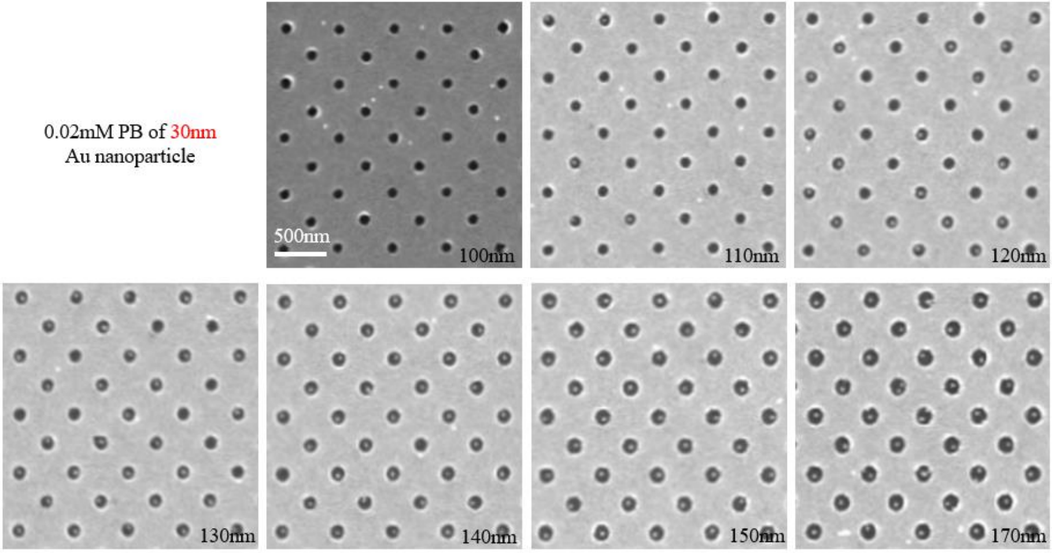

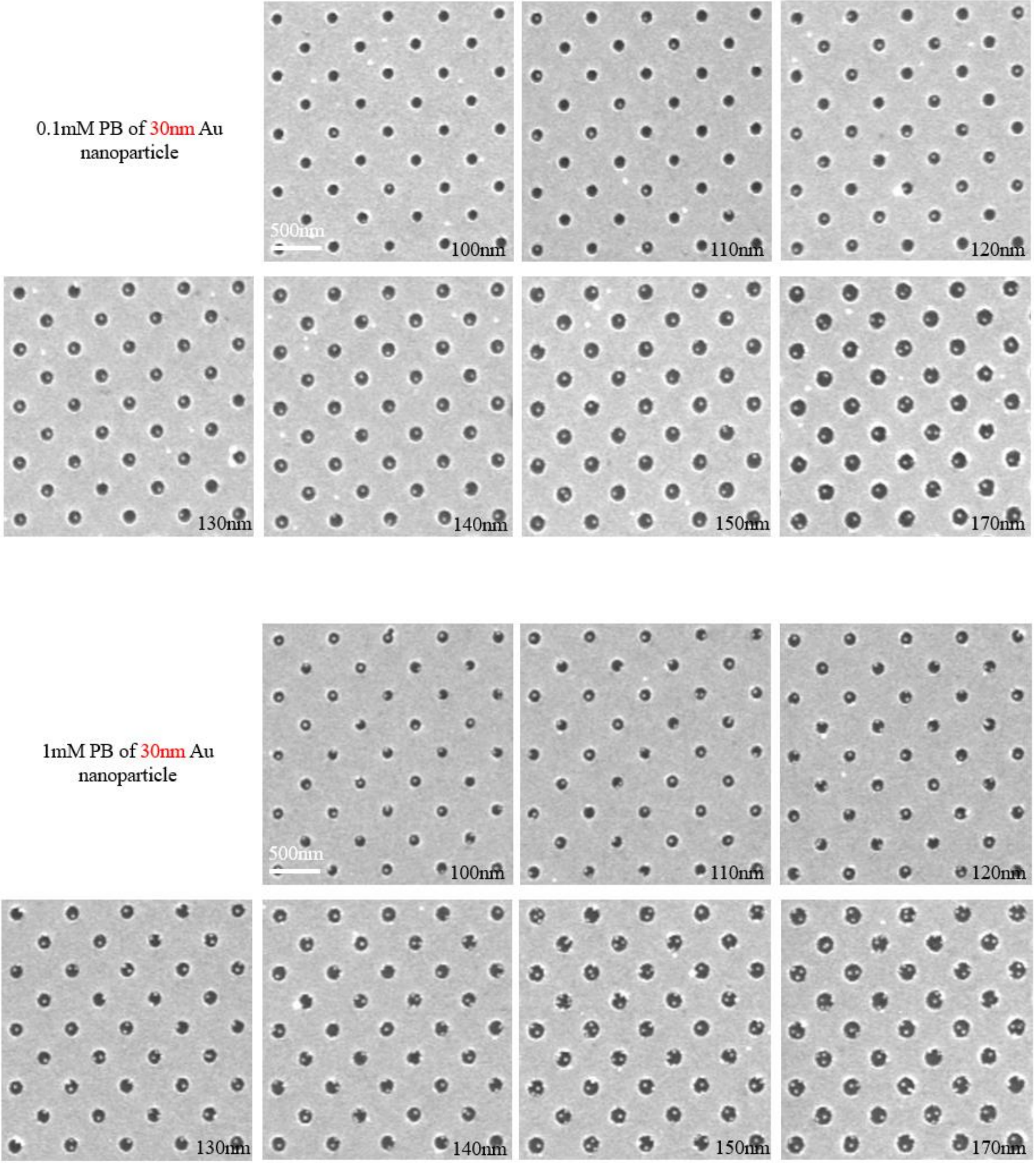

Fig 71 0.02mM, 0.1mM, and 1mM ion concentration for 30nm gold nanoparticle placement SEM with different circle diameters (Partial location)

30 nm AuNP (190319)				
Cicrle diameter [nm]	0.02 mM	0.1 mM	1mM	3mM
100	15	67	476	480
110	107	176	472	481
120	274	334	481	481
130	389	448	451	481
140	467	476	459	481
160	481	480	481	481
170	481	481	481	481

Table 4 30nm particle Attachment with differ ion concentration and circle diameter

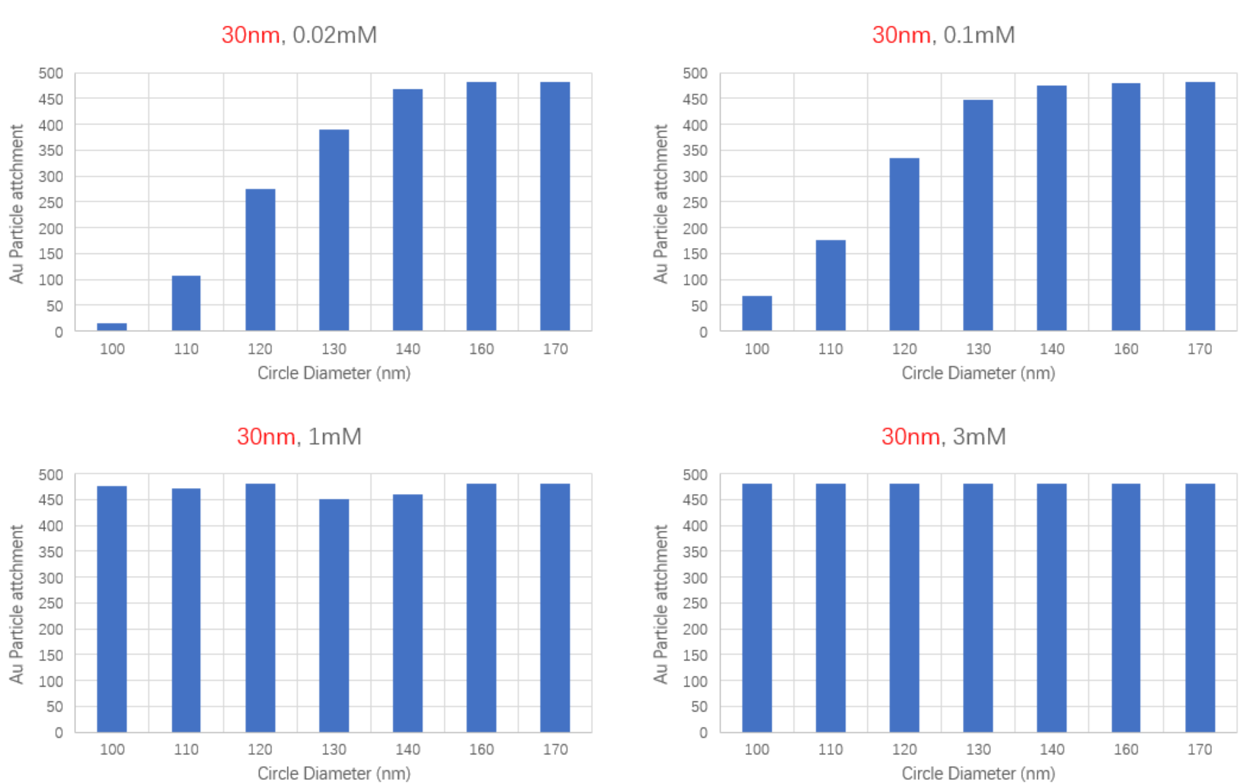

Fig 72 Column chart of circle diameter vs particle (30nm) attachment with different ion concentration

4.18 Ion Concentration and Circle Diameter (50nm Au particle)

We investigated using Au nanoparticles which have 50nm in diameter. This result gives us an idea about if the changing of the particle size may affect the attachment rate through the same pH and ion concentration. Moreover, from the below analysis, the conclusion is obvious that the large the nanoparticle size the less the attachment rate.

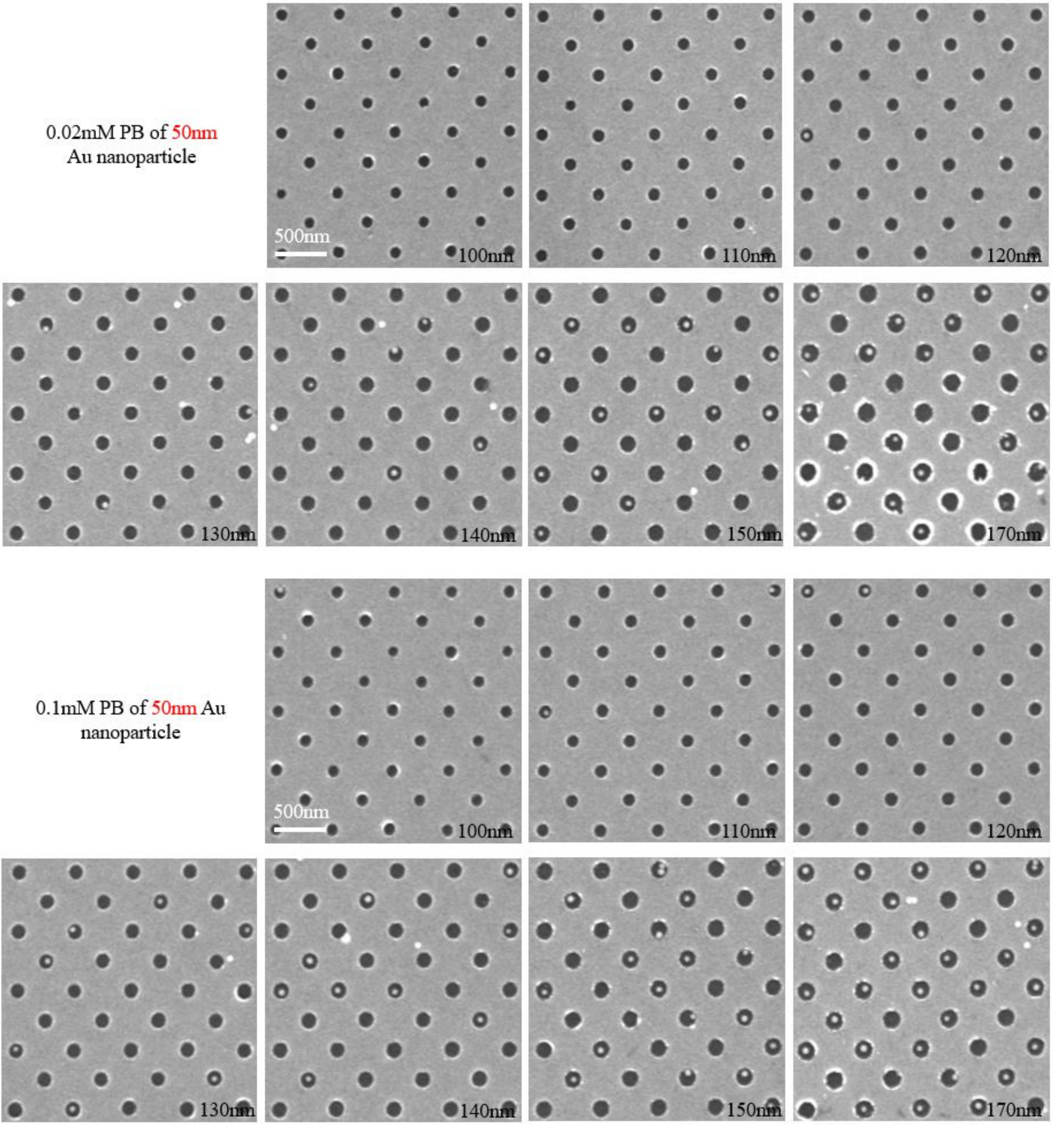

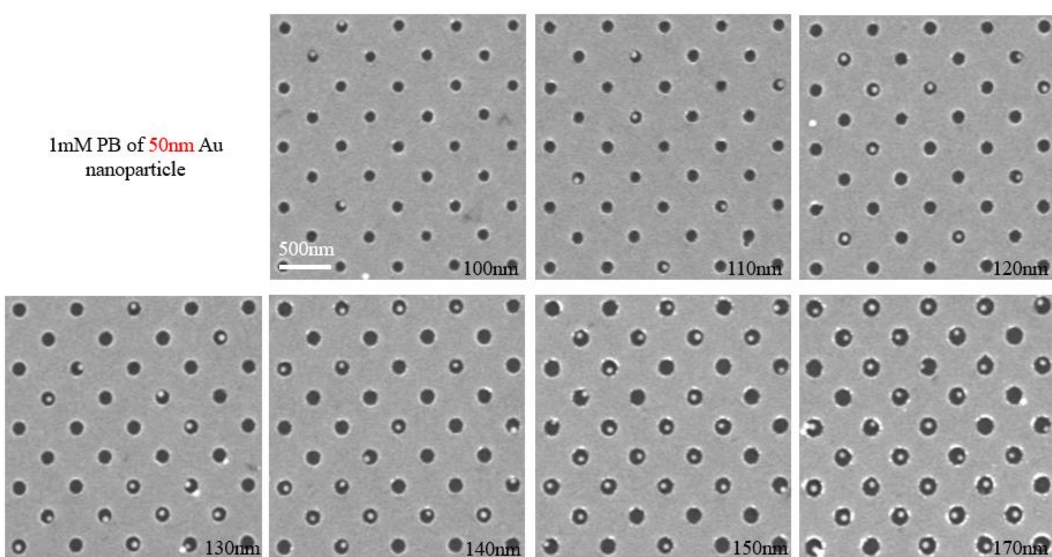

Fig 73 0.02mM, 0.1mM, and 1mM ion concentration for 50nm gold nanoparticle placement SEM with different circle diameters (Partial location)

50 nm AuNP (190320)				
Cicrle diameter [nm]	0.005 mM	0.1 mM	1mM	3mM
100	1	3	4	69
110	2	6	28	91
120	3	5	61	194
130	8	25	107	264
140	24	64	156	268
160	110	135	269	425
170	228	149	295	404

Table 5 50nm particle Attachment with differ ion concentration and circle diameter

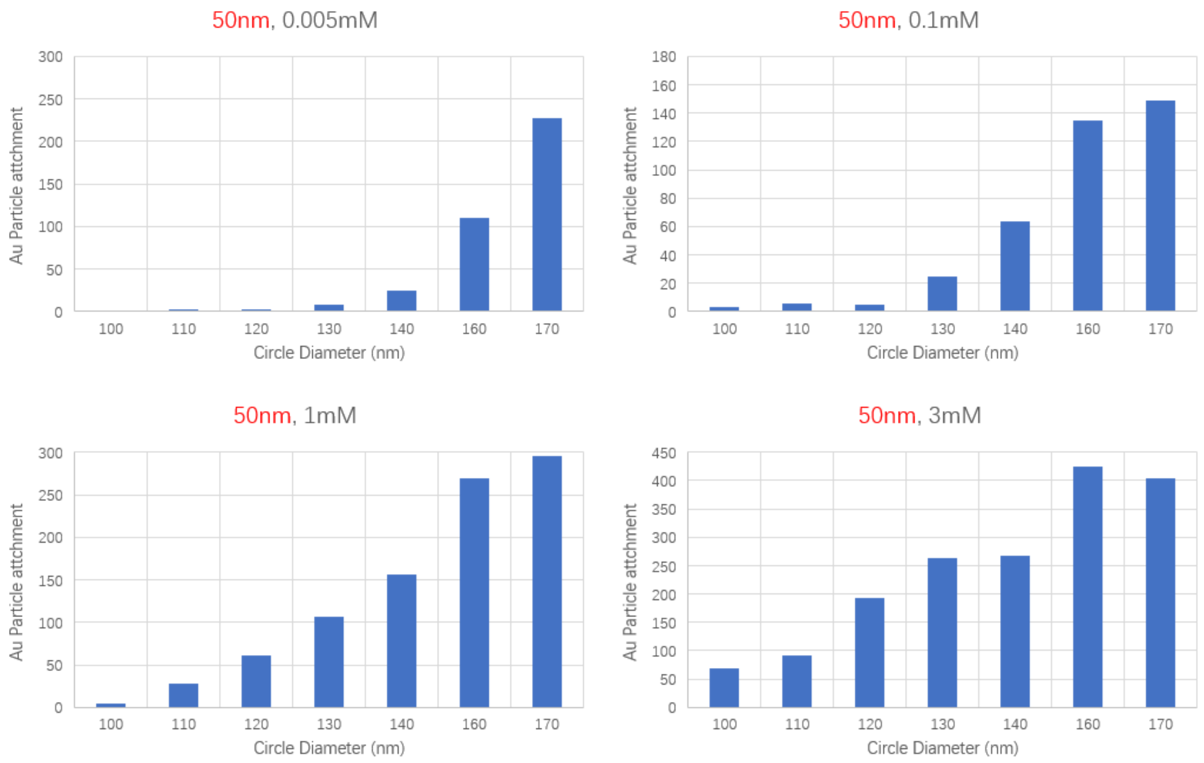

Fig 74 Column chart of circle diameter vs particle (50nm) attachment with different ion concentration

4.19 Single, Double, and Triple Attachment (30nm Au particle)

Since the previous experiment and results, we target our ion concentration from 0.1mM to lower region. Because over the 1mM ion concentration especially the diameter 30nm particle showing the almost full attachment rate, we want to the control among the lower ion concentration, this can let us have a better understanding of the micro selectively of Au nanoparticle placement. Instead of using the 16X16 plus 15X15 pattern array, we redraw the pattern with 8X8 plus 7X7 array; this reduce the total number of circles in one area from 481 to 113,

which make the counting job a little bit easier. In addition, we can also include the double and triple attachment.

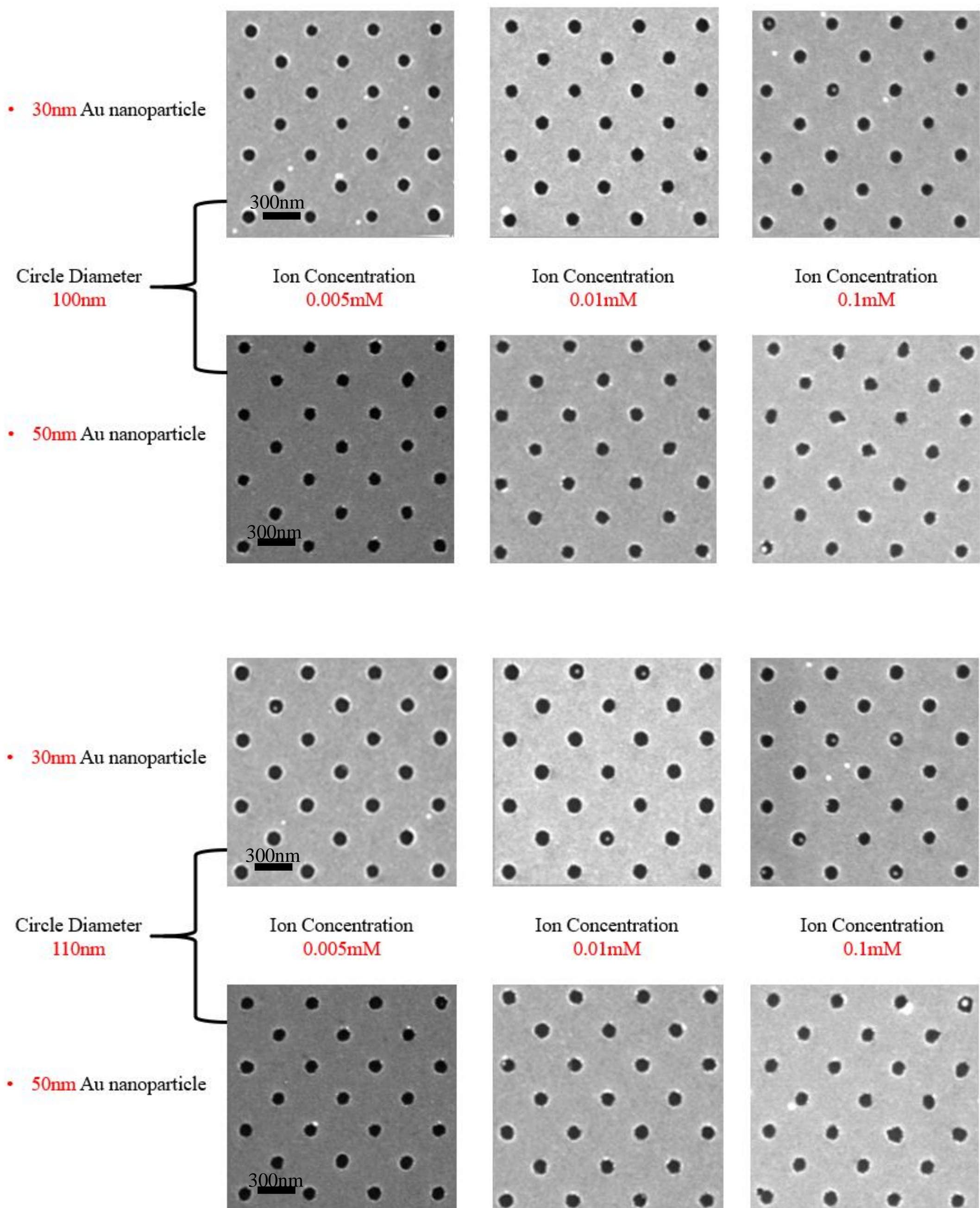

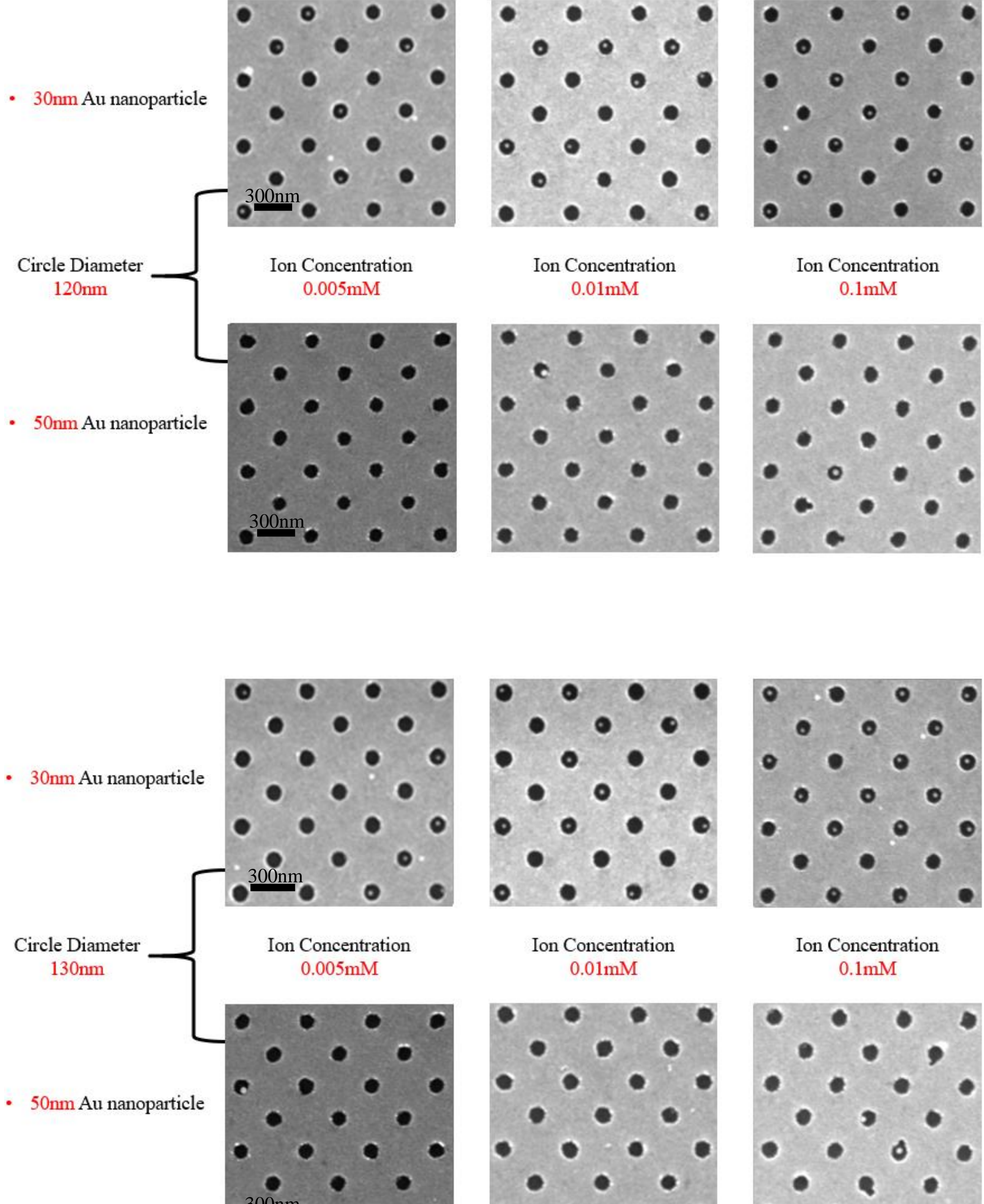
30nm Au nanoparticle
300nm
Circle Diameter
120nm
Ion Concentration
0.005mM
Ion Concentration
0.01mM
Ion Concentration
0.1mM
50nm Au nanoparticle
300nm
30nm Au nanoparticle
300nm
Circle Diameter
130nm
Ion Concentration
0.005mM
Ion Concentration
0.01mM
Ion Concentration
0.1mM
50nm Au nanoparticle
300nm

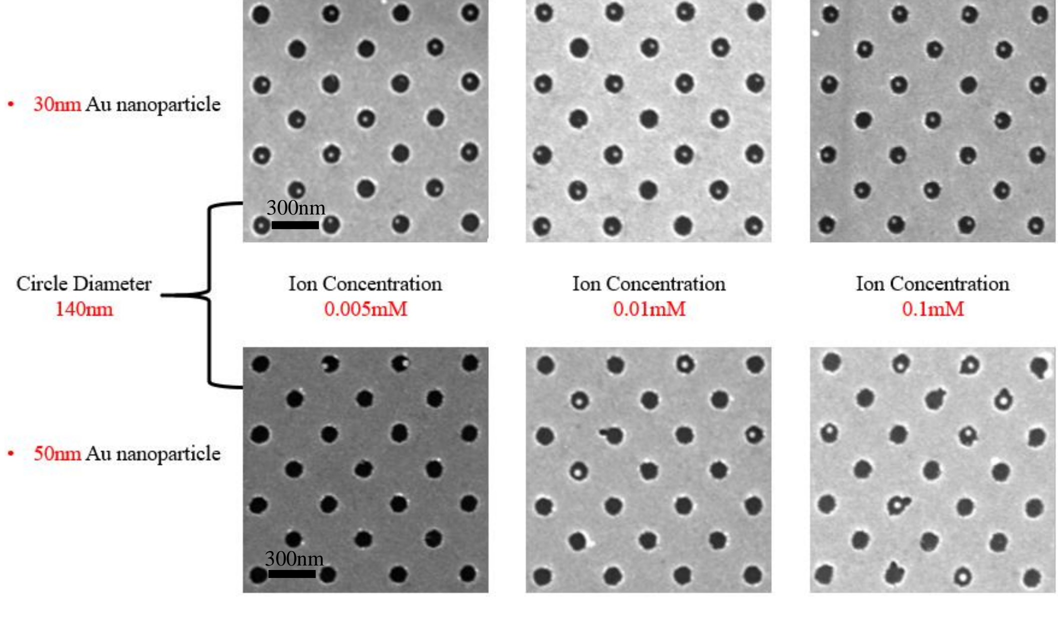
• 30nm Au nanoparticle
300nm
Circle Diameter
140nm
Ion Concentration
0.005mM
Ion Concentration
0.01mM
Ion Concentration
0.1mM
300nm
• 50nm Au nanoparticle

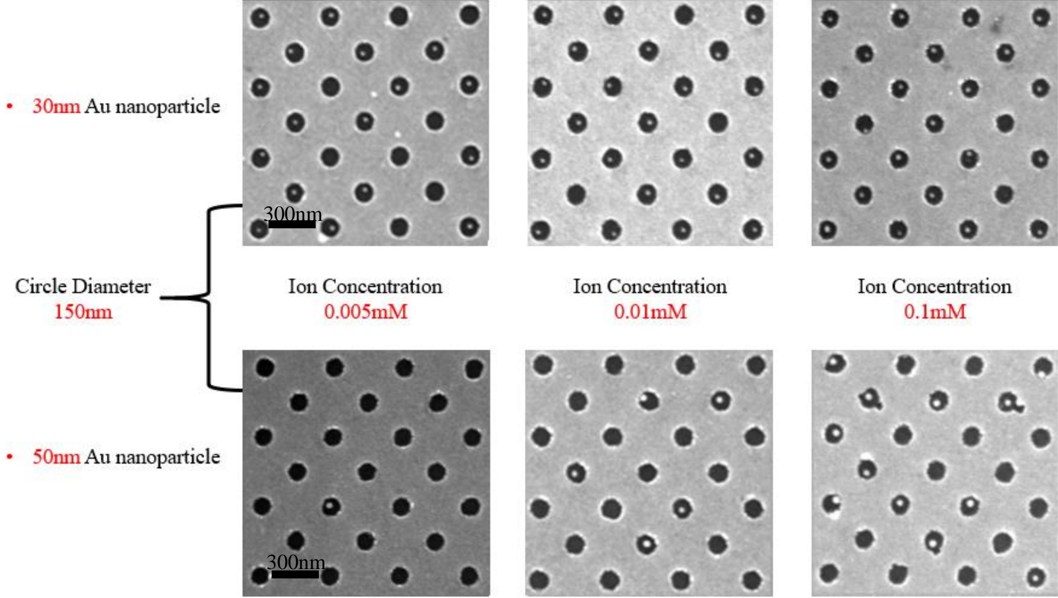
• 30nm Au nanoparticle
300nm
Circle Diameter
150nm
Ion Concentration
0.005mM
Ion Concentration
0.01mM
Ion Concentration
0.1mM
300nm
• 50nm Au nanoparticle

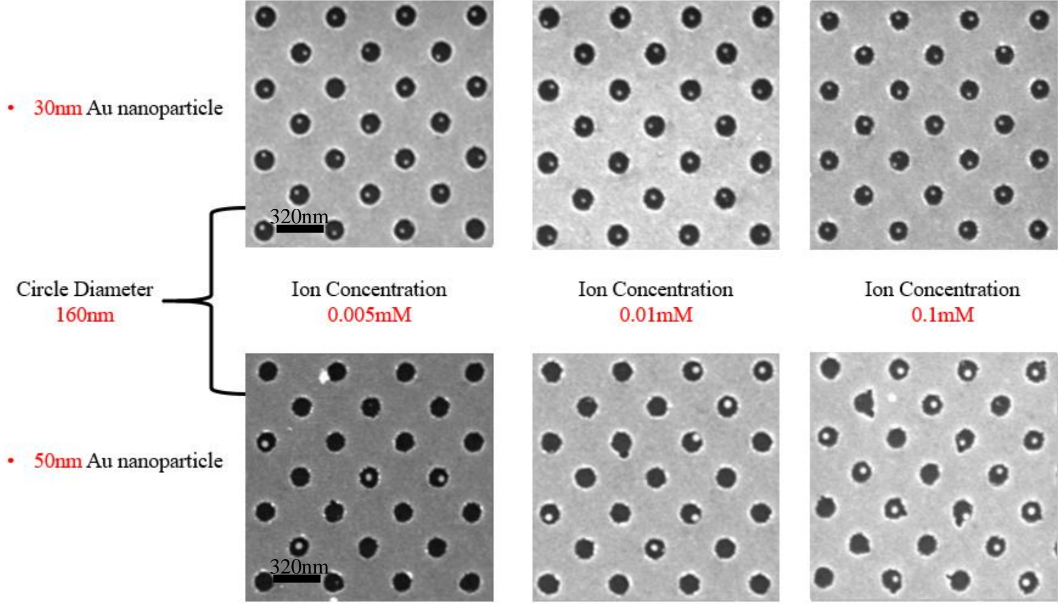
• 30nm Au nanoparticle
320nm
Circle Diameter
160nm
Ion Concentration
0.005mM
Ion Concentration
0.01mM
Ion Concentration
0.1mM
• 50nm Au nanoparticle
320nm

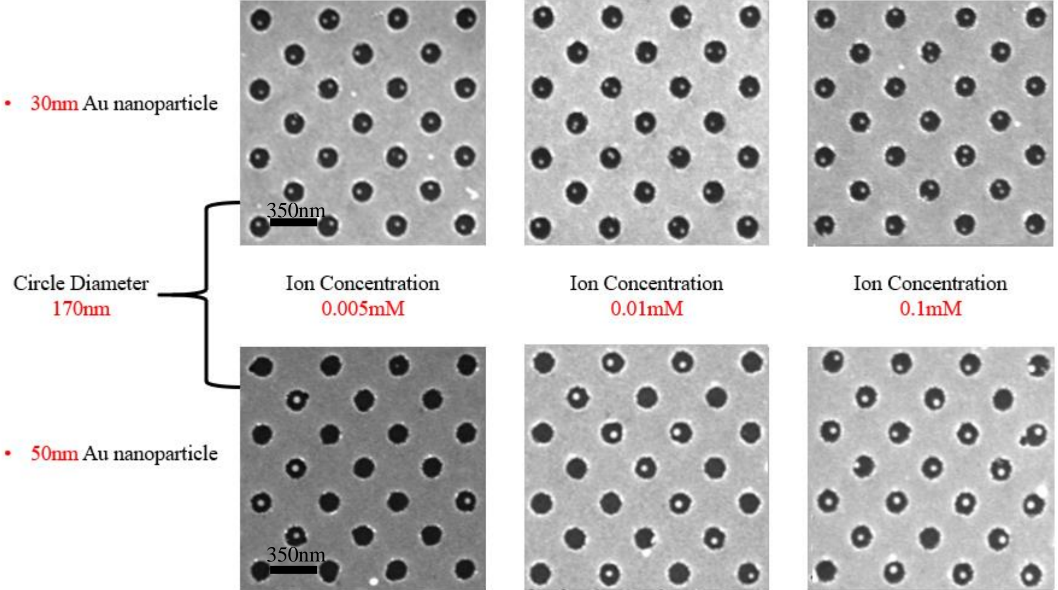
• 30nm Au nanoparticle
350nm
Circle Diameter
170nm
Ion Concentration
0.005mM
Ion Concentration
0.01mM
Ion Concentration
0.1mM
• 50nm Au nanoparticle
350nm

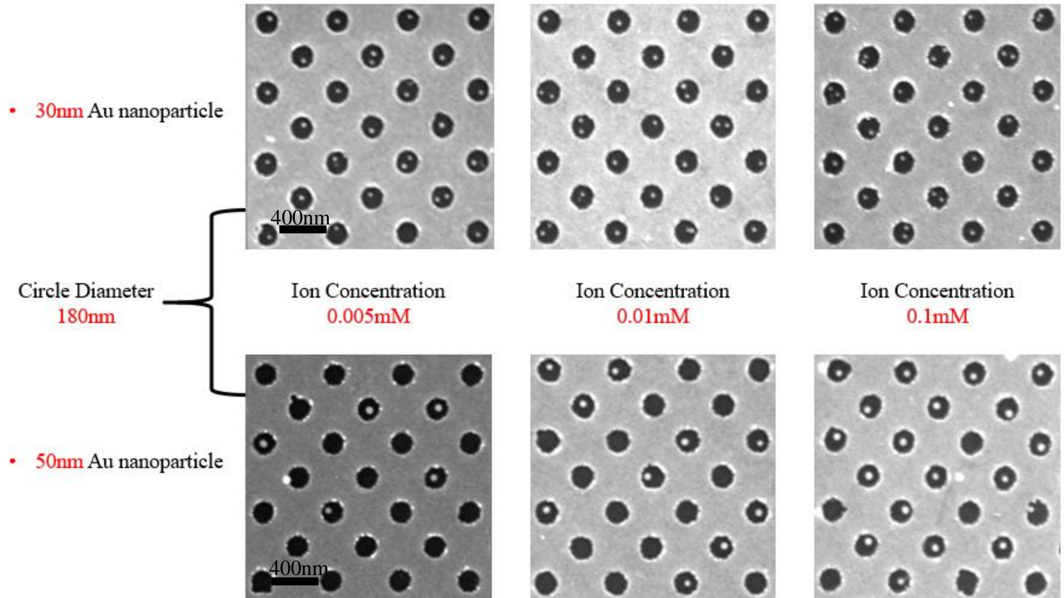

Fig 75 0.005mM, 0.01mM, and 0.1mM ion concentration for 30nm and 50nm gold nanoparticle placement SEM with circle diameters from 100nm to 180nm (Partial location)

30 nm AuNP	0.005mM		
Cicrle diameter [nm]	Single Attachment	Double Attachment	Triple Attachment
100	3	0	0
110	5	0	0
120	19	0	0
130	46	0	0
140	72	0	0
150	90	0	0
160	96	2	1
170	102	3	0
180	105	12	0

30 nm AuNP	0.01mM		
Cicrle diameter [nm]	Single Attachment	Double Attachment	Triple Attachment
100	6	2	0
110	19	1	0
120	34	2	1
130	59	0	0
140	88	0	0
150	98	1	0
160	107	3	1
170	113	11	0
180	112	24	1

30 nm AuNP	0.1mM		
Cicrle diameter [nm]	Single Attachment	Double Attachment	Triple Attachment
100	3	0	0
110	21	2	0
120	31	0	0
130	60	2	0
140	91	1	0
150	103	3	0
160	108	4	0
170	113	12	2
180	112	28	0

Single Attachment | Double Attachment | Triple Attachment

Table 6 30nm particle Attachment with differ ion concentration and circle diameter in 8X8 plus 7X7 array

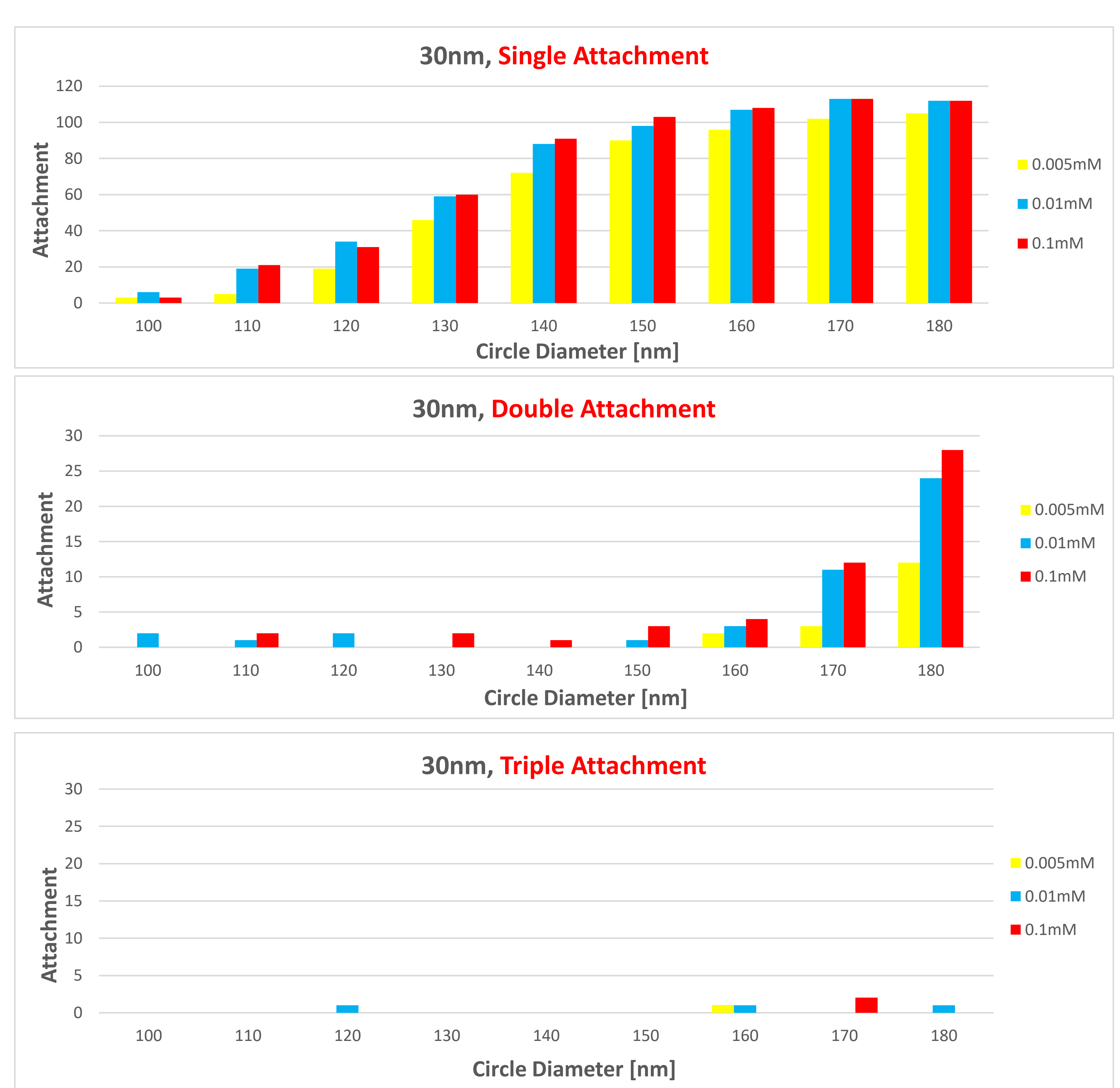

Fig 76 Column chart of circle diameter, ion concentration with single, double, and triple attachment

4.20 Single, Double, and Triple Attachment (50nm Au particle)

With the same conditions and 8X8 plus 7X7 patterns, we conducted one more time of the Au nanoparticle placement using the 50nm diameter of Au nanoparticle. A new deposition rate (10nm Cr and 20nm Au) was applied to enhance the lift-off process which proved useful. Because of the particle size increased bring up the repulsing force between each Au particle resulting in reduced attachment rate through the different circle diameter and ion concentration.

Especially for the double and triple attachment, both do not appear in this 50nm particle batch.

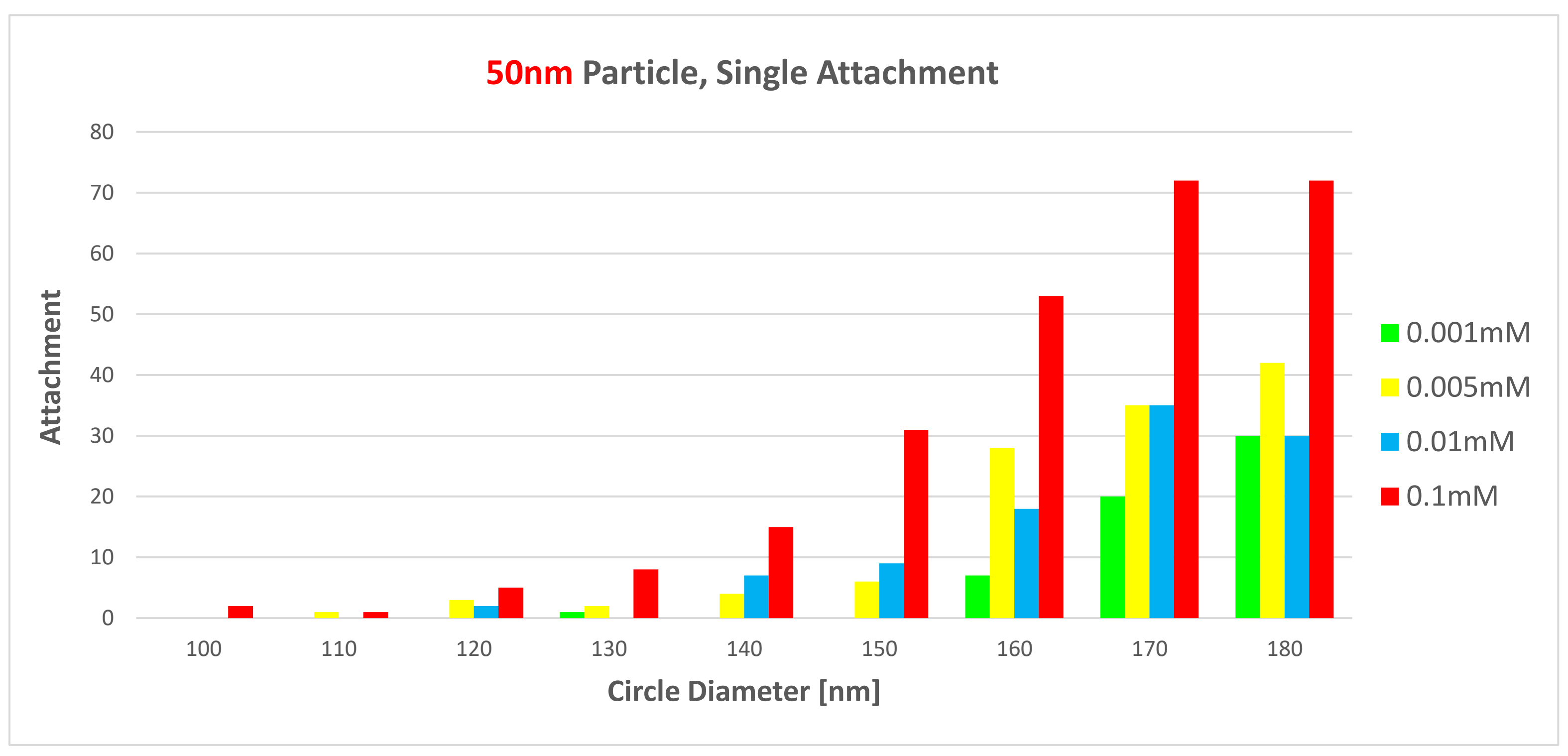

Fig 77 Column chart of circle diameter, ion concentration with single attachment

4.21 APTES Stability

After the results of both 30nm and 50nm Au nanoparticle attachments with different ion concentration, pattern circle size, and pH value. We did some data analysis work, and based on the all the investigation we start to conduct the experiment on the pattern circle which are two different diameters of circle rows alternating each other, the purpose is to control the 50nm Au nanoparticle place into the circle has large diameter, and the 30nm Au nanoparticle only go into the small diameter circle. The alternating circle we used are 130-180nm, 130-190nm, and 130-200nm. The process is placing the 50nm particle first on the substrate with low ion concentration, then apply 30nm particle with relatively high ion concentration. The result shows the 30nm particle attachment is almost not present. The reason is the APTES layer can be taken out by water during the first 50nm particle placement, resulting in the later 30nm particle has no APTES layer to attached with.

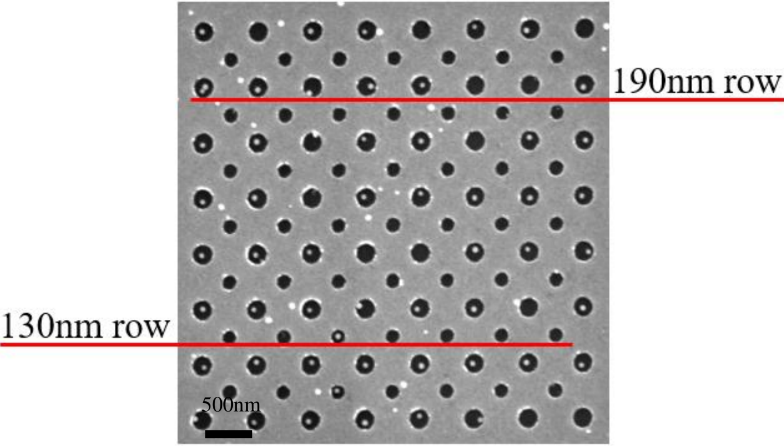

Fig 78 130-19nm alternating pattern, after 0.005mM 50nm+0.1mM 30nm particle placement

4.22 Heat Treatment for APTES Layer

APTES layer is unstable if the formation process under room temperature. To be able to solve this problem the heat treatment can be applied after the APTES layer formation. The temperature and treatment time can be critical for the substrate surface condition. Because higher temperature can cause the gold layer start to diffuse and may affect the later MHA layer formation on the gold surface. Several temperature tests being conducted 70℃, 80℃, 90℃, 100℃, and 110℃ for 2 minutes, plus another 110℃ and 60℃ for 10 minutes. The results show that the heat treatment makes a huge difference to the APTES layer; the APTES stability had a significant increase with the increase of the temperature. The problem also appears as the APTES layer becoming overstable after heating, cause the 50nm Au nanoparticle in low ion concentration even start to attach with the small size circle pattern, and the results also show the APTES layer after the 50nm placement somehow become unstable or defunctionalized with no later 30nm particle attachment and leave the empty circle pattern on the substrate.

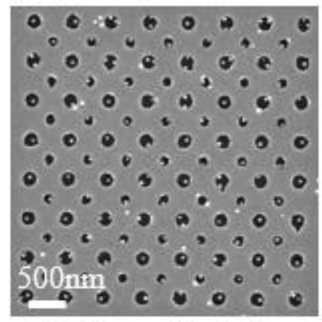

60 Degree, 10minutes
0.001mM 50nm + 0.1mM 30nm

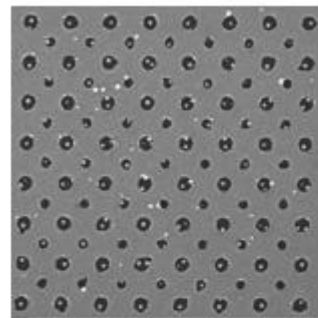

70 Degree, 2minutes
0.001mM 50nm + 0.1mM 30nm

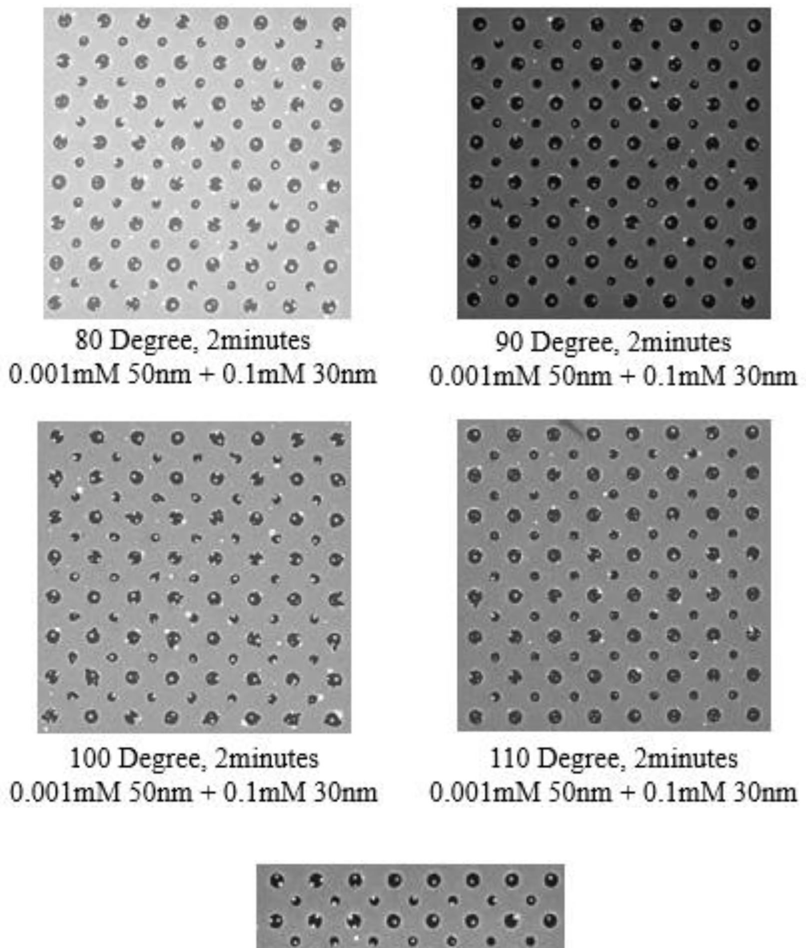

80 Degree, 2minutes
0.001mM 50nm + 0.1mM 30nm

90 Degree, 2minutes
0.001mM 50nm + 0.1mM 30nm

100 Degree, 2minutes
0.001mM 50nm + 0.1mM 30nm

110 Degree, 2minutes
0.001mM 50nm + 0.1mM 30nm

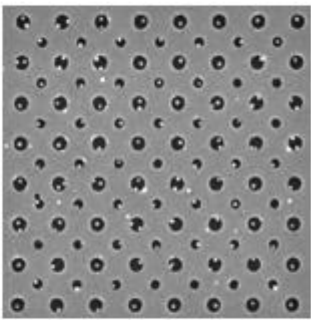

110 Degree, 10minutes
0.001mM 50nm + 0.1mM 30nm

Fig 79 Different temperature heat treatment result of multi nanoparticle placement

4.23 Double SAM's Layer Formation

The other method that we investigated is double SAM's layer formation. Since the APTES layer cannot be stable after the first 50nm particle placement and defunctionalized for the later 30nm particle placement, we decide to do two times of SAM's layer on the substrate. Because of the APTES layer can be degraded in the water, therefore a water immersion to remove the APTES layer after 50nm particle placement is added. This step is to clean out all the APTES on the SiO_2 surface since the second APTES layer will be formed later, the first APTES layer is not necessary after the 50nm particle placement. The step illustration shows below. The SEM results express the double SAM's layer method is relatively working, it is not entirely solved the problem, but it is clearly on the right track. The 50nm particles attached less in small circle pattern, and there are more 30nm particles inside the small circle.

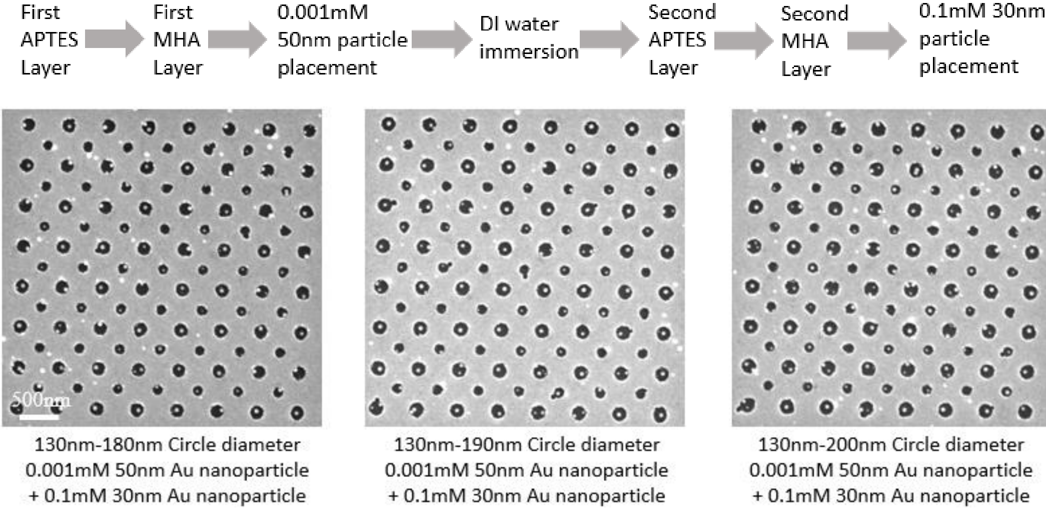

Fig 80 Double SAM's layer formation results with alternating pattern circle

CHAPTER 5 CONCLUSION

In this study, a novel approach for fabricating multi-element metastructures has been investigated. The placements of single 30 nm nanoparticles and single 50 nm Au nanoparticles on target substrate positions have been studied, where the effects of ion concentration, pH, diameter of the circular patterns on the nanoparticle placement have been investigated. The following have been achieved: Well-defined substrate patterns with circular wells (diameters from 100nm to 200nm) were successfully fabricated. Various process parameters for E-beam lithography and thin film deposition (such as e-beam dose, resist effect, lift-off, development, and film thickness) were investigated and optimized process conditions were obtained.

I. Procedures to conjugate DNA with Au nanoparticles were developed. Low pH (pH ~3) was used for the thiolated DNA to approach the Au surfaces easily during the conjugation. The DNA-functionalized Au nanoparticles were stable even in 1M NaCl.

II. An effective substrate cleaning procedure was developed that implements IPA sonication and ethanol immersion. This enabled reliable formations of APTES and MHA SAMs, resulting in good selectivity in the attachment of Au nanoparticles on the Au and SiO_2 surfaces.

III. Electrostatic interactions between DNA-functionalized Au nanoparticles and the substrate surface functionalized with SAMs (APTES SAMs on SiO_2

and MHA SAMs on Au) were investigated by varying colloid pH's, ion concentrations, and pattern sizes. For 30 nm Au nanoparticles, exactly one nanoparticle was placed at the center of each circular well when the ion concentration was 0.1 mM and the circular diameters were between 140 nm and 160 nm. For 50 nm Au nanoparticles, single-particle placement was made when the ion concentration was 0.01 mM and the circular diameters were between 180 nm and 200 nm.

IV. The stability of APTES SAMs upon heat treatment has been investigated. The post-bakeout of the APTES SAMs at 110°C for 10 minutes appears to enhance the stability of APTES as observed by more nanoparticle attachment for the same conditions compared to the APTES SAMs without the post-bakeout.

V. As a potential application of the accurate nanoparticle placement, the formation of SiO_2 nanopillars was investigated, where SiO_2 layer is vertically etched using RIE with Au nanoparticles used as etch hardmasks. Reliable RIE process conditions were established for the formation of nanoscale SiO_2 pillars as follows:

- RIE Power: 500W
- Pressure: 150 mTorr
- CF_4: 20 sccm
- O_2: 1.2 sccm

Although this study investigated the element-specific placement for two different sizes of Au nanoparticles (30 nm and 50 nm Au nanoparticles), this approach could be used for other nanoparticles, such as silver, silicon, CdSe, copper, SiO_2 nanoparticles, etc.

REFERENCES

[1] Anandan, V., Rao, Y. L. & Zhang, G. Nanopillar array structures for enhancing biosensing performance. International journal of nanomedicine 1, 73-79 (2006).
[2] Choudhury, B. D. et al. Silicon nanopillar arrays with SiO_2 overlayer for biosensing application. Opt. Mater. Express 4, 1345-1354, doi:10.1364/ome.4.001345 (2014).
[3] Xie, C., Hanson, L., Cui, Y. & Cui, B. Vertical nanopillars for highly localized fluorescence imaging. Proceedings of the National Academy of Sciences of the United States of America 108, 3894-3899, doi:10.1073/pnas.1015589108 (2011).
[4] Brust, M. & Kiely, C. J. Some recent advances in nanostructure preparation from gold and silver particles: a short topical review. Colloids and Surfaces A: Physicochemical and Engineering Aspects 202, 175-186, doi:https://doi.org/10.1016/S0927-7757(01)01087-1 (2002).
[5] Duyne, R. P. V., Haes, A. J. & McFarland, A. D. Nanoparticle optics: sensing with nanoparticle arrays and single nanoparticles. Vol. 5223 OP (SPIE, 2003).
[6] Wei, Q. H., Su, K. H., Durant, S. & Zhang, X. Plasmon Resonance of Finite One-Dimensional Au Nanoparticle Chains. Nano Letters 4, 1067-1071, doi:10.1021/nl049604h (2004).
[7] Liu, S. & Tang, Z. Nanoparticle assemblies for biological and chemical sensing. Journal of Materials chemistry 20, 24-35 (2010).
[8] Zywietz, U. et al. Electromagnetic Resonances of Silicon Nanoparticle Dimers in the Visible. ACS Photonics 2, 913-920, doi:10.1021/acsphotonics.5b00105 (2015).
[9] Spasova, M. et al. Magnetic properties of arrays of interacting Co nanocrystals. Journal of Magnetism and Magnetic Materials 240, 40-43, doi:https://doi.org/10.1016/S0304-8853(01)00723-5 (2002).
[10] Zywietz, U., Evlyukhin, A. B., Reinhardt, C. & Chichkov, B. N. Laser printing of silicon nanoparticles with resonant optical electric and magnetic responses. Nat. Commun. 5, 3402, doi:10.1038/ncomms4402 (2014).
[11] Cheng, X. in Nanolithography (ed Martin Feldman) 348-375 (Woodhead Publishing, 2014).
[12] Ingert, D. & Pileni, M. P. Nanocrystals Used as Masks for Nanolithography. The Journal of Physical Chemistry B 107, 9617-9619, doi:10.1021/jp030381d (2003).
[13] Brabazon, D. & Rafferty, A. 53-85 (2015).
[14] Haynes, C. L. & Van Duyne, R. P. Nanosphere Lithography: A Versatile Nanofabrication Tool for Studies of Size-Dependent Nanoparticle Optics. The Journal of Physical Chemistry B 105, 5599-5611, doi:10.1021/jp010657m (2001).
[15] Juillerat, F., Solak, H. H., Bowen, P. & Hofmann, H. Fabrication of large area ordered arrays of nanoparticles on patterned substrates. Nanotechnology 16, 1311-1316, doi:10.1088/0957-4484/16/8/055 (2005).
[16] Hung, A. M. et al. Large area spatially ordered arrays of gold nanoparticles directed by lithographically confined DNA origami. Nature Nanotechnology 5, 121, doi:10.1038/nnano.2009.450
[17] Zhang, H. et al. Direct Assembly of Large Area Nanoparticle Arrays. ACS Nano 12, 7529-7537, doi:10.1021/acsnano.8b02932 (2018).

[18] Zhang, G., Wang, D. & Möhwald, H. Ordered Binary Arrays of Au Nanoparticles Derived from Colloidal Lithography. Nano Letters 7, 127-132, doi:10.1021/nl062284c (2007).
[19] Yang, T. & Crozier, K. B. Dispersion and extinction of surface plasmons in an array of gold nanoparticle chains: influence of the air/glass interface. Opt. Express 16, 8570-8580, doi:10.1364/oe.16.008570 (2008).
[20] Hooper, D. C. et al. Second Harmonic Spectroscopy of Surface Lattice Resonances. Nano Letters 19, 165-172, doi:10.1021/acs.nanolett.8b03574 (2019).
[21] Yildirim, O. et al. Monolayer-directed Assembly and Magnetic Properties of FePt Nanoparticles on Patterned Aluminum Oxide. Vol. 11 (2010).
[22] Mikolajick, T. & Weber, W. Vol. 100 1-25 (2015).
[23] Niquet, Y. M. et al. Electronic structure of semiconductor nanowires. Physical Review B 73, 165319, doi:10.1103/PhysRevB.73.165319 (2006).
[24] Kuhn, K. J. Considerations for ultimate CMOS scaling. IEEE transactions on Electron Devices 59, 1813-1828 (2012).
[25] Mikolajick, T. et al. in 2007 International Symposium on VLSI Technology, Systems and Applications (VLSI-TSA). 1-4 (IEEE).
[26] Specht, M. et al. Novel dual bit tri-gate charge trapping memory devices. IEEE Electron Device Letters 25, 810-812 (2004).
[27] Wagner, R. & Ellis, W. Vapor-liquid-solid mechanism of single crystal growth. Applied physics letters 4, 89-90 (1964).
[28] Givargizov, E. in Vapour Growth and Epitaxy 20-30 (Elsevier, 1975).
[29] Morales, A. M. & Lieber, C. M. A laser ablation method for the synthesis of crystalline semiconductor nanowires. Science 279, 208-211 (1998).
[30] Cheung, C. L., Nikolić, R., Reinhardt, C. & Wang, T. Fabrication of nanopillars by nanosphere lithography. Nanotechnology 17, 1339 (2006).
[31] Jiang, P. & McFarland, M. J. Wafer-scale periodic nanohole arrays templated from two-dimensional nonclose-packed colloidal crystals. Journal of the American Chemical Society 127, 3710-3711 (2005).
[32] Elimelech, M., Chen, W. H. & Waypa, J. J. Measuring the zeta (electrokinetic) potential of reverse osmosis membranes by a streaming potential analyzer. Desalination 95, 269-286 (1994).
[33] Hunter, R. J. Zeta potential in colloid science: principles and applications. Vol. 2 (Academic press, 2013).
[34] Maurer, B. W. Flocculation and Filtration in the Geotextile Tube Environment, Syracuse University, (2011).
[35] Zukoski IV, C. & Saville, D. The interpretation of electrokinetic measurements using a dynamic model of the stern layer: I. The dynamic model. Journal of colloid and interface science 114, 32-44 (1986).
[36] Fixman, M. Thin double layer approximation for electrophoresis and dielectric response. The Journal of Chemical Physics 78, 1483-1491 (1983).
[37] Bell, G. M., Levine, S. & McCartney, L. N. Approximate methods of determining the double-layer free energy of interaction between two charged colloidal spheres. Journal of colloid and interface science 33, 335-359, doi:https://doi.org/10.1016/0021-9797(70)90228-6 (1970).

[38] Poorakbar, E. et al. Synthesis of magnetic gold mesoporous silica nanoparticles core shell for cellulase enzyme immobilization: Improvement of enzymatic activity and thermal stability. Process Biochemistry 71, 92-100, doi:https://doi.org/10.1016/j.procbio.2018.05.012 (2018).
[39] Stern, E. et al. Importance of the Debye Screening Length on Nanowire Field Effect Transistor Sensors. Nano Letters 7, 3405-3409, doi:10.1021/nl071792z (2007).
[40] Bryant, D. A. Debye length in a kappa-distribution plasma. Journal of Plasma Physics 56, 87-93, doi:10.1017/s0022377800019115 (1996).
[41] Mack, C. A. Field guide to optical lithography. Vol. 6 (SPIE Press Bellingham, WA, 2006).
[42] Vieu, C. et al. Electron beam lithography: resolution limits and applications. Applied surface science 164, 111-117 (2000).
[43] Tseng, A. A., Chen, K., Chen, C. D. & Ma, K. J. Electron beam lithography in nanoscale fabrication: recent development. IEEE Transactions on electronics packaging manufacturing 26, 141-149 (2003).
[44] Dill, F. H., Hornberger, W. P., Hauge, P. S. & Shaw, J. M. Characterization of positive photoresist. IEEE transactions on Electron Devices 22, 445-452 (1975).
[45] Liu, Y. Novel Parylene Filters for Biomedical Applications, California Institute of Technology, (2016).
[46] McIntire, T. M., Nizkordov, S. A. & Edwards, K. SELF-ASSEMBLED MONOLAYERS (SAMs). nature 13, 14.
[47] Aswal, D., Lenfant, S., Guerin, D., Yakhmi, J. & Vuillaume, D. Self-assembled monolayers on silicon for molecular electronics. Analytica chimica acta 568, 84-108 (2006).
[48] Love, J. C., Estroff, L. A., Kriebel, J. K., Nuzzo, R. G. & Whitesides, G. M. Self-assembled monolayers of thiolates on metals as a form of nanotechnology. Chemical reviews 105, 1103-1170 (2005).
[49] Acres, R. G. et al. Molecular structure of 3-aminopropyltriethoxysilane layers formed on silanol-terminated silicon surfaces. The Journal of Physical Chemistry C 116, 6289-6297 (2012).
[50] Haddada, M. B. et al. Optimizing the immobilization of gold nanoparticles on functionalized silicon surfaces: amine-vs thiol-terminated silane. Gold Bulletin 46, 335-341 (2013).
[51] Nuzzo, R. G., Zegarski, B. R. & Dubois, L. H. Fundamental studies of the chemisorption of organosulfur compounds on gold (111). Implications for molecular self-assembly on gold surfaces. Journal of the American Chemical Society 109, 733-740 (1987).
[52] Güllü, Ö. & Türüt, A. Electronic Properties of Cu/n-InP Metal-Semiconductor Structures with Cytosine Biopolymer. Acta Physica Polonica, A. 28 (2015).
[53] Sinden, R. R. DNA structure and function. (Elsevier, 2012).
[54] Zanchet, D., Micheel, C. M., Parak, W. J., Gerion, D. & Alivisatos, A. P. Electrophoretic isolation of discrete Au nanocrystal/DNA conjugates. Nano Letters 1, 32-35 (2001).
[55] Zu, Y. & Gao, Z. Facile and controllable loading of single-stranded DNA on gold nanoparticles. Analytical chemistry 81, 8523-8528 (2009).

[56] Hurst, S. J., Lytton-Jean, A. K. & Mirkin, C. A. Maximizing DNA loading on a range of gold nanoparticle sizes. Analytical chemistry 78, 8313-8318 (2006).
[57] Ma, L.-C. et al. Electrostatic Funneling for Precise Nanoparticle Placement: A Route to Wafer-Scale Integration. Nano Letters 7, 439-445, doi:10.1021/nl062727c (2007).
[58] Deal, B. E. & Grove, A. S. General Relationship for the Thermal Oxidation of Silicon. Vol. 36 (1965).
[59] Kao, D.-B., McVittie, J. P., Nix, W. D. & Saraswat, K. C. Two-dimensional thermal oxidation of silicon—I. Experiments. IEEE transactions on Electron Devices 34, 1008-1017 (1987).
[60] Gosálvez, M. A., Zubel, I. & Viinikka, E. in Handbook of Silicon Based MEMS Materials and Technologies (Second Edition) (eds Markku Tilli et al.) 470-502 (William Andrew Publishing, 2015).
[61] Nayak, A. P., Islam, M. S. & Logeeswaran, V. J. in Encyclopedia of Nanotechnology (ed Bharat Bhushan) 2829-2830 (Springer Netherlands, 2012).
[62] Logeeswaran, V. et al. A perspective on nanowire photodetectors: current status, future challenges, and opportunities. IEEE Journal of selected topics in quantum electronics 17, 1002-1032 (2011).
[63] Nojiri, K. Dry etching technology for semiconductors. (Springer, 2015).
[64] Bhardwaj, J., Ashraf, H. & McQuarrie, A. in Proc. Symp. Microstructures and Microfabricated Systems, ECS. 1-13.
[65] Jansen, H., Gardeniers, H., de Boer, M., Elwenspoek, M. & Fluitman, J. A survey on the reactive ion etching of silicon in microtechnology. Journal of micromechanics and microengineering 6, 14 (1996).